*Glorious diffraction spikes in The Cave*

# Astrophotographers take note!

This space is reserved for your B&W or greyscale images. Give us your best shots!



Gerry Smerchanski of the Winnipeg Centre adopted the hard way to record the crater Vieta on September 27 last year. Gerry combined paper and pencil at the end of a Celestron Ultima 8 with a binoviewer at 200× to capture the crater with its small central hill and off-centre craterlet. Gerry notes that "Crater Vieta usually gets overlooked by me as it is near Gassendi, which is a favourite of mine. But the lighting was perfect to go from Gassendi down along an arc of dramatically lit craters—including Cavendish—to Vieta where the terminator was found." Vieta is 80 km in diameter with 4500-m walls on the west side and 3000-m walls to the east. To the southeast lies the crater Fourier.

Michael Gatto caught the elusive "Werner X" during its few hours of visibility on November 20 from 9 to 9:45 p.m. Michael used an 8-inch f/7.5 Newtonian on a Dob mounting from Dartmouth, N.S., in average-to-poor seeing. The sketch was done at the eyepiece with various pencils and a blending stump on paper, then scanned and darkened in Photoshop. Werner X (or the Lunar X) is visible for only a short time when the Moon is at just the right phase.

# contents / table des matières

***Front cover*** *— Blair MacDonald captured the Cave Nebula (Sh2-155) in Cepheus with his Canon 60Da at the prime focus of a 200-mm Sky-Watcher Newtonian (with a Tele Vue Paracorr) at f/5.7. Exposure was 24×5 m at ISO 1600 from St. Croix Observatory in Nova Scotia. The Cave is a part of a much larger region of dust and ionized gas lying at a distance of 2400 light-years.*

# Letter to the Editor

*Open letter from Sidney van den Bergh to Victor Gaizauskas*

Dear Vic,

I have read the first two installments of your fine articles on "The Grand Schism." If I may, I should like to make one small correction. You write "...Carlyle Beals' strategy—before he retired as Dominion Astronomer—to create an institution of astronomy attached to a major university in Western Canada. The threat that this strategy posed for the ambitions of Toronto's Astronomy Department goes a long way towards explaining the bitterness of the ensuing dispute."

This statement is not correct. I was at the University of Toronto for the entire period 1958 to 1979. During this period, I never once heard any reference to rivalry between the University of Toronto and a major university in Western Canada. The objections by UofT to the development of Mt. Kobau were always entirely based on the poor weather conditions at the Mt. Kobau site.

It might be of interest to your readers if, in the last installment of your paper, you could publish a table comparing the number of clear hours of observing with the Sun below 18 degrees at the Mt. Kobau, Mauna Kea, and Cerro Tololo sites. These data provided the sole and devastating argument of the Toronto astronomers against building a major observatory in B.C.

With kindest regards and best wishes.

Sidney ✳

## The Royal Astronomical Society of Canada

### Vision
To inspire curiosity in all people about the Universe, to share scientific knowledge, and to foster collaboration in astronomical pursuits.

### Mission
The Royal Astronomical Society of Canada (RASC) encourages improved understanding of astronomy for all people, through education, outreach, research, publication, enjoyment, partnership, and community.

### Values
The RASC has a proud heritage of excellence and integrity in its programs and partnerships. As a vital part of Canada's science community, we support discovery through the scientific method. We inspire and encourage people of all ages to learn about and enjoy astronomy.

# News Notes / En manchettes

*Compiled by Andrew I. Oakes*
*(copernicus1543@gmail.com)*
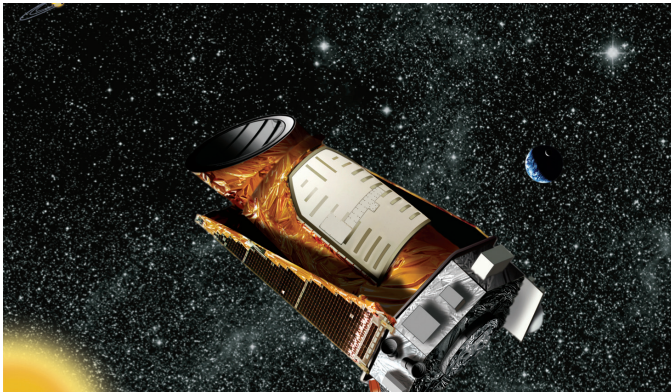


*Figure 1 —* Kepler *in space — an artist's concept.*
*Source: NASA/Ames/JPL-Caltech.*

## NASA's *Kepler* mission begins extension

The *Kepler Space Telescope*'s three-and-a-half-year primary mission to search for planets like the Earth came to a successful end in 2012 and was followed by the start of an extended mission that could last up to four more years. The primary mission identified more than 2300 planet candidates; more than 100 planets were confirmed. Hundreds of Earth-sized planet candidates were also found, in addition to contenders that orbit the so-called "habitable zones" around stars. Such zones are the region in an extra-solar planetary system where liquid water might exist on the surface of a planet.

With *Kepler*'s collected data in place, work is now underway to find true Sun-Earth analogues—Earth-size planets with a one-year orbit around stars similar to the Sun.

*Kepler* was launched 2009 March 6 and began the search for small worlds like Earth on 2009 May 12 after two months of commissioning. The space mission's results have indicated that the Milky Way Galaxy is teeming with planetary systems and that planets are prolific. A third of the stars seem to have planets, which translates to a total number in the billions for the whole galaxy.

To locate planets, the space telescope searched for candidates (exoplanets) orbiting distant suns by continuously monitoring the brightness of more than 150,000 stars. When a planet candidate transited the star from the spacecraft's vantage point, the light from a star underwent a small fading and recovery. The amount of starlight blocked would reveal the planet's size relative to its star.

A highlight from the prime mission included the first reported case of a planet orbiting a double-star system. This discovery was the result of a joint effort of amateur astronomers and scientists, with "citizen scientists" participating in Planet Hunters, a program led by Yale University that enlisted the public to comb through *Kepler* data for signs of transiting planets.

## Mercury harbours water ice and frozen volatiles

The planet Mercury appears to contain abundant water ice and other frozen volatile materials located in its permanently shadowed polar craters. This long-held hypothesis is supported by new observations by *MESSENGER*, an exploratory spacecraft now orbiting the innermost planet.

The conclusion is reinforced by three independent lines of evidence:

- The first measurements of excess hydrogen at Mercury's north pole with *MESSENGER*'s Neutron Spectrometer;

- The first measurements of the reflectance of Mercury's polar deposits at near-infrared wavelengths with the Mercury Laser Altimeter (MLA); and

- The first detailed models of the surface and near-surface temperatures of Mercury's north polar regions that utilize the actual topography of the surface as measured by the MLA.

The new findings appeared in three papers published in late November 2012 in *Science Express*, an online publication that offers electronic copies of selected scientific papers in advance of their printing in *Science*. The papers were titled:

- "Bright and Dark Polar Deposits on Mercury: Evidence for Surface Volatiles."

- "Evidence for Water Ice Near Mercury's North Pole from *MESSENGER* Neutron Spectrometer Measurements."

- "Thermal Stability of Volatiles in the North Polar Region of Mercury."
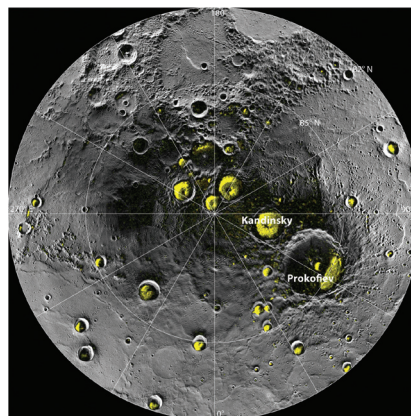


*Figure 2 — A mosaic of* MESSENGER *images of Mercury's north polar region with all of the larger polar deposits located on the floors or walls of impact craters while deposits farther from the pole are concentrated on the north-facing sides of craters. Source: NASA/Johns Hopkins University Applied Physics Laboratory/Carnegie Institution of Washington/National Astronomy and Ionosphere Center, Arecibo Observatory.*

Because the tilt of Mercury's rotational axis is almost zero—less than one degree—there are pockets at the planet's poles that never see sunlight. Scientists suggested decades ago that there might be water ice and other frozen volatiles trapped in these sunless regions. In 1991, the Arecibo radio telescope in Puerto Rico detected radar-bright patches at Mercury's poles—spots that reflected radio waves in the way one would expect if there were water ice. These patches also corresponded to the location of large impact craters mapped by the *Mariner 10* spacecraft in the 1970s.

There are a strong indications that:

- water ice is the major constituent of Mercury's north polar deposits;

- ice is exposed at the surface in the coldest of those deposits; and

- ice is buried beneath an unusually dark material across most of the deposits (in areas where temperatures are a bit too warm for ice to be stable at the surface itself).

The material is trapped in a region with temperatures that remain below 100 K (-280 °F or -173 °C). According to scientists, the dark material is likely a mix of complex organic compounds delivered to Mercury by the impacts of comets and volatile-rich asteroids. They add that the organic material may have been darkened further by exposure to the harsh radiation at Mercury's surface, even in permanently shadowed areas.

## Dwarf planet reveals itself during rare occultation

Telescopes in Chile and Brazil have assisted astronomers in reaching some preliminary conclusions about dwarf planet Makemake, originally discovered in March 2005. Pronounced *MAH'-kay MAH'-kay*, Makemake (named after the creator of humanity and god of fertility in the myths of the native people of Easter Island) is one of five known dwarf planets orbiting in our Solar System. Makemake is about two-thirds the size of Pluto and travels around the Sun in a distant path that lies beyond that of Pluto but closer to the Sun than Eris, the most massive known dwarf planet in the Solar System.

Scientists succeeded in gaining new knowledge about Makemake by measuring changes in the stellar brightness when the dwarf planet occulted a background star. The event was a rare opportunity, as occultations are particularly uncommon in the case of Makemake, because the dwarf planet moves in an area of the sky with relatively few stars.

Makemake passed in front of the faint star on 2011 April 23. The scientific team observed this event using seven different telescopes across Brazil and Chile. The occultation lasted about one minute, while astronomers utilized a specialized high-speed camera known as ULTRACAM and a high-speed infrared imager named ISAAC to capture the event. The new

observations also have allowed astronomers to check for the first time whether Makemake is surrounded by an atmosphere.

With its orbit lying in the cold outer Solar System, Makemake was expected to have an atmosphere like Pluto, but the new observations show that this is not the case. Although there is no global Pluto-like atmosphere at a level of one thousandth that of Pluto's atmosphere, it may have a local atmosphere that only covers part of the surface, which is possible in theory and is not excluded by the observations.

Astronomers have measured how much of the Sun's light Makemake's surface reflects—its albedo—which is at about 0.77. This albedo is comparable to that of dirty snow, higher than that of Pluto, but lower than that of Eris. Makemake's density is 1.7 ± 0.3 grams per cubic centimetre. Astronomers have inferred the dwarf planet's shape and appearance is that of an oblate spheroid with axes of 1430 ± 9 kilometres and 1502 ± 45 kilometres.

A paper titled *"Albedo and atmospheric constraints of dwarf planet Makemake from a stellar occultation"* providing details of the research appeared in the 2012 November 22 issue of the journal *Nature*.

## Gas bridge connects galaxy clusters

Astronomers have detected a "bridge" of hot gas connecting two galaxy clusters, *Abell* 399 and *Abell* 401, that are located at red-shift z~0.07 or about one billion light-years away from



*Figure 3 — The* Planck *space telescope has discovered a bridge of hot gas that connects galaxy clusters Abell 399 (lower centre) and Abell 401 (top left). The gas bridge extends approximately 10 million light-years between them. Source: Sunyaev-Zel'dovich effect (orange): ESA &* Planck *Collaboration; optical image: STScI Digitized Sky Survey.*

Earth. The bridge filament extends across some 10 million light-years of intergalactic space and contains gas with a temperature of about 80 million K. Scientists believe that part of this gas might derive from the so-called warm-hot intergalactic medium (WHIM), an elusive web of gaseous filaments that is said to pervade the Universe.

The European Space Agency's *Planck* space telescope—its primary task is to capture the most ancient light of the cosmos, the cosmic microwave background (CMB)—has made the first conclusive detection of the bridge of hot gas. When CMB light interacts with hot gas permeating huge cosmic structures, its energy distribution is modified in a characteristic way known as the Sunyaev–Zel'dovich (SZ) effect. Astronomers have not only detected the individual signal from the gas in each of the Abell 399 and Abell 401 clusters, but also a stream of gas linking the two. A scientific paper, titled *Planck intermediate results. VIII. Filaments between interacting clusters* and published in the journal *Astronomy & Astrophysics*, provides more detail on the results of the phenomenon.

## Asteroid 2007 PA8 imaged by radar

Recent images of near-Earth asteroid 2007 PA8 reveal the existence of possible craters, boulders, an irregular and asymmetric shape, and a very slow rotation. The asteroid, imaged via radar in October and November 2012 by NASA's 70-metre Deep Space Network antenna at Goldstone, California, measures about 1.6 kilometres wide. The space traveller came to some 6.5 million kilometres from Earth, 17 times the distance between Earth and the Moon. The 2012 flyby was the closest since 1880. The next flyby closer than this latest one will be in 2488, at which the asteroid is expected to approach no closer than 5.8 million kilometres.
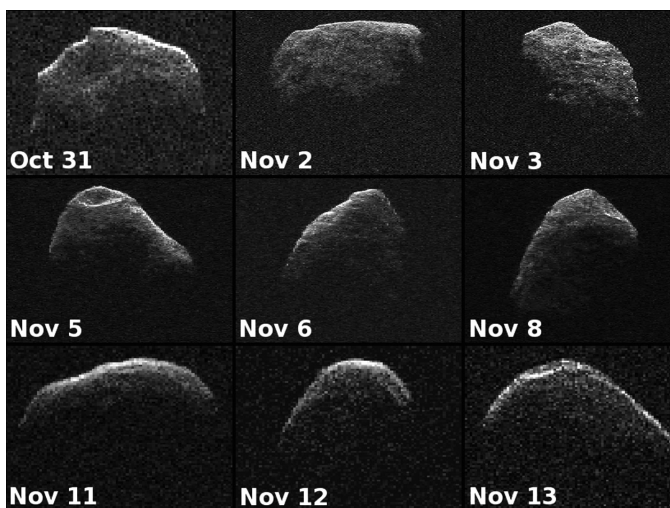


*Figure 4 — NASA's 70-metre Deep Space Network antenna at Goldstone, California collected data creating new radar images of near-Earth asteroid 2007 PA8. The images were obtained between 2012 October 31 and 2012 November 13. Source: NASA/JPL-Caltech.*

Each of nine radar images (Figure 4) shows one image per day. All images are oriented so rotation is counterclockwise and are shown at the same scale, covering 1.7 kilometres from top to bottom. The resolution of the images varied from day to day as the asteroid's distance changed, ranging from 18.75 to 3.75 metres per pixel during the passage.

## Patrick Moore, a giant in amateur astronomy and an RASC Honorary Member



*Figure 5 — Sir Patrick Moore. Source: Cambridge University Press.*

Sir Patrick Moore, an internationally acclaimed amateur astronomer and long-time Honorary Member of the RASC, "passed away peacefully" at his home in Selsey, West Sussex, U.K., on 2012 December 9. He was 89. Sir Patrick's life-long passion for astronomy led him over many years to attain a prominent status as a writer, researcher, radio commentator, and television host.

Born on 1923 March 4 at Pinner, Middlesex, Patrick Alfred Caldwell-Moore's love for astronomy began when, as a child, he received from his mother a copy of G.F. Chambers's book, *The Story of the Solar System*. He became the author of over 70 books on astronomy and host of the world's longest-running television series with the same original host in place—the British Broadcasting Corporation's *The Sky at Night*. Moore hosted the first broadcast of the show on 1957 April 24, and he last appeared in an episode televised on the Monday before he died.

Moore was appointed an Honorary Member of the RASC in 1993 and received a knighthood from the Queen for his services to astronomy in 2001. He was a former president of the British Astronomical Association, co-founder and former president of the Society for Popular Astronomy, a specialist in lunar observation, and the creator of the *Caldwell Catalogue*, an astronomical list of 109 bright star clusters, nebulae, and galaxies for observation by amateur astronomers. The book has served as a complement to the Messier Catalogue.

After the death of his fiancée, killed by a bomb during World War II, Moore chose never to marry.

Although a quiet ceremony of interment was held in December 2012, a farewell event is planned for what would have been Moore's 90th birthday in March 2013. ★

# The Red Giant Branches of Milky Way Globular Clusters: A Near-Infrared Perspective

*Jeff Webber[1] and Graeme H. Smith[2]*

[1] *Department of Physics, University of California, Santa Cruz CA 95064 USA*

[2] *University of California Observatories, University of California, Santa Cruz CA 95064 USA*

*graeme@ucolick.org*
*2012 August 11*

## Abstract

Utilizing near-infrared data from the Two-Micron All-Sky Survey for 24 of the brightest and closest globular clusters in the Milky Way, colour-magnitude diagrams have been derived that plot the absolute magnitude $M_{K_S}$ versus $(J - K_S)$ colour. The morphology of the red giant branch in these diagrams has been characterized through measurements of (i) the colour at a fixed reference magnitude and (ii) the absolute magnitude of the brightest stars. These parameters in turn have been documented as a function of metallicity and compared with predictions based on Dartmouth model isochrones. The colour of the red giant branch and the maximum $K_S$-band luminosity both vary with metallicity in a manner consistent with the model isochrones. Measurements of the slope of the upper part of the red giant branch have been obtained from the work of Ivanov & Borrisova (2002) and are found to also behave with metallicity in a similar manner to that of the isochrones.

## Résumé

En utilisant des données proches-infrarouges provenant du 2MAAS touchant 24 des plus brillants et proches amas globulaires de la Voie lactée, des diagrammes de la couleur-magnitude ont été relevés traçant la couleur de la magnitude absolue $M_{K_S}$ versus $J - K_S$. La morphologie de la branche des géantes rouges dans ces diagrammes est précisée en (i) mesurant la couleur à un point de magnitude référentielle fixe et (ii) de la magnitude absolue des plus brillantes étoiles. A leur tour, ces paramètres ont été recensés en fonction de la métallicité et comparés avec les prévisions basées sur les isochrones du modèle Dartmouth. La couleur de la branche des géantes rouges et la luminosité maximale de la bande $K_S$ varient, toutes deux, selon la métallicité d'une façon compatible avec les isochrones du modèle. Les mesures de la pente de la partie supérieure des géantes rouges sont tirées de l'ouvrage d'Ivanov & de Borrisova (2002), et aussi ont un agissement en métallicité semblable à celle des isochrones.

## 1. Introduction

A colour-magnitude diagram (CMD) is one of the most useful tools in stellar astronomy. Such a diagram consists of a plot of absolute magnitude versus colour in some photometric system for an ensemble of stars. Globular clusters of the Milky Way provide systems of $10^4$–$10^6$ stars that fall along well-defined sequences or *branches* in a CMD. Study of the morphologies of these branches and their inter-connections has provided an important basis for deciphering the evolution of low-mass stars.

Much of the work on CMDs of globular clusters has been based on photometry obtained at visible wavelengths. Commencing in the 1970s, the introduction of infrared photometers led to an extension of globular-cluster colour-magnitude studies into the 1.0–2.3 μm wavelength range (Cohen *et al.* 1978; Frogel *et al.* 1979, 1981; Persson *et al.* 1980; Da Costa *et al.* 1981). For example, CMDs of globular clusters based on near-infrared imaging data have been published by Davidge & Simons (1994a,b), Davidge & Harris (1995, 1996, 1997), Davidge & Courteau (1999), and Sarajedini (2004), while systematic studies as a function of cluster metal abundance have been done by Ferraro *et al.* (2000), Ivanov & Borissova (2002), and Valenti *et al.* (2004). Near-infrared colour-magnitude diagrams are of considerable utility in star-cluster studies for a number of reasons. The spectral energy distributions of cluster red giants peak near 1-2 μm, and such stars are brighter at these wavelengths than in visible light. In comparison with visible wavelengths shortward of 0.5 μm, spectra in the wavelength range 1-2.5 μm of the brightest globular cluster stars are less subject to blanketing by atomic absorption lines. Interstellar extinction and reddening are both reduced in the infrared compared to visible wavelengths.

The Two-Micron All-Sky Survey (2MASS) of the northern and southern skies (Cutri *et al.* 2003a; Skrutskie *et al.* 2006) has produced near-infrared magnitudes for red giant stars in many of the globular clusters of the Milky Way. The aim of this article is to illustrate how 2MASS data that are readily accessible via the Internet can be used to study the red-giant region of the CMDs of globular clusters.

## 2. The Two-Micron All-Sky Survey

The Two-Micron All-Sky Survey (2MASS) was carried out between 1997 and 2001 (Skrutskie *et al.* 2006). Near-infrared $J, H,$ and $K_S$ magnitudes were measured for approximately 300 million stars. The $J, H,$ and $K_S$ filter passbands have effective wavelengths of 1.25 μm, 1.65 μm, and 2.16 μm, respectively. These filters define a photometric system similar to that

introduced by Johnson (1962), except that the so-called $K$-short filter, denoted $K_S$, has a long-wavelength limit of 2.31 μm. The 2MASS survey employed two 1.3-metre telescopes. Each telescope was equipped with an infrared camera comprised of three NICMOS3 HgCdTe 256×256 detector arrays having a pixel size of 2.0 arcsec. At a given pointing on the sky, six integrations of 1.3 sec duration each were made for a total exposure time of 7.8 sec. Observations began in the northern hemisphere in June 1997 on Mount Hopkins, Arizona, while southern observations commenced in March 1998 at Cerro Tololo Inter-American Observatory in Chile. Observations officially ended in February 2001.

More information on the Two-Micron All-Sky Survey, as well as a number of data products that have been derived from it, can be found at the Web site www.ipac.caltech.edu/2mass maintained by the Infrared Processing and Analysis Center.

## 3. The Near-Infrared Colour-Magnitude Diagram of a Globular Cluster

One of the best examples of a colour-magnitude diagram based on 2MASS data of a globular cluster is shown in Figure 1. In this diagram, the $K_S$ apparent magnitude is plotted versus $(J - K_S)$ colour for stars having projected angular separations of 5–12 arcmin from the centre of the southern cluster 47 Tucanae (NGC 104). Three stellar sequences are seen in the diagram: the red giant branch (RGB), the red horizontal branch (RHB), and the asymptotic giant branch (AGB). The
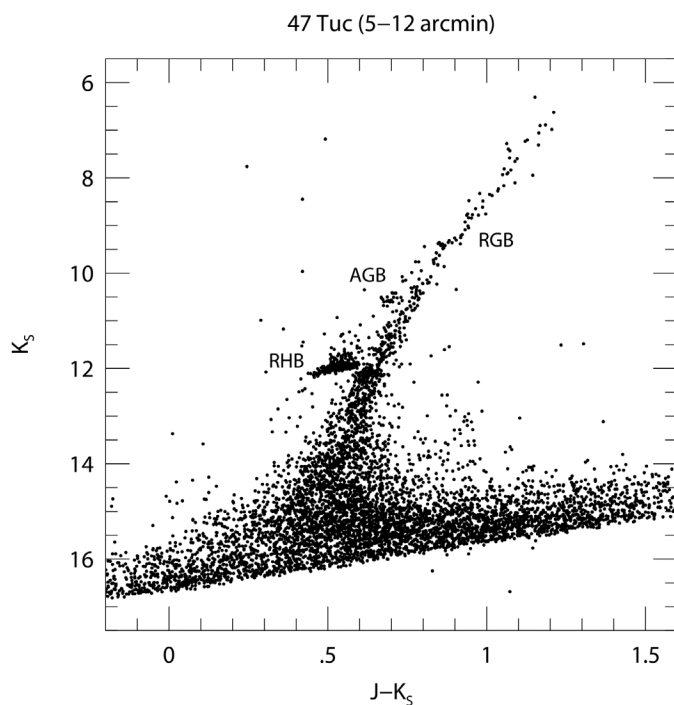


47 Tuc (5–12 arcmin)

*Figure 1 — A $K_S$ versus J - $K_S$ colour-magnitude diagram for stars within 5-12 arcmin of the centre of the cluster 47 Tucanae. The red giant branch (RGB), red horizontal branch (RHB), and asymptotic giant branch (AGB) sequences of stars are labelled.*

red giant branch extends from $K_S \sim 6.5$ to $K_S > 14.0$, and is composed of stars fusing hydrogen to helium in a thin shell outside an inert helium-rich core. The increasing width of the RGB for $K_S > 12.0$ is the result of increasing photometric error, while the greatly increased scatter at $K_S > 15.0$ indicates the sensitivity limit of the photometry. The red horizontal branch is located at $0.4 \leq (J - K_S) \leq 0.6$ within a narrow magnitude range from $K_S \sim 11.5$–12.0. Stars in the RHB phase of evolution are fusing helium in their core. An asymptotic giant branch is populated over the magnitude range $9.5 < K_S < 11.5$, where it is offset to the blue of the red giant branch by 0.05-0.10 mag in $(J - K_S)$ colour. Stars on the AGB have exhausted helium in a now carbon-rich core, and are burning He in a thin shell surrounding that core. It is the upper domain of the RGB that is the focus of this article.

## 4. The Red Giant Branch

There are three basic parameters that determine the colour and absolute magnitude of a star: age, mass, and chemical composition. Elements heavier than helium are collectively referred to as "heavy elements" or "metals" by astronomers. Precision abundance measurements of heavy elements in globular clusters have often focused on the element iron because it presents numerous absorption lines in the spectrum of a red giant star. As a consequence, the iron abundance is often used as a tracer of the overall content of heavy elements in a cluster. This is valid to the extent that the abundances of other heavy elements scale with the iron abundance. The so-called "metallicity" of a star is often referenced to the Sun and defined as the iron-to-hydrogen ratio on a logarithmic scale as given by

$$[Fe/H] = \log_{10} ((N_{Fe} / N_H)star / (N_{Fe} / N_H)_\odot), \qquad (1)$$

where $N_{Fe}$ and $N_H$ are the atoms per cubic centimetre of iron and hydrogen in a stellar atmosphere. Most globular clusters are thought to have ages of around 12–14 billion years, although exceptions are known (Dotter *et al.* 2010, 2011). At the large ages found among globular clusters, the main-sequence turnoff mass is $\sim 0.8\ M_\odot$, and the difference in mass between much of the red giant branch and the main sequence turnoff is relatively small. Hence the similarity in ages among globular clusters translates into a similarity in the masses of their red giants.[1] Metallicity on the other hand can vary within the range $-2.5 \leq [Fe/H] \leq 0.0$ among Milky Way globular clusters. This large range leaves metallicity as a key variable governing RGB morphology among globular clusters.

Metallicity affects the opacity of gas within a red giant star.[2] Opacity in turn plays an important role in setting the size of a red giant by regulating the flux of radiation propagating through the atmosphere, and by controlling the characteristic pressure of the atmosphere (Prialnik 2000). Metallicity also affects the timing of the helium-core-flash event that causes a red giant star to transition to the horizontal branch. The effects

of metallicity upon the morphology of the RGB of a globular cluster can be illustrated by using numerical stellar models. Theoretical isochrones were selected for this purpose from the Dartmouth Stellar Evolution Database (Web site http://stellar.dartmouth.edu) described by Dotter *et al.* (2008). The isochrones are derived from stellar evolutionary tracks computed by the Dartmouth Stellar Evolution Program (Bjork & Chaboyer 2006; Dotter *et al.* 2007). The Dartmouth models are particularly useful in the present context, because theoretical luminosities and effective temperatures have been transformed into absolute magnitudes and colours of the 2MASS photometric system.

Figure 2 shows a plot of stellar luminosity (normalized to the solar luminosity) versus effective temperature for four different stellar isochrones. The models plotted in Figure 2 cover the RGB but not the RHB or AGB phases of stellar evolution.[3] All were chosen to have an age of 12 Ga, a helium mass fraction given by $Y = 0.245 + 1.6Z$, where $Z$ is the heavy-element mass fraction, and a ratio between Fe and α-element abundances of [α/Fe] = +0.2. Advancing from left to right, the isochrones have metallicities of [Fe/H] = −2.2, −1.6, −1.0 and −0.4, respectively. Three characteristics of the upper half of the RGB change as the metallicity is increased: (i) the effective temperature at a fixed luminosity decreases, (ii) the slope of the isochrones at a fixed luminosity decreases, and (iii) the

luminosity at the tip of the red giant branch increases. Such behaviour has been known since the stellar model analyses of Rood (1972) and Sweigart & Gross (1978). Using 2MASS data for a selection of 24 globular clusters, it is possible to verify these expected trends and to compare the observed correlations directly with the Dartmouth models.

## 5. The Data

Data from the 2MASS Point Source Catalog (Cutri *et al.* 2003b) have been used to produce near-infrared CMDs of globular clusters. A sample of clusters was chosen from among the closest and brightest systems included in the *Catalog of Parameters for Milky Way Globular Clusters* compiled and maintained by Harris (1996). The 2003 version of this catalogue was employed. Most clusters were selected on the basis of distance from the Sun (to ensure bright RGBs) and the integrated visual magnitude (to ensure a large sample of stars per cluster). Several additional clusters of interest were chosen, specifically those with relatively high metallicities. A list of the selected clusters, with the metallicity [Fe/H] from Harris (1996; 2003 version), can be found in Table 1, along with the absolute integrated visual magnitude $M_{V,t}$ (the brighter, *i.e.* the more negative this magnitude, the greater the number of stars in a cluster).

The VizieR astronomical catalogue server (Ochsenbein *et al.* 2000) developed by the Strasbourg Astronomical Observatory[4] was used to download $J$ and $K_S$ magnitudes for all stars included in the 2MASS database within the field of each cluster. Most stellar-magnitude measurements catalogued by 2MASS have an associated error. Near the centre of a cluster, the photometric errors can be significant due to the crowding of stellar images. A first step in producing a relatively clean CMD for a particular object was to set a *minimum* separation from the cluster centre for the stars to be considered. This step was accomplished through inspection of plots of the error in $K_S$ magnitude versus projected distance $r$ from the cluster centre. Reducing the presence of non-cluster stars in a CMD was done by setting a *maximum* radius to each search. Colour-magnitude diagrams for each cluster were constructed for several different outer radii, and a judgement was made of a radius that produced a relatively clean but well-populated red giant branch. The preferred outer radius differed among clusters, and was most problematic for objects along lines of sight toward the galactic bulge. The adopted radial range considered for each cluster is listed in column 2 of Table 2.



*Figure 2 — Theoretical Dartmouth isochrones for red giant branches of age 12 Ga are shown in the luminosity versus effective-temperature plane. Model luminosities are normalized to that of the Sun. Metallicities of the isochrones running from left to right are [Fe/H] = -2.2, -1.6, -1.0, -0.4. The RGB locus corresponds to that portion of each curve brighter than log(L/L☉) ~1.0. That part of each isochrone for log(L/L☉)<0.0. is known as the main sequence; it is populated not by red giants but by stars like the Sun that are fusing hydrogen into helium in a central core.*

Eight CMDs derived from the 2MASS data are shown in Figures 3 and 4. The apparent $K_S$ magnitude is plotted against $(J − K_S)$ colour, no corrections having being made for interstellar absorption or distance modulus. Clusters represented in Figure 3 (NGC 6397, M10, M4, and M71) are among the closest of those listed in Table 1. Figure 4 contains CMDs for the more distant systems M92, M13, M95 and

| NGC | Other Name | $d_{kpc}$ (kpc) | $D_M$ mag | $M_{V,t}$ mag | E (B − V) mag | E (J − $K_S$) mag | A($K_S$) mag | [Fe/H] |
|---|---|---|---|---|---|---|---|---|
| 104 | 47 Tuc | 4.5 | 13.27 | −9.42 | 0.04 | 0.02 | 0.01 | −0.76 |
| 288 | — | 8.8 | 14.72 | −6.74 | 0.03 | 0.01 | 0.01 | −1.24 |
| 362 | — | 8.5 | 14.65 | −8.41 | 0.05 | 0.02 | 0.02 | −1.16 |
| 1851 | — | 12.1 | 15.41 | −8.33 | 0.02 | 0.01 | 0.01 | −1.22 |
| 2808 | — | 9.6 | 14.91 | −9.39 | 0.22 | 0.11 | 0.08 | −1.15 |
| 3201 | — | 5.0 | 13.49 | −7.46 | 0.32 | 0.16 | 0.12 | −1.58 |
| 5139 | ω Cen | 5.3 | 13.62 | −10.29 | 0.12 | 0.06 | 0.04 | −1.62 |
| 5272 | M3 | 10.4 | 15.09 | −8.93 | 0.01 | 0.00 | 0.00 | −1.57 |
| 5904 | M5 | 7.5 | 14.38 | −8.81 | 0.03 | 0.01 | 0.01 | −1.27 |
| 5927 | — | 7.6 | 14.40 | −7.80 | 0.45 | 0.22 | 0.16 | −0.37 |
| 6121 | M4 | 2.2 | 11.71 | −7.20 | 0.36 | 0.18 | 0.13 | −1.20 |
| 6171 | M107 | 6.4 | 14.03 | −7.13 | 0.33 | 0.16 | 0.12 | −1.04 |
| 6205 | M13 | 7.7 | 14.43 | −8.70 | 0.02 | 0.01 | 0.01 | −1.54 |
| 6218 | M12 | 4.9 | 13.45 | −7.32 | 0.19 | 0.09 | 0.07 | −1.48 |
| 6254 | M10 | 4.4 | 13.22 | −7.48 | 0.28 | 0.14 | 0.10 | −1.52 |
| 6341 | M92 | 8.2 | 14.57 | −8.20 | 0.02 | 0.01 | 0.01 | −2.28 |
| 6352 | — | 5.7 | 13.78 | −6.48 | 0.21 | 0.10 | 0.08 | −0.70 |
| 6397 | — | 2.3 | 11.81 | −6.63 | 0.18 | 0.09 | 0.07 | −1.95 |
| 6656 | M22 | 3.2 | 12.53 | −8.50 | 0.34 | 0.17 | 0.12 | −1.64 |
| 6752 | — | 4.0 | 13.01 | −7.73 | 0.04 | 0.02 | 0.01 | −1.56 |
| 6809 | M55 | 5.3 | 13.62 | −7.55 | 0.08 | 0.04 | 0.03 | −1.81 |
| 6838 | M71 | 4.0 | 13.01 | −5.60 | 0.25 | 0.12 | 0.09 | −0.73 |
| 7078 | M15 | 10.3 | 15.06 | −9.17 | 0.10 | 0.05 | 0.04 | −2.26 |
| 7099 | M30 | 8.0 | 14.52 | −7.43 | 0.03 | 0.01 | 0.01 | −2.12 |

Table 1 — Globular Cluster Properties

| Cluster NGC | r arcmin | (J − $K_S$)₄ eye | $M_{Ks}$ (tip) | (J − $K_S$)₄ IB02 | $M_{Ks}$ (tip) IB02 |
|---|---|---|---|---|---|
| (1) | (2) | (3) | (4) | (5) | (6) |
| 104 | 5–12 | 0.88 | −6.55 | 0.87 | −6.86 |
| 288 | 1–7 | 0.79 | −6.20 | 0.76 | −6.67 |
| 362 | 1–6 | 0.75 | −5.95 | — | — |
| 1851 | 1–6 | 0.80 | −6.30 | 0.79 | −6.31 |
| 2808 | 1.5–8 | 0.80 | −6.05 | — | — |
| 3201 | 1–8 | 0.68 | — | — | — |
| 5139 | 5–6.5 | 0.71 | −5.90 | 0.68 | −6.02 |
| 5272 | 2–10 | 0.73 | −5.95 | — | — |
| 5904 | 2–8 | 0.75 | −5.95 | — | — |
| 5927 | 1–5 | 0.86 | −6.55 | — | — |
| 6121 | 2–10 | 0.85 | −6.15 | 0.74 | — |
| 6171 | 2–8 | 0.83 | −5.70 | 0.71 | −6.47 |
| 6205 | 2–10 | 0.70 | −6.00 | 0.70 | −6.03 |
| 6218 | 1–8 | 0.80 | −6.10 | — | — |
| 6254 | 2–8 | 0.75 | −5.55 | — | — |
| 6341 | 2–7 | 0.65 | −5.70 | — | — |
| 6352 | 0–4 | 0.92 | −6.75 | — | — |
| 6397 | 1.5–8 | 0.68 | −5.65 | — | — |
| 6656 | 1–8 | 0.71 | −5.95 | — | −5.98 |
| 6752 | 2–10 | 0.74 | — | — | — |
| 6809 | 2–10 | 0.71 | −5.30 | 0.70 | −5.87 |
| 6838 | 0–4 | 0.81 | −6.65 | 0.75 | — |
| 7078 | 1–8 | 0.65 | −5.50 | — | −5.63 |
| 7099 | 2–10 | 0.66 | −5.70 | 0.65 | −5.83 |

Table 2 — Parameters of the Red Giant Branch.

NGC 5927, the first three of which are among the best known globular clusters in the northern sky. The panels are arranged such that the most metal-poor cluster in each figure is in the top left panel, whereas the most metal-rich is in the bottom-right panel. Each panel in Figures 3-4 is labelled with not only the cluster name, but also the range in projected distance from each cluster centre covered by the plotted stars (which is as listed in Table 2).

The apparent magnitude and colour data for the stars within a chosen cluster annulus were transformed to absolute magnitude and intrinsic colour by correcting for distance modulus, interstellar extinction, and reddening. Values for the $E(B − V)$ reddening of each cluster were obtained from the catalogue of Harris (1996; 2003 version) and converted to the equivalent for the 2MASS $E (J − K_S)$ colour. Based on reddening ratios quoted in the literature (*e.g.* Valenti *et al.* 2004) the following
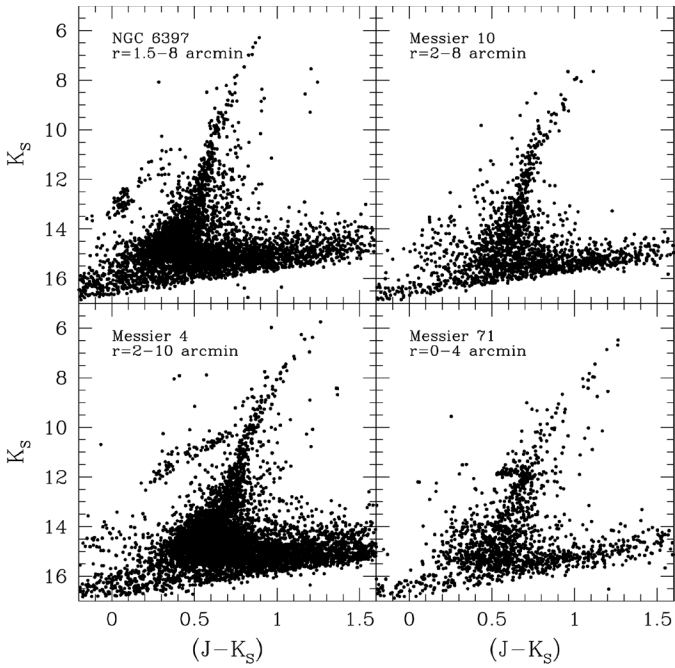
*Figure 3 — Infrared colour-magnitude diagrams from 2MASS data for the globular clusters NGC 6397, M10, M4, and M71. The panels are ordered such that metallicity increases from the top left to the bottom right. The projected distance from cluster centre covered by a CMD is given in each panel (as well as listed in Table 2).*



*Figure 4 — Colour-magnitude diagrams from 2MASS data for the globular clusters M92, M13, M5, and NGC 5927. Cluster metallicity increases from top left to bottom right. The projected distance from cluster centre covered by a CMD is noted in each panel (and listed in Table 2). The four clusters represented in this figure are at greater distances from the Sun than the clusters of Figure 3.*

correction was applied to get the reddening in $(J-K_S)$:

$$E(J-K_S) = 0.49E(B-V). \qquad (2)$$

The extinction in $K_S$ was obtained in a similar fashion:

$$A(K_S) = 0.366E(B-V). \qquad (3)$$

The adopted values of $E(B-V)$, $E(J-K_S)$, and $A(K_S)$ for the program clusters are given in Table 1. Also listed is the distance from the Sun $d_{kpc}$ in units of kiloparsecs, again from the Harris (1996; 2003 version) catalogue, and the equivalent distance modulus $D_M = 5\log_{10}(10^3 d_{kpc}) - 5$. These parameters were used to produce colour-magnitude diagrams in which the absolute magnitude $M_{K_S} = K_S - D_M - A(K_S)$ of cluster stars was plotted versus their intrinsic colour $(J-K_S)_0 = (J-K_S) - E(J-K_S)$. Several characteristics of the RGB were derived from such colour-magnitude diagrams.

## 5.1. A Fiducial Colour for the Red Giant Branch

The $(J-K_S)_0$ colour of the RGB at a fiducial magnitude of $M_{K_S} = -4.0$ was determined by eye from plots of each colour-magnitude diagram. We denote this colour as $(J-K_S)_4$ and values for all 24 clusters in the sample are collected in column 3 of Table 2. This fiducial colour is plotted versus cluster metallicity [Fe/H] in Figure 5. Filled circles depict measurements for clusters with absolute magnitudes of $M_{V,t} < -7.5$,

*i.e.* the higher-mass clusters in the plot, whereas open circles denote lower-mass systems with $M_{V,t} > -7.5$. The most massive cluster in the galaxy is ω Centauri, which is shown as a filled triangle.

A second technique was also employed to derive a value of $(J-K_S)_4$ from a colour-magnitude diagram. The locus of the RGB was approximated by a linear least-squares fit, and the value of this fit was computed at $M_{K_S} = -4.0$ for 22 of the 24 clusters in Table 1. The upper RGB is not expected to be precisely linear, as the isochrones in Figure 2 and the plots in Figures 3 and 4 indicate. Therefore the linear fits were generally limited to stars within ±1 mag of $M_{K_S} = -4.0$ (or ±2 mag in some cases). The difference $\delta(J-K_S)_4$ between the eye-estimated value and the linear-fit value of $(J-K_S)_4$ was calculated for each cluster. The distribution of $\delta(J-K_S)_4$ values has a mean of −0.005 mag and a standard deviation of 0.016 mag. This comparison suggests that the random error in the $(J-K_S)_4$ determinations is on the order of 0.02 mag.

## 5.2. Determining the Brightest Stars of Each Red Giant Branch

An estimate of the absolute magnitude $M_{K_S}$ (tip) of the tip of the red giant branch was obtained by adopting the absolute magnitude of the star that was judged to be the brightest red giant in the CMD of each cluster. This magnitude is listed in column 4 of Table 2. It has been rounded off to the nearest

0.05 mag because our method of obtaining $M_{K_s}$(tip) can be uncertain when the upper region of a RGB is lightly populated or exhibits fluctuations in the magnitude distribution of the red giants.[5] Such effects can make the true tip of the RGB hard to locate. This was the case for NGC 3201 and NGC 6752, for which no value of $M_{K_s}$(tip) is given in Table 2. In our CMD of NGC 3201, there is a spread in colour among the brightest giants, with one star located near the extrapolated locus of the RGB at a much brighter magnitude than the second brightest star. In NGC 6752 there may be a sparsely populated extension to the RGB reaching to an absolute magnitude of $M_{K_s}$~ −6.9, which is significantly brighter than the theoretically expected tip of the giant branch. Regarding the clusters NGC 288, M4, M10, NGC 6352, and M30, the value of $M_{K_s}$(tip) is made somewhat uncertain by the fact that there are only five or fewer RGB stars within 1 mag of the expected tip of the red giant branch.

A plot of the tip magnitude versus [Fe/H] is shown in Figure 6. The brightest magnitude theoretically attainable by a cluster giant for a given [Fe/H] and age can be read from the isochrone tables for the same sets of age and composition specified in Section 4. These model values are also shown in Figure 6. The symbols used in Figure 6 are coded on the basis of cluster integrated magnitude, with filled and open symbols



Figure 6 — The absolute magnitude of the tip of the red giant branch in the $K_S$ bandpass (from column 4 of Table 2) versus cluster metallicity. The solid line shows the calculated RGB-tip magnitudes from the Dartmouth 12-Ga isochrones. Clusters with integrated magnitudes of $M_{V,t}$ < -7.50 are shown as filled symbols, while fainter clusters are depicted with open symbols. In addition, ω Cen, M10, M55, and M107 are depicted with a filled triangle, open triangle, filled box, and open box, respectively.

corresponding to objects for which $M_{V,t}$ is brighter or fainter than −7.5 respectively.

## 5.3. Data from Ivanov & Borissova (2002)

The behaviour of the RGBs of 27 globular clusters was previously studied by Ivanov & Borissova (2002; IB02 in Table 2) through the use of 2MASS data. They explored the metallicity dependence of the morphology of the RGB for a somewhat different sample of clusters, although they did not compare their results with isochrones. Values of $M_{K_s}$(tip) were derived by them for ten of the clusters in Table 1, and these values are listed in column 6 of Table 2. Furthermore, Ivanov & Borissova made linear least-squares fits to the locus of the RGB in the $(K_S, J–K_S)$ diagram of 22 clusters. The coefficients of their fits allow values of $(J – K_S)_4$ to be calculated for ten of the clusters in Table 2, and these values are listed in column 5. Ivanov & Borissova employed stars above the level of the horizontal branch in deriving their RGB fits. Consequently, many of those clusters that were incorporated into the present sample, but not that of Ivanov & Borissova (2002), appear to be systems in which the HB is not well defined in the 2MASS colour-magnitude diagrams.



Figure 5 — The $(J–K_S)_0$ colour of the red giant branch at an absolute magnitude of $M_{K_S}$ = -4.0 (column 3 of Table 2) versus cluster metallicity. Closed symbols refer to clusters with integrated visual magnitudes $M_{V,t}$ > -7.50, i.e., the intrinsically brightest clusters in the sample, while open symbols are for the fainter clusters with $M_{V,t}$ > -7.50. The filled triangle depicts the cluster ω Centauri. A solid line shows the least-squares fit given by equation (4), while a dashed line corresponds to the predictions of the Dartmouth 12-Ga isochrones.

# 6. Results

## 6.1. The Colour of the Red Giant Branch

In Figure 5, the $(J-K_S)_4$ colour of the RGB is plotted as a function of metallicity [Fe/H]. There is an almost linear relationship. The solid line in the figure shows a linear least-squares fit to the plotted data, which is given by the equation:
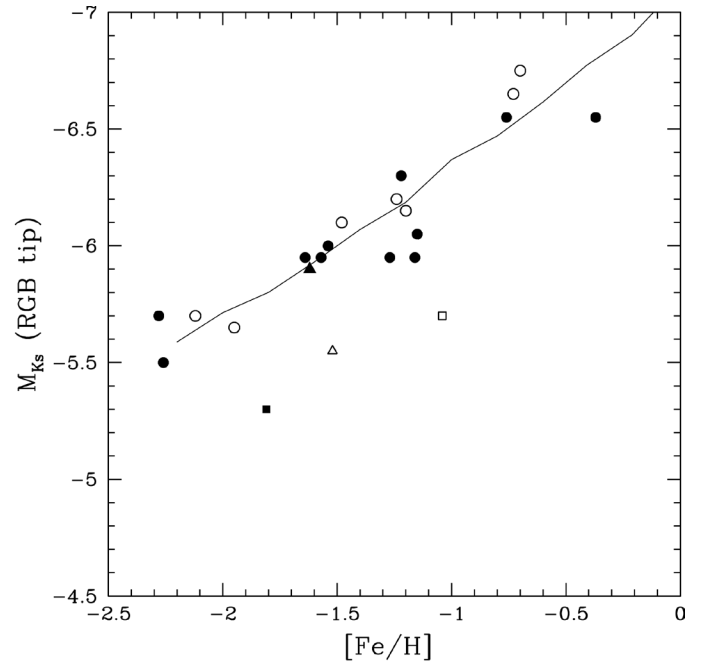
$$(J-K_S)_4 = 0.954 + 0.139[\text{Fe/H}], \qquad (4)$$

with the standard deviation in the slope of this line being 0.014. The root-mean-square deviation in $(J-K_S)_4$ about this fit is 0.032 mag, which is comparable to the random errors in $(J-K_S)_4$ ascertained in Section 5.1. Open circles in Figure 5 exhibit a greater dispersion about equation (4) than the filled symbols, suggesting that the eye-estimated values of $(J-K_S)_4$ are more uncertain for the lower-mass clusters. A dashed line shows the predictions of the 12-Ga Dartmouth models plotted in Figure 2. The models and equation (4) agree to within 0.02 mag in $(J-K_S)_4$ colour.

The cluster ω Centauri is worth noting. It is not only the most massive globular cluster in the Milky Way, but has a large internal metallicity dispersion (*e.g.* Johnson & Pilachowski *et al.* 2010 and references therein), that leads to an intrinsically broad red giant branch. Nonetheless, the eye estimated value of $(J-K_S)_4$ agrees well with both equation (4) and the isochrone locus in Figure 5.

Generally, the values of $(J-K_S)_4$ derived in the present work agree to within ~0.03 mag of those found by Ivanov & Borissova (2002), with three notable exceptions: M4, M71, and M107. The colour-magnitude diagram of M4 exhibits a well-populated AGB that parallels the RGB by ~0.09 mag in the $(J-K_S)$ colour. Inclusion of AGB stars could lead to an anomalous value of $(J-K_S)_4$. The colour found in our work falls redward of equation (4) by 0.05–0.08 mag, while the value of Ivanov & Borissova is a closer match to the isochrone prediction. In the case of M107, the value of $(J-K_S)_4$ found here is a notably better match to both equation (4) and the isochrone predictions, with the value of Ivanov & Borissova being too blue. The $(J-K_S)_4$ colour derived here for M71 agrees more closely with the isochrone locus in Figure 5, although both the present and Ivanov & Borissova values are bluer than the isochrone colour and the linear fit given by equation (4).

## 6.2. The Tip of the Red Giant Branch

Figure 6 shows the relationship between the absolute magnitude of the tip of the red giant branch (from column 4 of Table 2) and cluster metallicity. On average, the tip becomes brighter in the $K_S$ band with increasing metallicity. The solid line in Figure 6 shows the prediction from the Dartmouth isochrones, which provides a reasonable upper envelope to the
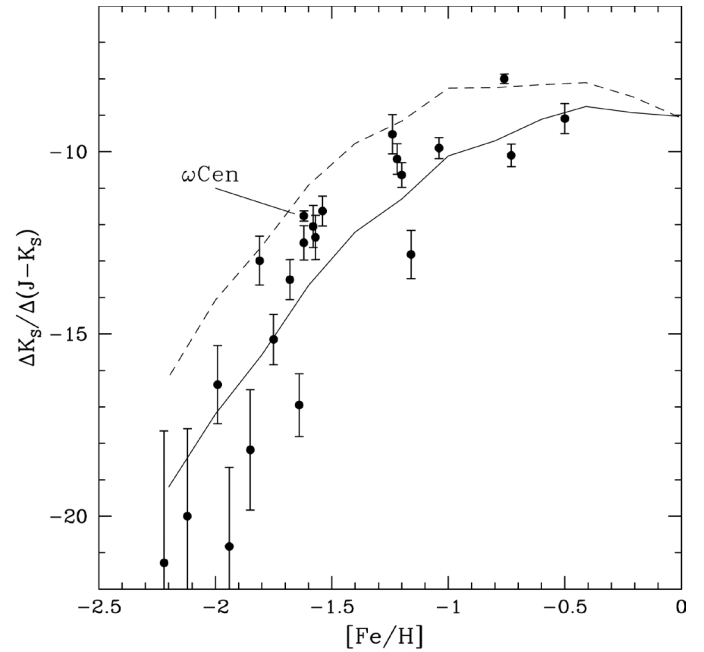


*Figure 7 — The slope of the red giant branch $\Delta K_S/\Delta(J\text{-}K_S)$ based on the data of Ivanov & Borissova (2002) versus cluster metallicity. Two parameters derived from Dartmouth 12-Ga isochrones are plotted, $\Delta_{-4.0}^{-5.0}$, and $\Delta_{-3.0}^{-4.0}$, as the dashed and solid lines respectively.*

data points. The fact that some RGB tips appear to be fainter than the model predictions may be brought about by sampling limitations if the upper part of the branch is not well populated with stars. In cases where the observed tip lies above the theoretical curve in Figure 6, the star that was identified as the tip of the RGB could actually be an AGB star (such stars can theoretically attain higher luminosities than RGB stars) or a field star, or else this could be a consequence of photometric errors in the 2MASS magnitudes. In addition, some of the brighter giants may be long-period variables, particularly in clusters of higher metallicity such as 47 Tuc (Frogel & Elias 1988), and such stars could contribute to scatter both above and below the theoretical curve in Figure 6. Errors in cluster distance modulus could also lead to scatter.

Two of the most discrepant points in Figure 6 correspond to M55 (filled square) and M107 (open square), and are both based on samples that excluded stars within 2 arcmin of the cluster centre. By contrast, Ivanov & Borissova (2002) found much brighter values of $M_{K_S}$(tip) for these two objects by using 2MASS CMDs that included the cluster central regions. Consequently, a second set of diagrams was produced for M55 and M107 that extended to the cluster centre. In the case of M107, the CMD within 0-8 arcmin of the cluster centre was found to exhibit stars up to a magnitude of $K_S \approx 7.65$, *i.e.*, $M_{K_S}$ (tip) ~ −6.5, which is in excellent agreement with both the value found by Ivanov & Borissova (2002) and the prediction of the Dartmouth isochrones. Similarly, for M55 there are four red giants within 2 arcmin of the projected cluster centre that are notably brighter than giants in the 2-10 arcmin sample.

The tip of the RGB in the central regions was concluded to be $M_{Ks}(\text{tip}) \approx -5.85$ to $-5.45$. The brighter estimate is very close to the result of Ivanov & Borissova (2002) and the Dartmouth isochrones. These examples illustrate how estimates of $M_{Ks}(\text{tip})$ can be subject to sampling statistics, and suggest that the very brightest red giants may be located in the innermost regions of some clusters.[6] The cluster M10 (open triangle) also sits notably below the theoretical curve in Figure 6, which may again be a sampling effect given that it falls in the lower half of the mass range of the clusters plotted.

### 6.3. The Slope of the Red Giant Branch

The linear fits made by Ivanov & Borissova (2002) to the locus of the RGB in the 2MASS $(K_S, J-K_S)$ diagram yield systematic measurements of the slope of that branch. The values of $\alpha = d(J-K_S)/dK_S$ for 22 clusters from Ivanov & Borissova (2002) have been converted to a slope $\Delta K_S/\Delta(J-K_S)$, which is plotted versus cluster metallicity in Figure 7. Error bars in the figure are based on the errors in $\alpha$ quoted by Ivanov & Borissova. The metallicity [Fe/H] is again taken from the Harris (1996; version 2003) catalogue. In order to compare with numerical models, the Dartmouth isochrones were used to calculate a parameter defined as

$$\Delta_l^u = \frac{M_{Ks,u} - M_{Ks,l}}{(J-K_S)u - (J-K_S)_l} ,\qquad (5)$$

where $u$ and $l$ denote two fiducial points on an isochrone for which the absolute magnitudes are $M_{Ks,u}$ and $M_{Ks,l}$ and the colours are $(J-K_S)_u$ and $(J-K_S)_l$ respectively. The behaviour of this parameter is shown as a function of [Fe/H] in Figure 7, with the dashed and solid lines corresponding to $(u,l) = (-5.0, -4.0)$ and $(-4.0, -3.0)$ respectively. The more negative the value of this parameter, the steeper is the RGB over the specified magnitude range. Except at near-solar metallicities, the giant branch is characterized by $\Delta_{-3.0}^{-4.0} < \Delta_{-4.0}^{-5.0}$, which means that it becomes steeper at fainter magnitudes. The models show qualitatively the same trend as the observations[7] in that the RGB is steeper at lower metallicities, particularly for [Fe/H] ≤ −1.0. Theoretically this trend is much more subdued at higher metallicities, however there are few clusters having [Fe/H] ≤ −1.0 in the Ivanov & Borissova (2002) sample with which to test the isochrones.

## 7. Conclusions

In summary, red giant branches of globular clusters derived from 2MASS photometry show three morphological trends with metallicity:

(i)  The $(J-K_S)$ colour of the RGB at a reference magnitude of $M_{Ks} = -4.0$ correlates linearly with [Fe/H].

(ii) The absolute magnitude $M_{Ks}$ of the tip of the RGB becomes brighter with increasing metallicity.

(iii) The slope of the RGB becomes steeper with decreasing metallicity, although at [Fe/H] > −0.5 this correlation is quite weak.

All three trends are well matched by the Dartmouth stellar models. Such correlations provide photometric tools that can be used to derive values of [Fe/H] for globular clusters.

Various combinations of the above observational trends have previously been documented from non-2MASS infrared-imaging data by Ferraro *et al.* (2000) and Valenti *et al.* (2004). The demonstration of the first two trends via infrared photometry harkens back to the pioneering work of Frogel *et al.* (1983a, 1983b), who measured *(J, H, K)* magnitudes of red giants in globular clusters through the use of single-channel photometers. 2MASS has now made analogous investigations possible without going to a telescope. Furthermore, whereas near-infrared cameras are not commonplace in amateur astronomy, 2MASS makes a virtual infrared observatory available to both professional and amateur astronomers alike.

The current work is but a sampling of what 2MASS can contribute to the investigation of globular clusters. The study presented here could be extended and refined in a number of ways. We conclude by presenting some suggestions for further work.

(i)  For clusters in which proper motions of individual stars have been measured, such as ω Cen (van Leeuwen *et al.* 2000), field stars could be identified in the colour-magnitude diagrams. The present method of restricting the radius from cluster centre of stars in a CMD is an imperfect approach to minimizing the inclusion of field stars.

(ii) Since 2MASS is an all-sky survey, the number of clusters for which CMDs can be derived is much greater than in the sample chosen for this paper. For example, clusters at low galactic latitude or in regions of higher interstellar extinction could be investigated.

(iii) Because 2MASS imaged entire clusters, it could be possible to investigate how stars in different regions of the CMD are distributed spatially within a cluster. This could allow a systematic study of an issue noted in Section 6.2, namely whether in some clusters the brightest red giants have different radial distributions than stars lower down the giant branch.

## 8. Acknowledgments

## References

Bjork, S.R. & Chaboyer, B. (2006). Theoretical Uncertainties in Red Giant Branch Evolution: The Red Giant Branch Bump. *ApJ, 641*, 1102.

Cohen, J.G., Persson, S.E., & Frogel, J.A. (1978). Infrared Photometry, Bolometric Magnitudes, and Effective Temperatures for Giants in M3, M13, M92 and M67, 1978. *ApJ, 222*, 165.

Cordoni, J.-P., & Auriere, M. (1984). Magnitudes and colours for stars in the central part of the globular cluster NGC 7099 (M30). *A&AS, 58*, 559.

Cutri, R.M., *et al.* (2003a). *Explanatory Supplement to the 2MASS All Sky Data Release*, Pasadena: IPAC www.ipac.caltech.edu/2mass/releases/allsky/doc/explsup.html.

Cutri, R.M., et al. (2003b). *2MASS All-Sky Point Source Catalog*, VizieR On-line Data Catalog: II/246.

Da Costa, G.S., Frogel, J.A., & Cohen, J.G. (1981). The giant branch of the globular cluster NGC 3201. *ApJ, 248*, 612.

Davidge, T.J. & Simons, D.A. (1994a). Deep infrared array photometry of globular clusters. I. M4. *ApJ, 423*, 640.

Davidge, T.J. & Simons, D.A. (1994b). Deep infrared array photometry of globular clusters. II. M71. *ApJ, 435*, 207.

Davidge, T.J. & Harris, W.E. (1995). Deep infrared array photometry of globular clusters. III. M13. *ApJ, 445*, 211.

Davidge, T.J. & Harris, W.E. (1996). Deep infrared array photometry of globular clusters. IV. M22 (NGC 6656). *ApJ, 462*, 255.

Davidge, T.J. & Harris, W.E. (1997). Deep infrared array photometry of globular clusters. VI. NGC 288. *ApJ, 475*, 584.

Davidge, T.J. & Courteau, S. (1999). High angular resolution JHK imaging of the centres of the metal-poor globular clusters NGC 5272 (M3), NGC 6205 (M13), NGC 6287, and NGC 6341 (M92). *AJ, 117*, 1297.

Dotter, A., Chaboyer, B., Jevremović, D., Baron, E., Ferguson, J.W., Sarajedini, A., & Anderson, J. (2007). The ACS Survey of Galactic Globular Clusters. II. Stellar Evolution Tracks, Isochrones, Luminosity Functions, and Synthetic Horizontal-Branch Models. *AJ, 134*, 376.

Dotter, A., Chaboyer, B., Jevremović, D., Kostov, V., Baron, E., & Ferguson, J.W. (2008). The Dartmouth Stellar Evolution Database. *ApJS, 178*, 89.

Dotter, A., *et al.* (2010). The ACS Survey of Galactic Globular Clusters. IX. Horizontal Branch Morphology and the Second Parameter Phenomenon. *ApJ, 708*, 698.

Dotter, A., Sarajedini, A., & Anderson, J. (2011). Globular Clusters in the Outer Galactic Halo: New Hubble Space Telescope/Advanced Camera for Surveys Imaging of Six Globular Clusters and the Galactic Globular Cluster Age-metallicity Relation. *ApJ, 738*, 74.

Ferraro, F.R., Montegriffo, P., Livia, O., & Fusi Pecci, F. (2000). A New Infrared Array Photometric Survey of Galactic Globular Clusters: A Detailed Study of the Red Giant Branch Sequence as a Step toward the Global Testing of Stellar Models. *AJ, 119*, 1282.

Frogel, J.A., Cohen, J.G., & Persson, S.E. (1983a). Globular cluster giant branches and the metallicity scale. *ApJ, 275*, 773.

Frogel, J.A. & Elias, J.H. (1988). Red variables in globular clusters - Their classification and evidence for mass loss. *ApJ, 324*, 823.

Frogel, J.A., Persson, S.E., & Cohen, J.G. (1979). Infrared colors, CO band strengths, and physical parameters for giants in M71. *ApJ, 227*, 499.

Frogel, J.A., Persson, S.E., & Cohen, J.G. (1981). Infrared photometry of red giants in the globular cluster 47 Tucanae. *ApJ, 246*, 842.

Frogel, J.A., Persson, S.E., & Cohen, J.G. (1983b). Infrared photometry, bolometric luminosities, and effective temperatures for giant stars in 26 globular clusters. *ApJS, 53*, 713.

Guhathakurta, P., Webster, Z.T., Yanny, B., Schneider, D.P., & Bahcall, J.N. (1998). Globular Cluster Photometry with the Hubble Space Telescope. VII. Color Gradients and Blue Stragglers in the Central Region of M30 from Wide Field Planetary Camera 2 Observations. *AJ, 116*, 1757.

Harris, W.E. (1996). A Catalog of Parameters for Globular Clusters in the Milky Way. *AJ, 112*, 1487.

Ivanov, V.D. & Borissova, J. (2002). Red giant branch stars as probes of stellar populations. I. 2MASS calibration and application to 2MASS GC01. *A&A, 390*, 937 (IB02).

Johnson, C.I. & Pilachowski, C.A. (2010). Chemical Abundances for 855 Giants in the Globular Cluster Omega Centauri (NGC 5139). *ApJ, 722*, 1373.

Johnson, H.L. (1962). Infrared stellar photometry. *ApJ, 135*, 69.

Ochsenbein, F., Bauer, P., & Marcout, J. (2000). The VizieR database of astronomical catalogues. *A&AS, 143*, 23.

Persson, S.E., Cohen, J.G., Matthews, K., Frogel, J.A., & Aaronson, M. (1980). The spread in CO absorption and effective temperature among the giants in omega Centauri. *ApJ, 235*, 452.

Prialnik, D. (2000). *An Introduction to the Theory of Stellar Structure and Evolution.* Cambridge University Press: New York.

Rood, R.T. (1972). Metal-Poor Stars. V. Horizontal-Branch Morphology. *ApJ, 177*, 681.

Sarajedini, A. (2004). The 2MASS Color-Magnitude Diagram of the Globular Cluster Lyngå 7. *AJ, 128*, 1228.

Skrutskie, M.F., *et al.* (2006). The Two Micron All Sky Survey (2MASS). *AJ, 131*, 1163.

Sweigart, A.V. & Gross, P.G. (1978). Evolutionary sequences for red giant stars. *ApJS, 36*, 405.

Valenti, E., Ferraro, F.R., & Origlia, L. (2004). Red giant branch in near-infrared colour-magnitude diagrams - I. Calibration of photometric indices. *MNRAS, 351*, 1204.

van Leeuwen, F., Le Poole, R.S., Reijns, R.A., Freeman, K.C., & de Zeeuw, P.T. (2000). A proper motion study of the globular cluster ω Centauri. *A&A, 360*, 472.

## Endnotes

1 Mass loss from the more luminous red giants may reduce their total masses by ~0.1 $M_\odot$ during the RGB phase of evolution.

2 In particular, iron is one of the key suppliers of electrons for the formation of $H^-$ ions that govern the continuous opacity in the outer regions of red giants.

3 Models of RHB and AGB stars are subject to a greater range of stellar input parameters than RGB models. The morphology of the RHB in particular is sensitive to the occurrence of mass loss during the preceding red giant phase of evolution.

4 The VizieR Catalogue Service was accessed via the Web site http://vizier.u-strasbg.fr.

5 At the tip of the RGB of the cluster 47 Tuc, the formal uncertainty in $K_S$ magnitudes as given in the 2MASS data set is ~ 0.025 mag. Thus 0.05 mag corresponds to a 2σ uncertainty in the $K_S$ photometry of the brightest cluster stars.

6 In other clusters, such as NGC 7099, the opposite may be the case, *e.g.* Cordoni & Auriere (1984) and Guhathakurta *et al.* (1998).

7 An exact match between models and data points would not be expected, since the observed slopes were derived by Ivanov & Borissova (2002) over a larger magnitude range than the model parameters.

# Observation of the October 2011 Orionid Meteor Shower by FM Radio

*by David Cleary, Edmonton Centre*
*(davecleary@shaw.ca)*

## Abstract

The Sky Scan Science Outreach Program uses FM-Radio Meteor Detectors for teaching astronomy in the Alberta Grade 9 school curriculum in Edmonton. The technique makes use of the basic forward-scatter method for observing over-the-horizon FM radio signals bounced off ionized meteor trails. This article reviews the equipment and method used for observing the Orionid meteor shower in October 2011, the results of the observations, and possible future development of this detector as an educational tool.

## Introduction

In the early part of the last decade, our Sky Scan educational project developed an FM-radio meteor detector. Last fall, I began testing a new antenna and refining the observing techniques using the sound-capture capabilities of Jim Sky`s *Radio–SkyPipe* (*RSP*) program. The goal was to expand our educational tools. For the 2011/12 school year, Sky Scan worked with 42 Edmonton-area schools to assist teachers with the astronomy portions of their curriculum in Grades 6 and 9. Nine schools at the Grade 9 level signed up to use the FM-radio meteor detector described in this article. I observed the Orionid meteor shower in order to test the new antenna and develop a guide for teachers that would allow them to use the more advanced features of *Radio–SkyPipe* for counting meteors and recording sound files.

## Observatory

Some characteristics of our observatory are listed in Table 1. When we originally decided to use FM radios to detect meteors, we tried a number of options including inexpensive analogue and digitally tuned radios, neither of which worked. Digital stereo receivers used in home entertainment systems were suitable but expensive. As we experimented with different radios, we developed a list of required characteristics. (Table 1)

Digitally tuned, used, car radios turned out to be excellent for the job because they are able to reject broadcast signals that spill into the inter-station bandwidth (narrow band pass), able to reject interference caused by the car engine, sensitive to radio signals and able to pick up distant stations while travelling, inexpensive to acquire when sourced from auto wrecking yards, and digitally tuned, as are most car radios manufactured in the last couple of decades.

| | |
|---|---|
| Radio | Chrysler radio model 4469088 |
| Antenna | Winegard HD6000 PROSTAR 1000 FM Antenna (HD-6000) |
| Azimuth | 180° |
| Altitude | 30° |
| Software | *Radio-SkyPipe v2.1.9* |
| Location | Edmonton, Alberta, Canada (population: 750,000) Latitude 53° 29′ 29″ N, Longitude 113° 39′ 06″ W |
| Environment | suburban |

*Table 1 — Observatory characteristics*

With a few modifications, they can easily be used for detecting meteors. I recently bought eight radios taken from Chrysler K-cars and Intrepids (1980s to '90s) for $15 Cdn apiece. Other brands may work as well. The modifications we made are shown in Figure 1.

The components that need to be added to the radio are:
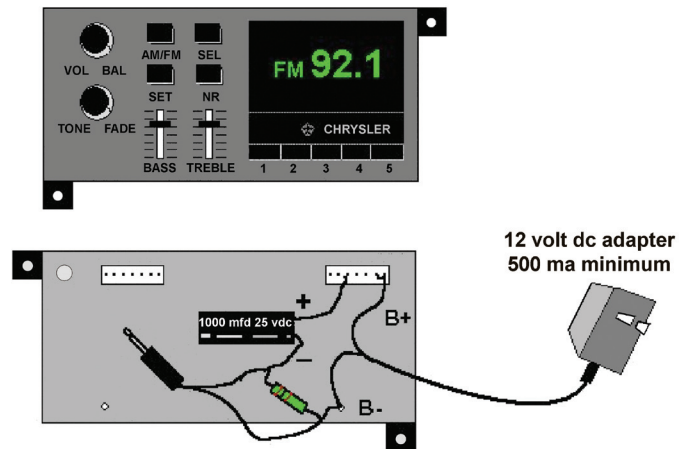


*Figure 1 — Front and rear modifications. Pictured here is a Chrysler radio model 4469088, front and rear view. The back of the radio is where all the connections and modifications are made so it will work as a radio meteor detector. All digital car radios have similar pin connections, although they are arranged in different configurations.*

- 2000-ohm resister (color bands are red, black, red, with a possible 4th color that can be ignored),

- 1/8-inch (3.5 mm) mono type headphone jack,

- 1000 μF electrolytic capacitor rated for 16–25 V,

- 12 VAC adapter rated at 800 mA to power the radio from a typical 110 V wall outlet (a 500 mA adapter can be used, but we recommend 800),

- 2 m of two-conductor stranded cable to connect the headphone jack to the radio. The headphone jack will eventually be connected to the "line-in" jack on the computer sound card.

Note that the one lead (marked "B+" on the diagram) of the DC adapter connects to both of the last two pins on the right hand set of pins on the back of the radio. The wire marked "+" on the electrolytic capacitor connects to the 3rd pin from the left on the right hand set of pins. The adapter wire marked "B−" on the diagram should be fastened to one of the screws on the back of the radio as a ground connection. One wire from the resistor and one from the audio jack should also connect to ground. The other wire on the resistor connects to the negative wire on the capacitor and to the other wire from the audio jack.

The capacitor and resistor combination is added because the speaker terminals sit at 1/2 the supply voltage (+6 V) with no output being generated. The capacitor and resistor level-shift the output down to be centred around the zero V that the computer sound card expects.

A Motorola antenna plug (also called Motorola connector) is soldered to the coax from the antenna. This plug goes into the circular hole (jack) on the top left-hand corner of the rear of the radio. For other makes of car radio, you will need to use a similar wiring configuration, but with different connections depending on the brand of radio.

## Antenna

We tried different Yagi antenna configurations, all cut to the centre of the VHF FM band (88–108 MHz) and using one to six elements. A good design that produced results with the smallest footprint and cost was a 3-element Yagi. RG-59 coaxial cable was used to connect the antenna to the car radio. Instructions for building a Yagi antenna can be found at the Web page www.skyscan.ca/equipment.htm.

I talked with Bill Lord at the SARA 2011 Annual Conference who had seen the original FM meteor detector on our Web site. He and Dick Castle used a Winegard HD6000 PROSTAR 1000 FM Antenna (HD-6000) and found it worked fine for them[1]. These are available from Solid Signal for $19.99 US plus shipping (www.solidsignal.com/). Basic

| CHANNEL | 88MHz | 98MHz | 108MHz |
|---|---|---|---|
| dB gain over reference dipole | 5 | 5 | 5.2 |
| beamwidth at half power points | 67° | 72° | 71° |
| front-to-back ratio | 6dB | 14dB | 16dB |

### Polar Patterns



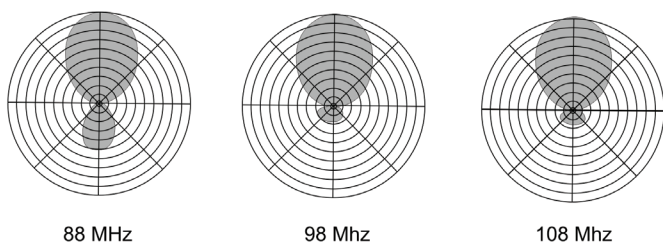88 MHz      98 Mhz      108 Mhz

*Figure 2 — HD-6000 antenna specifications*

specifications are shown in Figure 2. Since it was less trouble and looked a lot better than the home-built variety, I ordered one and installed it on a metal mast on my deck.

Because we were looking for over-the-horizon FM signals bounced off ionized meteor trails between 65 and 135 km (40–85 miles) above the Earth's surface, I oriented the antenna to an elevation of 30° above the southern horizon. Given our Edmonton location of 53° north latitude, almost all FM stations are south. The exact elevation angle did not seem to matter too much but could be adjusted somewhat to optimize reception based on the probable location of stations within the reception window that we determined using the geometry of meteor in-fall from particular showers.

## Software

For data collection, I use *Radio–SkyPipe Pro Edition* software. For graphical display of data results, I use the free software program *Colorgramme* from the *Radio Meteor Observing Bulletin (RMOB)* (Bill Lord and Dick Castle also use this software)[2].

## Operation

Since you are looking for FM stations that are over the horizon and not normally detectable on the radio, you have to find a channel in the FM band that is characterized by noise and not occupied by a local station. To do this, make a spreadsheet that lists all the FM channels from 87.9 to 107.9 MHz (101 channels). Start at the bottom of the band and work your way up, marking off each channel that has a local station present. Ideally, look for three clear channels adjacent to one another, since there is sometimes bleed-through of a station on one channel onto another. Because results can vary a bit from day to day, try this scan another day to see what results you get. Depending on your local circumstances, you may find more than one clear channel to use. You may also find no channels free due to the proliferation of local FM broadcast stations.

After the radio is connected to the computer sound card, *Radio–SkyPipe* needs to be set up to monitor the clear channel you have identified. Set the chart to record at 100-ms intervals (10 samples per second), and record for a 24-h period. This allows you to check a few things. First, you want to determine how stable the baseline noise level is—the smoother the better. If it's not smooth, try another clear frequency, if one is available to you. This will make it easier to set the event trigger for counting events using *Radio–SkyPipe Pro*'s event counter and to record audio files with its built-in WAV file recorder. Second, it's good to see how the radio behaves through the day. There may be baseline dropouts where the signal strength drops for a period of time (I don't know what causes this). Third, you are going to see some spikes through the day. Normally, you should see an increase in the number of meteors

at 6 a.m. local solar time, when the local leading edge of the Earth is sweeping through the highest number of sporadic meteors that fall into the atmosphere, much like rain on a car windshield. You will probably also see a minimum number at 6 p.m. when your location is opposite the leading edge.

Assuming that you are using the same or a similar radio to the one I used, when you first tune to a clear station, your radio may have a function that mutes the sound for a while before it is convinced that this is actually a channel you want to listen to. Noise should be heard after a short period.

The Pro version of *Radio-SkyPipe* has a WAV file recorder with several useful options. It allows the triggering of an audio recording based on events that change the signal strength beyond an upper or lower threshold (I only used the upper threshold trigger). You can adjust the amount of time prior to an event that sound will be kept (buffered) and added to the sound file, and how long each recording will be. WAV files take up considerable hard-drive space, so it's wise to set maximum file lengths. You can allow the recorder to accept multiple triggers. This produces a number of sound files that can then be reviewed with a handy visual display (see the Data Analysis section). I recorded all data using Universal Time (UT) to allow for corroboration with other data collections.

Due to the size and duration of the reflective characteristics of ionized meteor trails, sound files may record music and voices from radio stations or they may not contain anything. Underdense meteor trails produce spikes in the signal-strength data that show a sharp rise and a slower rate of decline, all of which occur in sub-second to several-seconds duration. Overdense meteor trails produce long-duration sound files and signal-strength data, lasting up to a minute or more depending on the energy of the meteor. These trails show up as a long period of higher signal strength and typically choppy audio recordings. While underdense audio recordings may or may not capture sound, it is unusual not to get discernible audio with overdense events[3].

## Orionids

There are two meteor showers in October each year: the Draconids centred on October 8; and the Orionids on October 21[4]. The dates given represent the peak of the showers. The names refer to the constellations from which the streams of meteoroids appear to come; for example, Orionids come from a point in the constellation Orion. This point in space is called the *radiant*. The same meteor showers recur annually because

their orbits cross Earth's orbit at the same point each year. The variations in intensity that occur from year to year are due to the history of shedding of material by the comet or asteroid that is the parent object.

In 2011, the Orionids were predicted to peak at 22 h UT on October 21 (3 p.m. local time in Edmonton) with the total event spanning two days. Orion rises at midnight and sets at 10 a.m. at this time of year[5]. The radiant was therefore below the horizon to the northwest at the predicted peak time, and essentially unavailable for viewing in Edmonton by either optical or radio methods.

The shower was predicted to have a Zenithal Hourly Rate (ZHR) of 20. The ZHR is the calculated maximum number of meteors an ideal observer would see in perfectly clear skies with the shower radiant overhead during one hour of viewing. Again, the stellar geometry of the shower in relation to my

| Oct | Total | 00h | 01h | 02h | 03h | 04h | 05h | 06h | 07h | 08h | 09h | 10h | 11h | 12h | 13h | 14h | 15h | 16h | 17h | 18h | 19h | 20h | 21h | 22h | 23h |
|-----|-------|-----|-----|-----|-----|-----|-----|-----|-----|-----|-----|-----|-----|-----|-----|-----|-----|-----|-----|-----|-----|-----|-----|-----|-----|
| 17 | 367 | 1 | 9 | 4 | 4 | 9 | 17 | 7 | 26 | 15 | 33 | 28 | 14 | 28 | 22 | 32 | 16 | 17 | 15 | 15 | 11 | 17 | 9 | 7 | 11 |
| 18 | 1056 | 5 | 3 | 4 | 6 | 5 | 9 | 10 | 9 | 7 | 8 | 13 | 6 | 11 | 6 | 21 | 70 | 417 | 293 | 32 | 25 | 44 | 19 | 24 | 9 |
| 19 | 511 | 12 | 6 | 11 | 11 | 4 | 11 | 13 | 13 | 7 | 20 | 15 | 17 | 10 | 7 | 29 | 12 | 20 | 13 | 10 | 33 | 14 | 51 | 97 | 75 |
| 20 | 725 | 147 | 135 | 23 | 49 | 71 | 11 | 21 | 17 | 21 | 36 | 11 | 6 | 8 | 6 | 18 | 35 | 31 | 13 | 24 | 8 | 13 | 17 | 2 | 2 |
| 21 | 578 | 0 | 7 | 15 | 8 | 19 | 13 | 28 | 30 | 38 | 23 | 22 | 18 | 26 | 25 | 25 | 43 | 47 | 18 | 36 | 30 | 32 | 50 | 24 | 1 |

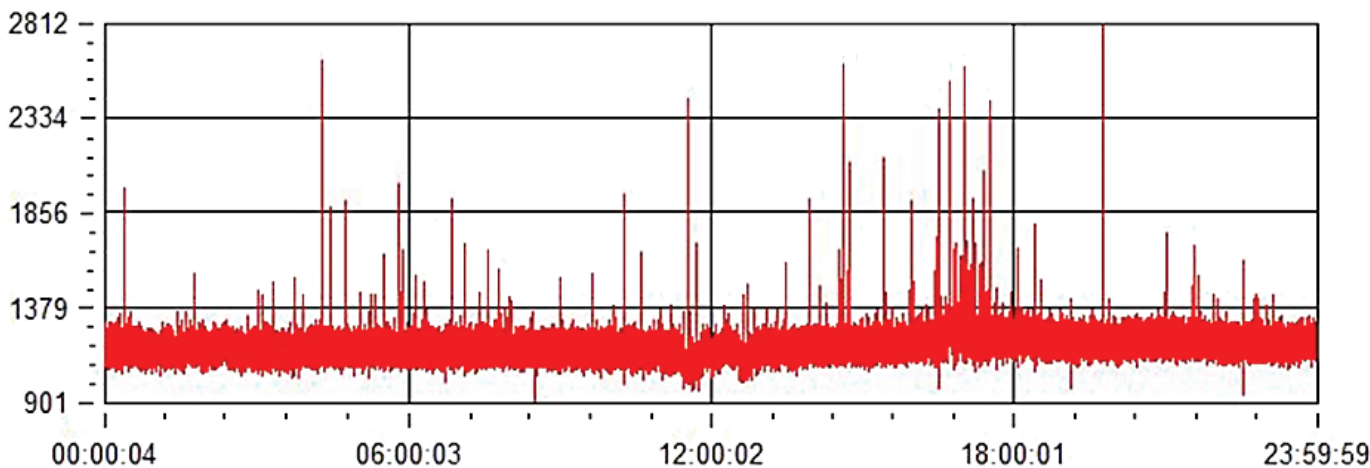*Figure 3 — Hourly meteor flux with peaks highlighted (hours in UT)*

Figure 4 — RSP file from 2011 October 18

## Data Analysis

observatory was poor for viewing due to the radiant being far below the horizon.

I collected 24 hours of data between 2011 October 14 and 26. There were a few days at the beginning where I had some downtime on my system as I fine-tuned my setup.

The *SkyPipe* files were set for 11,025 kHz mono 16-bit recording with sampling interval at 500 milliseconds (2 samples per second). As underdense events can occur with smaller durations than this, I probably missed some events and should have set *RSP* to sample at more than 10 times per second. If anything, then, my results probably understate the meteor flux that occurred during this period.

The data files showed an increase in activity between October 18 and 21, with peaks on the 18th at 16 UT (10 a.m. local time) and over the end and start of the day (Figure 3), respectively, on the 19th and 20th (3–7 p.m. local time). The *Colorgramme* portrayal of the data shown in Figure 6 shows this same data by days horizontally left to right, and hours



Figure 5 — Sound playback window

vertically top to bottom for data collected in October. The color-code key on the right shows the number of hits per hour. Note the correspondence between higher intensities shown in Figure 3 and the *Colorgramme* graphic.

Figure 4 is a *Radio–SkyPipe* chart that shows the pronounced increase in the number of hits between 15 and 17 hours UT on October 18. During the most intense period, the atmosphere was so ionized by the number of overdense meteor hits and the frequency of underdense events, that the baseline rises above the trigger level on a number of occasions. Unfortunately, I did not have the sound recording running on this day.

What I find to be the most fun with observing meteors is recording sound files of overdense events. We (students and project members) have recorded overdense events lasting more than a minute, with quite audible voices and music. Sometimes we have been lucky enough to also capture the station identi-fication, notably one a decade ago from Winnipeg, which is 1300 km from Edmonton. Station IDs allow confirmation that the signals being received are actually from meteor trails.

In previous years, we used VCRs to record audio files, but during this Orionid shower, I used *SkyPipe*'s triggered audio recording to capture overdense and some underdense events. The underdense events often did not have a long-enough duration to detect music or voices, but this was not the case with the overdense events.

At the bottom of the *RSP* sound playback screen shown in Figure 5 you can see the signature of an Orionid sound file captured on October 22 that contained the station IDs of 3 FM stations operated by Lane Community College (KLCC 89.7, my observing frequency) in Eugene, Oregon[6]. The green trace at the bottom of the window contains the announcer's voice that carries on for about 30 s before the ionization trail recombines to form neutral atoms and molecules and loses its reflective quality. The portion of the trace on the right shows what the normal background noise without a signal looks like.
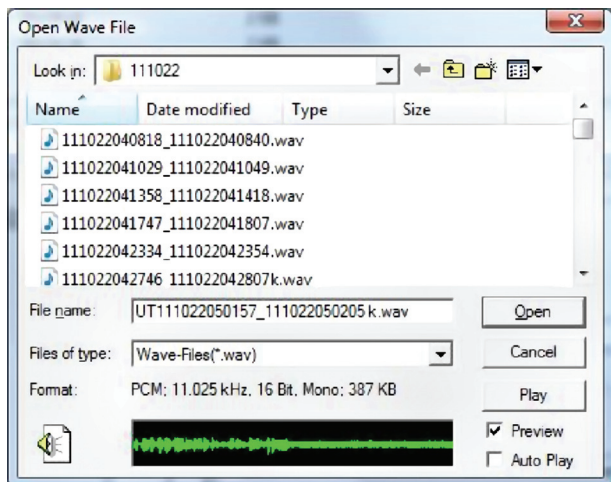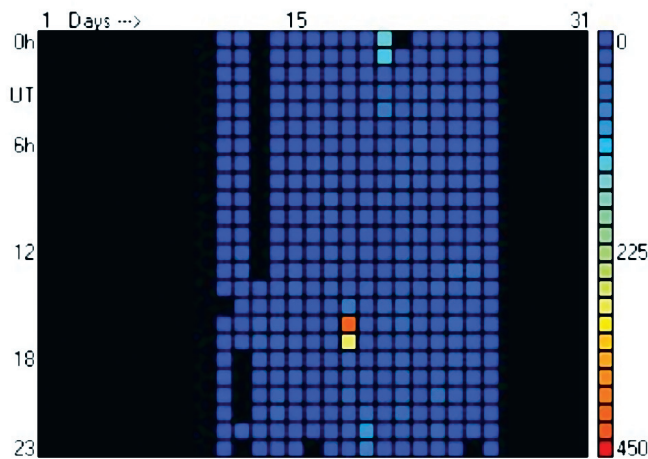
*Figure 6* — Colorgramme *representation of October 2011 data*

The pronounced thickness of the audio graphic above and below the centreline makes it easy to quickly scan through sound files to identify ones that contain reflected signals.

## Future development

Radio meteor detection is not new, going back to at least 1947, and much of the science of meteor detection using radio has been done. At the same time, there is value in reinventing the wheel by students, as is done when they use interference gratings to reproduce experiments that demonstrated the wave and particle nature of electromagnetic radiation.

Meteor events occur all the time. Knowledge accumulated over the last half century can be applied to observe meteor streams and their variability from year to year. As amateurs, we can support the work of professional astronomers, as happened in 2002 when our observations were cited by Dr. Robert McNaught of the Australian National University during the spectacular Leonid shower that year.

I am hoping we can expand and refine our techniques by pursuing some of the following ideas:

1) explore the use of the North American All-Sky Camera Network to make visual confirmation of overdense events[7], use two radio detectors in the same school, tuned to separate frequencies, to see how often radio meteor events coincide and how effective this arrangement is at rejecting interference,

2) try variations in the elevation angle and azimuth in relation to the radiant of individual meteor showers, and the effect this has on hourly rates. With several stations set up around the city it will be possible to try observations using these variations and correlating results to determine the effects,

3) use the transition to Digital Audio Broadcasting (DAB) occurring now across North America to identify stations. Apparently DAB stations still carry an analogue

component. If we can determine a way to capture both the digital ID and the analogue signal, it may be possible to get more information about direction without having to wait for a station to voice announce their call sign, and

4) could we use triangulation of fireballs to help in recovering meteorite fragments?

For us, the benefits of radio meteor detection are that it provides a useful means of carrying out ongoing observations, and meets a number of learning outcomes for Alberta Education's Science 9 Space Exploration unit. ✶

## References

1 www.tnskynet.com/Contact.php
   Bill and Melinda Lord's Web site with information about their project using a very similar FM radio meteor setup based on the Sky Scan setup. Accessed 2011 October 29

2 www.rmob.org
   *Radio Meteor Observing Bulletin* is a European site that has some useful software tools including *Colorgramme* for graphically displaying hourly meteor flux rates using data converted from Excel files. It also provides an FTP service for uploading data to a database maintained by RMOB. Files archived since 1997 including data up to the most recent month can be viewed on their web site. Accessed 2011 November 2.

3 www.imo.net/radio/reflection
   This page explains the characteristics of underdense and overdense radio meteor events. Accessed 2011 November 8.

4 *Meteors* by Margaret Campbell-Brown and Peter Brown, *Observer's Handbook 2013*, Royal Astronomical Society of Canada, p. 252. This annual publication contains information about meteors and a table describing meteor showers throughout each respective year covered by the Handbook. The Handbook can be ordered from the RASC at: rasc.ca/handbook. Accessed 2012 October 1.

5 www.imo.net/calendar/2011#octdec
   Accessed 2011 November 6.

6 transition.fcc.gov/mb/audio/fmq.html
   I used this Web site to identify radio stations operating at 89.7 MHz, my operating frequency. There are a number of other Internet services that can also be used. Accessed 2011 October 4.

7 allsky.ca/NAdatabase.html
   This site lists all-sky cameras used for optical meteor detection, their locations, and details about the observatories. Accessed 2011 October 30.

*David Cleary volunteers as Program Coordinator for the Sky Scan Science Outreach Program, a collaboration between the Edmonton Centre of The Royal Astronomical Society of Canada and the Department of Physics at the University of Alberta. He has been doing amateur radio astronomy on and off since 1997. His biggest radio-astronomy thrill was going up the big dish at the NRAO at the 2011 annual SARA conference in Greenbank.*

# LEDs in Astronomy

*by Robert Dick, RASC-LPAC and Canadian Scotobiology Group*
*(rdick@robertdick.ca)*

## Abstract

We propose a practical alternative to red LEDs for flashlights used in astronomy. Although low-brightness red LEDs do not affect our scotopic vision, they do not provide sufficient light for reading and navigation, especially across grassy fields. This conclusion is reached after study of the spectral sensitivity of our eyes and the spectrum of available solid-state light sources.

*Figure 1 — A star-night gathering at the Torrance Barrens Dark-Sky Preserve in 2010. About 50 observers take advantage of the dark skies in the Muskoka District in southern Ontario. Red LED lighting illuminates the legs of assorted telescopes to prevent accidents. The brightness of these lights is magnified by the long-time-exposure image.*

## Background

A typical star party, such as that shown in Figure 1, has people clustered around telescopes using red-light illumination to prevent individuals from tripping over equipment and each other. Forty years ago, it was easy to recommend a flashlight for stargazing. Most of us used an incandescent light wrapped in red cellophane. But the batteries only lasted a few weeks, so when light-emitting diodes (LEDs for short) became available in the 1970s, it was an easy switch to make. Even with a resistor of a few hundred ohms to limit the current, the batteries lasted for more than a year. The secret was in the technology.

The electric current delivered by the batteries in the old flashlights heated the bulb's tungsten filament to around 2000

degrees, so that some of its thermal radiation was shifted into the visual part of the spectrum. Clearly, incandescent bulbs are a very wasteful way to make light and so they are being phased out of circulation. Does your father still use incandescent bulbs? To quote a commercial for an Internet provider from over a decade ago: "How old is your dad?"

LEDs emit light when electrons supplied by the battery recombine with electron holes (a place where an electron is absent in an otherwise full electron shell) within a properly doped semiconductor. When a free electron drops into a hole, it is the equivalent of dropping from a higher orbital in an atom to a lower one, and the energy released is emitted as light. The individual colour is determined by the energy gap of the doped semiconductor.

LEDs remained a curiosity for most hobbyists, but amateur astronomers adopted them because they can be designed to emit light with a frequency that is about as far away from our critical scotopic vision as possible—in the red[1]. About 40 years ago, I fashioned a number of low-illumination-level LED flashlights by gutting burned-out incandescent bulbs and replacing their innards with LEDs and resistors.

A look at the action spectra for the two most obvious detectors in our eyes[2], cone and rod cells, shows why the red LEDs continue to be widely used (Figure 2).

The cone cells are the cells we use for our bright photopic vision, typically during the day. They are clustered mostly within the central 10-degree diameter field of view of our retina, giving us high-resolution views of scenery and the ability to read the fine print in cell-phone contracts. Cone cells contain photosensitive proteins called iodopsins that are composed of a protein called photopsin and an attached
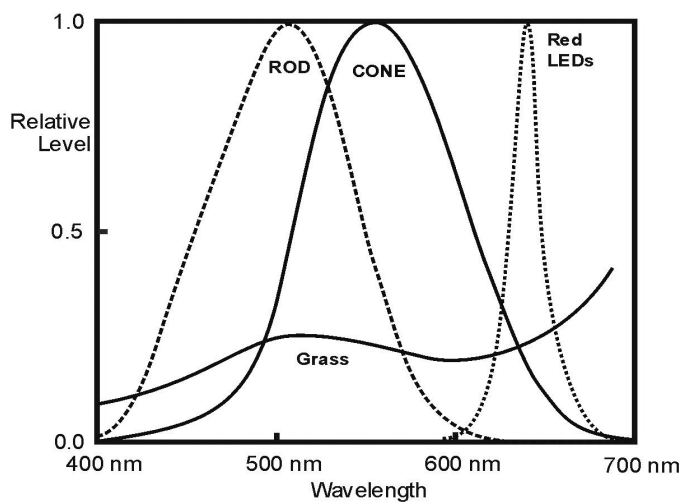


*Figure 2 — A comparison of the spectral sensitivity between human rod and cone cells, which provide our scotopic and photopic vision, respectively. The reflectivity of grass is relatively constant at 20 percent. The cone cells only faintly pick up the light of red LEDs. Therefore, very bright red light is needed to provide adequate illumination.*

chromophore or colour-sensitive molecule. There are three types of photopsin, individually responsible for sensitivity to blue, green, or red wavelengths[3]. Since they evolved for daylight use, they are not very sensitive, but given a sufficiently long period in darkness, the detection threshold for a cone cell will improve to only 200 photons at 555 nm wavelength.

The rod cells occupy the periphery of our field of view and provide our scotopic or night vision. Although they are plentiful—20× that of the cones[4]—there is only one type of rod cell, so they cannot differentiate colour. Graham Edge of *The Moody Blues* wrote a very good and poetic description of this failing colour discrimination under faint light on their album *The Days of Future Past*.

Studies in the 1960s measured the gain in sensitivity due to dark adaptation (Figure 3) and found it to range from 100× for cone cells to about 400× for the rod cells[5] (see also the e-book on vision[6]). However, there is a cost for the rod cells being more sensitive to light. To limit the number of rod cells randomly "firing" in faint light, they are grouped into clusters, and neuron logic determines if the detection of light is real or not, at the cost of reducing visual resolution and giving us a "grainy" image like a poorly tuned television station.

The rod cells contain a photosensitive rhodopsin molecule similar to the cone cells' iodopsin[7], making the width and shape of the rod-cell action spectrum (spanning over 200 nm) similar to that of the cone cells. The narrow emission band of the red LEDs, only 50 nm wide and lying outside the spectral band detected by rhodopsin, only triggers the much less sensitive photopic vision that we use mostly during the day.

Modern red LEDs require a higher voltage than the earlier products (about 3 volts compared to the earlier 1.5 volts), but they emit much more light as well. In figure 2, we can see that the red light has to be "bright" because our eyes are not very sensitive to that wavelength. We also see in the same figure that the amount of red light that reflects off green grass is only about 5 percent of that for white light. You will need a lot of



Figure 4 — An evening observing session at Starfest 2008. The observing field was speckled with red-filtered computer monitors. A strong sense of observing etiquette prevented the imaging observers from affecting the visual observers. The red LED-illuminated power switches on the telescopes and associated gear helped to prevent visitors from walking into the equipment.

red light to find a dropped pen, and so this prompted us to ask if the fixation on red light was still warranted.

Computer screens are the "viewing instrument" of choice for many astronomers (Figure 4). Computer monitors, however, are designed to emit a broad fluorescent spectrum of emission lines that in sum resemble the apparent colour of the Sun. Thick red cellophane is not sufficient to cut out all the green and blue light that shines on our rod cells—it can only attenuate it. This unfortunate circumstance can be overcome by using filters of the Kodak Wratten series (#24 to #29, with increasing short-wavelength rejection[8]) but these are more expensive than coloured cellophane. At a star party, you find a lot of people looking at computer monitors .

Except for visual observers, there really isn't much need for red light in astronomy. Given the very poor sensitivity of our cone cells to red light, and the poor reflectivity of grass to narrow-band red light, could there be a better choice of light for many in astronomy? If so, what properties should it have?

## Ideal Spectrum for an Astronomy Light

As daytime creatures, we need some light at night to read star charts and navigate around the telescope and its environs. We make virtually no use of our cone cells when observing faint objects, but must protect our scotopic vision as much as possible if we are to see those faint fuzzies after a walk to the nearest outhouse.
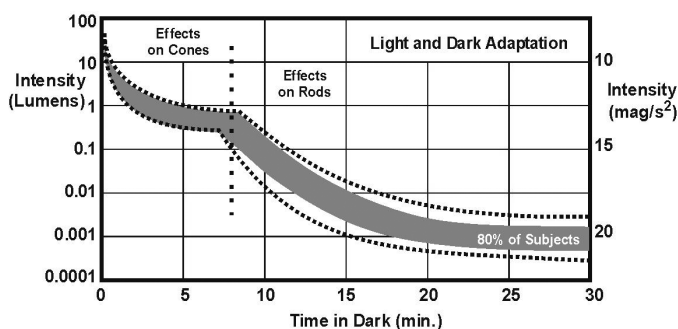


Figure 3 — The photopic and scotopic dark-adaptation curves show the improvements in our vision over time. Although our cone cells need relatively little time to reach full dark adaptation (5 minutes), our scotopic vision continues to improve even after 30 minutes.
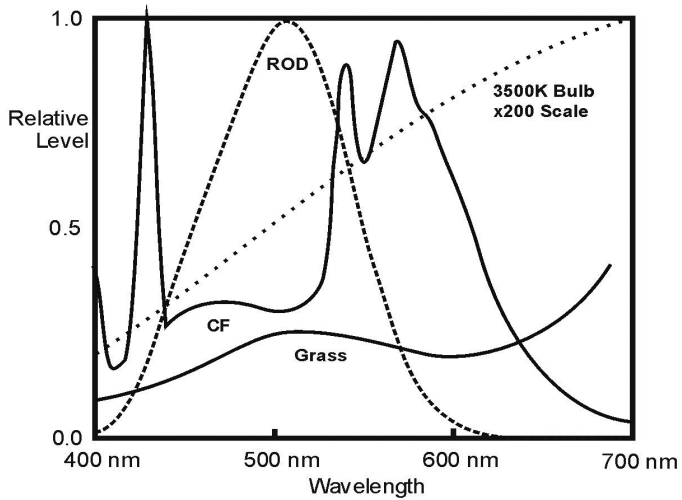
*Figure 5 — The emission of a popular compact fluorescent (CF) bulb compared to our scotopic action spectrum. This is compared to the old incandescent 3500K bulb, which emits very little short wavelength blue light. Both provide broad-band illumination to help navigate at night.*

During the summer, the predominant landscape is green, so we should use a light that provides enough green, yellow, and orange light to illuminate the grass while minimizing the blue and green to which our scotopic vision is most sensitive. The more effective the light spectrum for this, the less light we need to use.

Incandescent bulbs emit too broadly to protect the sensitivity of our rod cells, and filters absorb light, reducing the luminous efficiency of the light fixture. The recently introduced compact fluorescent (CF) bulbs have a broad emission-type spectrum (Figure 5) and so a filter can be placed over the bulb to remove most of the light that will affect our scotopic vision. However, it would be more effective if the spectrum of the emitted light avoids the rod cells' action spectrum in the first place, a goal that is currently achieved with red LEDs.

## Spectra of LED Products

Red LEDs are not particularly common except in astronomy circles and red traffic lights. Manufacturers prefer to produce flashlights with white LEDs for the mass market, which does not include astronomers. What does the spectrum of a typical consumer LED flashlight look like? Figure 6 shows two versions of LEDs—cool and warm white[9].

There are two main components to the spectrum of white LEDs: a blue peak and a broad amber emission. The technology used to create this mimic of white light is relatively new: a very efficient deep-blue LED excites a phosphor that re-emits the energy at longer wavelengths (Figure 7). This structure is optimized for for its emission characteristics while keeping the phosphor relatively cool[10]. The specifics of the phosphor vary between LED manufacturers and are proprietary, but their
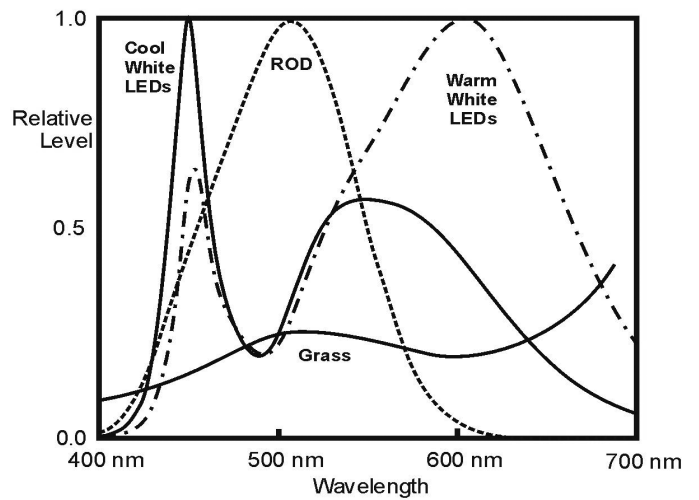


*Figure 6 — White-light LEDs are compared to red LEDs. The main differences between the warm and cool LEDs are the height of their blue peak emission, and the relative heights and position of the amber emission bands. As more of the blue light is phosphor-converted into amber, the amber peak shifts to longer wavelengths, enveloping the red-LED emission peak.*

spectra all have this general form. In general, the more amber we get, the lower the blue peak and the further the amber emission band is shifted to the red.

The geometry of the emitter is also important, because the blue exciter LED can be quite hot, which degrades the phosphor, reduces its operational life and shifts the emitted colour. It is imperative to keep the LED cool. For every 40 °C of the LED's junction temperature that is above room temperature, operational life decreases by a factor of ten[11]! For example, the thermal resistance of an LED between the semiconductor junction and its case is between 6 °C and 10 °C per watt. A temperature difference of 30 °C between the case and the air is considered good thermal management for natural convection, so a 100,000-hour LED is probably only going to last 10,000 hours, yet this is still more than 4× better than most light bulbs.
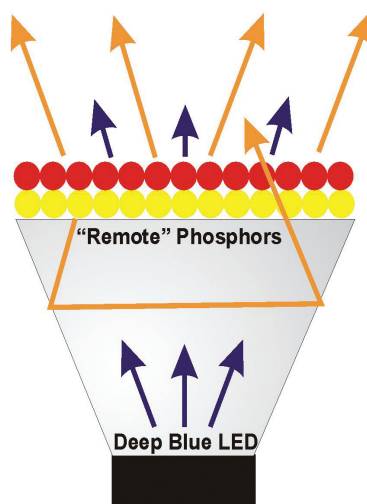


*Figure 7 — This configuration of a phosphor-converted LED is based on recent developments. The material between the LED and phosphor collating enhances the LED emission (efficacy) and helps keep the phosphor cool.*
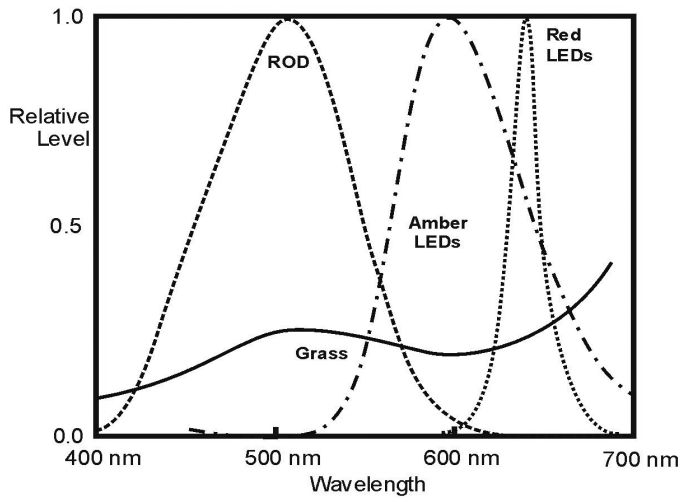
Figure 8 — The emission spectra of "true amber" and red LEDs are compared to the action spectrum of our scotopic rod cells. The spectral reflectivity of green grass is also shown for reference. The impact of amber LEDs on our scotopic vision is much less than most people would expect. Amber also increases the visibility of hazards in grass-like ground cover.



Figure 9 — A visual demonstration of the apparent colour difference between white and "true amber" LEDs. Most city dwellers are used to the amber colour from street lighting. "True amber" LEDs are readily available to flashlight manufacturers. However, most consumer flashlights are being sold with white LEDs, which are unsuitable for astronomy. The drive voltage for amber LEDs is about 3 volts so they may not require current-limiting resistors, except to reduce the LED brightness, which is considerable!

When we compare the white LED spectrum to the sensitivity of our eyes, we find the main problem with the white LEDs is the blue peak. It will affect our scotopic vision and at the same time, does not help us see the grass! Also, the short wavelength side of the broadband amber emission interferes with our rod cells. We would like a compromise between the red LEDs and the amber emission band of a white LED shifted as far to the longer wavelengths as practical. We could use a blue-blocking filter, but this cuts the light, reducing the efficacy (amount of light per watt) of the light fixture. However, the amount of electricity used by LEDs is so low that energy efficiency may be secondary to the complexity and cost of using fragile filters. LEDTECH CANADA (ledtechcanada.com) is developing these filters.

We don't see these amber LEDs in the consumer market because it has been decided by the lighting-fixture manufacturers that white-coloured LEDs are the way to go. However LEDs that approximate the ideal light source above do exist and can be ordered from the LED manufacturers.

Figure 8 compares the emission spectrum of a Philips amber LED to the sensitivity of rod cells, to a red LED, and to grass cover. The amber LED[12] has very little emission below 500 nm yet provides sufficient illumination for grass[13] and the recognition of other colours.

By convolving the sensitivity of the rod and cone cells's action spectra by the emission of the amber LED, we can approximate the relative visibility of amber by the rod and cone cells. The amber spectrum "contaminates" our scotopic vision by about 13 percent and our photopic (cone cell) vision by 51 percent. The efficacies of the amber and red LEDs are approximately the same[14], so amber LEDs will require about 1/4 the

power of emitted light to provide the same visibility as red LEDs and with much better colour rendering.

There is an obvious shift in the colour (Figure 9), though this is primarily due to the absence of a narrow blue emission spike. Since most of the visual spectrum from 500 nm to 700 nm is illuminated, there is a reasonable colour-rendering index (CRI). There does not seem to have been any measurement of the CRI for amber LEDs (as defined in this paper), but a light source with the relatively smooth black-body curve of the Sun (5800K) is defined as having a CRI=100. Emission-line sources that only sporadically sample the visual spectrum have much lower CRIs (20-80 for High Pressure Sodium lights[15]) with higher values for emission spectra that approach the black-body curve. In the opinion of this author, the broad amber-emission spectrum, though lacking in blue, is a fair compromise. We will see the colour codes on the star chart better by using amber than with red LEDs.

## Summary

"True amber" LEDs, with emissions >500 nm, are viable alternatives to red LED light sources for astronomy.

Red LEDs are ideal for illumination when our eyes are fully dark adapted as when viewing the sky, observing at the telescope, using binoculars, or observing meteors. However, they provide very little light within the range of our photopic vision for walking about, where navigation markers and hazards are mixed in with green grass. Grass absorbs most of the incident red light, making the ground look very dark in both scotopic and photopic vision. We need a very bright red LED flashlight to be able to navigate safely when walking about.

Low-level amber light provides much better visibility while not seriously affecting our scotopic vision. It improves visibility for navigation and hazard avoidance over the use of red light. However, in reviewing LED product literature, we found that some LEDs emitting a colour called "amber" also emit significant levels of blue. LED products destined for astronomical use should be tested with a spectrograph to ensure that they conform to our "true amber" definition.

## Acknowledgements

We thank ComDev Limited, Ottawa, for assistance in obtaining the LED spectra. ✴

## Endnotes

1   Philips Lumileds (2012). LUXEON® Rebel Technical Datasheet DS68. www.philipslumileds.com/uploads/265/DS68-pdf Accessed 2012 May 27

2   Luminous Efficiency, (n.d.) www.cvrl.org/lumindex.htm Accessed 2012 May 27

3   Cone Cell. (n.d.) http://en.wikipedia.org/wiki/Cone_cell Accessed 2012 May 29

4   Dale Purves, *et al.* Editors (2001). Neuroscience, 2nd edition, Chapter 11, Sinauer Associates, ISBN-10: 0-87893-742-0 www.ncbi.nlm.nih.gov/books/NBK10799/ Accessed 2012 May 28

5   Pirenne, MH (1962). Dark Adaptation and Night Vision. Chapter 5. In: Davson, H. (ed), *The Eye*, vol 2. London, Academic Press.

6   Kolb, H., *et.al.* Editors (2011). Webvision: Organization of the Retina and Visual System http://webvision.med.utah.edu/ Accessed 2012 May 29

7   Photopsin http://en.wikipedia.org/wiki/Photopsin Accessed 2012 May 29

8   Peed, A.C. (n.d.) Transmission of Wratten Filters. Eastman Kodak Company www.karmalimbo.com/aro/pics/filters/transmision%20of%20wratten%20filters.pdf Accessed 2012 May 29

9   CREE. (2012). CREE Product Literature for Xlamp XP-C LEDs, CLD-DS19 REV 6A, Page 5. www.cree.com/products/pdf/xlamp7090xr-e.pdf Accessed 2012 May 29

10  Zhu, Y. & Narendran, N. (2010). Investigation of Remote-Phosphor White Light-Emitting Diodes with Multi-Phosphor Layers, *Japanese Journal of Physics, 49* (2010) 100203, (DOI: 10.1143/JJAP.49.100203)

11  Toshiba, Products, Reliability Information, Semiconductor Device Reliability, Reliability Testing, Accelerated Lifetime Tests (2012) www.semicon.toshiba.co.jp/eng/product/index.html Accessed 2012 May 27

12  Philips Lumileds (2010). Philips Luxeon Rebel Phosphor-Converted Amber LED, Technical Datasheet DS62 www.philipslumileds.com/uploads/34/DS62-pdf Accessed 2012 May 29

13  Farooq, S. (n.d.) Spectral Reflectance of Land Covers, Department of Geology, Aligarh Muslim University, Aligarh (India) www.cps-amu.org/sf/notes/m1r-1-8.htm Accessed 2012 May 12

14  Philips Lumileds (2010). Ibid. Page 5 Accessed 2012 May 29

15  Pacific Gas and Electric Company (1997). *High Pressure Sodium Lamps, A Pacific Energy Center Factsheet* www.lightingassociates.org/i/u/2127806/f/tech_sheets/High_Pressure_Sodium_Lamps.pdf Accessed 2012 May 29

# Pen & Pixel



Figure 1 — Lynn Hilborn provided the Journal with this image of NGC 1055 (left) and M77 (right) nestled in their stellar background in the constellation Cetus. The two galaxies form a binary system at an approximate distance of 52 million light-years. NGC 1055 is a marvellous edge-on galaxy while its companion is an active Seyfert galaxy nearly face on. Exposure was 12×10 min in L, and 6×10 min in each of RGB. Lynn used a TEC 140 telescope at ƒ/5.6 and an SBIG ML 8300 camera from his WhistleStop Observatory near Grafton, Ontario.



Figure 2 — André Paquette of the Ottawa Centre joins the suite of Journal photo contributors with this image of Comet Hergenrother, one of the several comet gems at the end of last year. Comet Hergenrother was not expected to attain a significant magnitude, but an outburst and fragmentation allowed it to reach 8th magnitude. Andre used a 14-inch Celestron Edge HD at ƒ/7.7 with a Celestron Nightscape 8300 camera. The image is constructed from 9×10-minute subs.

# Pen & Pixel

Figure 3 — *Klaus Brasch sent us this mosaic of two overlapping images of the Milky Way, taken from his observatory at Flagstaff. The images were acquired with a Hutech-modified Canon 50D using a 50-mm ƒ/1.8 lens at ISO 800. The Lagoon and the Trifid Nebulae are prominent in the centre of the image, but many more clusters and gas clouds are visible in the scene.*
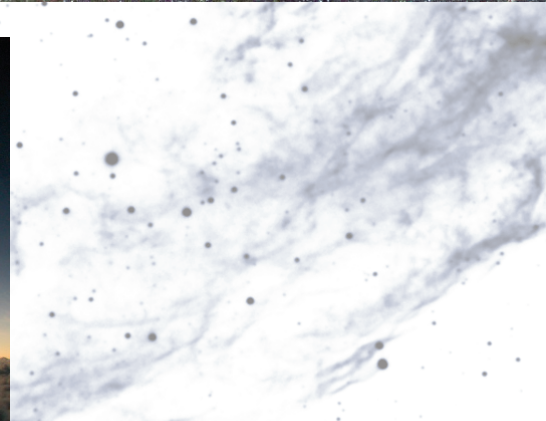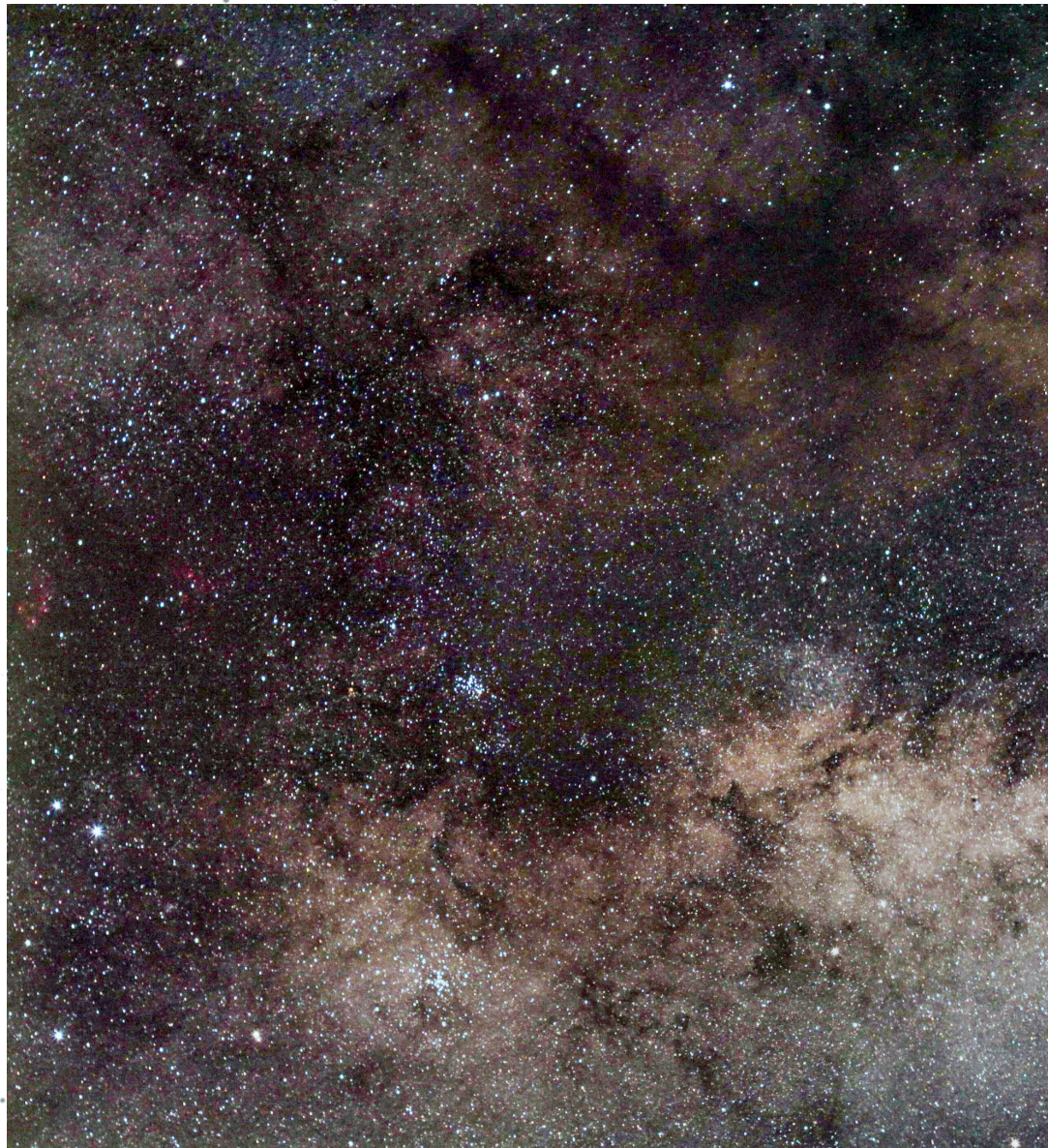
Figure 4 — *When clouds intervened, Dr. Jay Pasachoff took to the air to photograph the November total eclipse in Australia. This intriguing image captures the Sun from a helicopter just before second contact and the beginning of totality.*
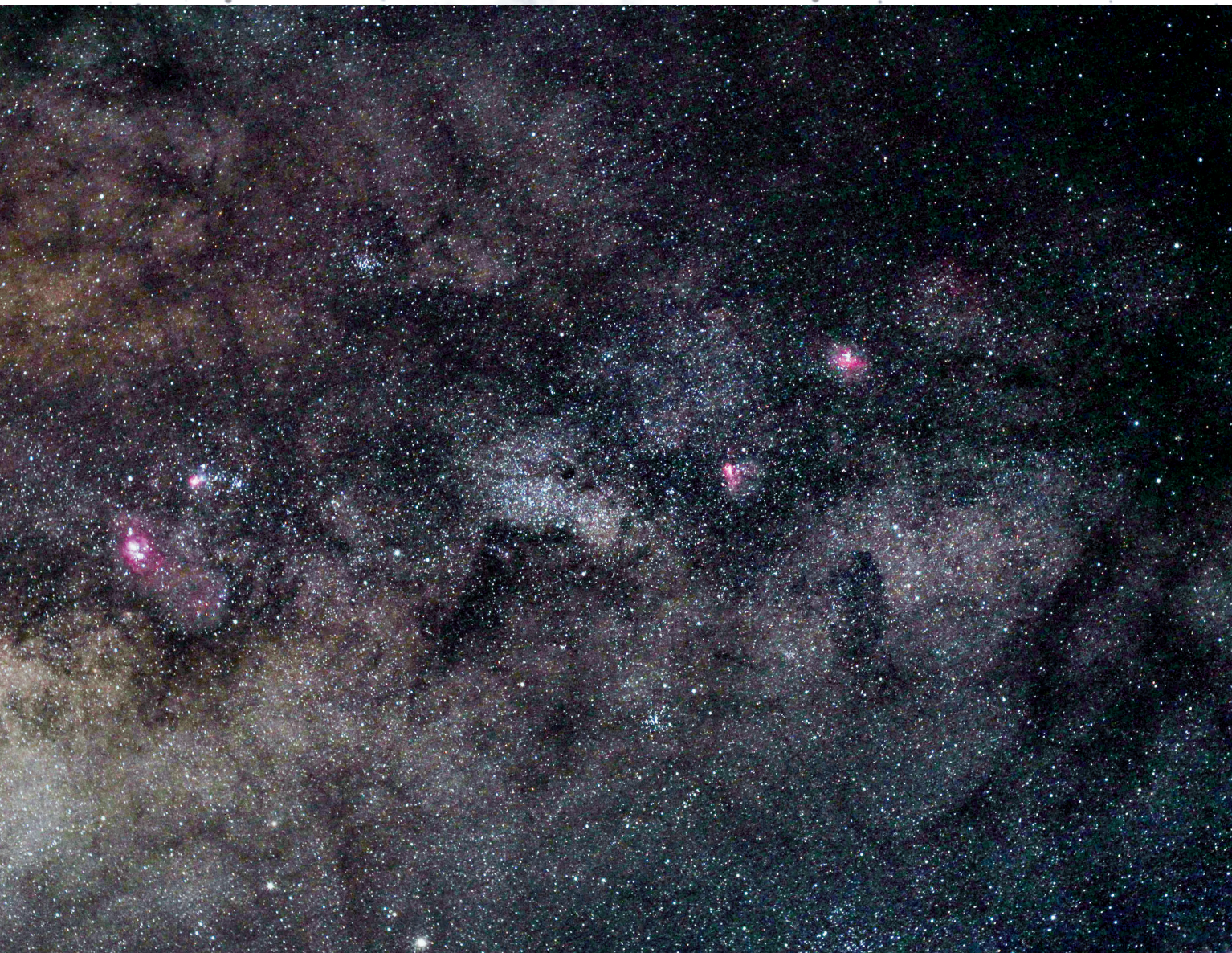
*Figure 5 — Lynn Hilborn just about owns a personal page in the* Journal *with the many excellent photographs that he supplies to us. This image, of the spiral galaxy IC 342 in Camelopardalis also graces the cover of his new book* Time Machine, *which shows many of his superb photographs. The 3-colour image was acquired on October 12 and 26 with a TEC 140 at ƒ/5.6 using an FLI ML8300 camera. Exposure was L: 23×15m; RGB: 18×5m; Hα 5×15m for a total of 8½ hours. Many more of Lynn's images can be found at* www.nightoverontario.com.

# Pen & Pixel



Figure 6 — Dalton Wilson sends us this exquisite image of the Crab Nebula in Taurus, one of winter's highlights, but a difficult object to photograph well. The Crab is a well-known supernova remnant, expanding from an explosion witnessed in 1054. Dalton used an AstroTech 10-inch Ritchey–Chrétien telescope and a QSI 540wsg camera. Exposure was 9x900s in LRGB on December 12 last year.
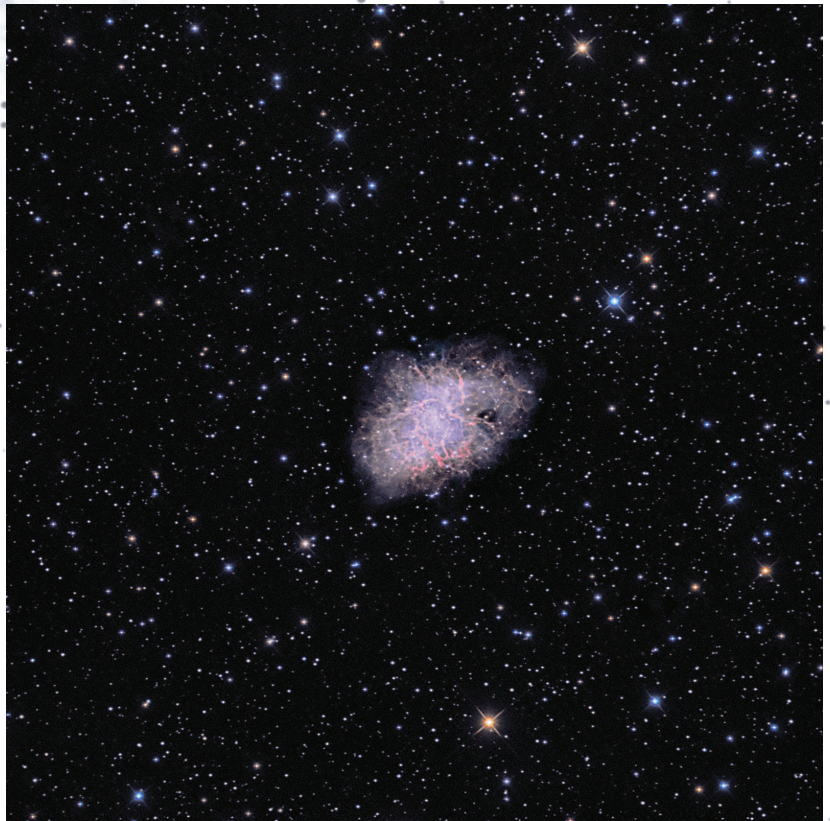


Figure 7 — Winnipeg's Sheila Wiwchar couldn't resist a long-awaited clear sky and headed north to Norris Lake to take in a little sky-shooting. In Sheila's words, "the sky was amazing and remained clear from about 10 p.m. until all batteries died in the camera!" She also noted that "you can keep warm by running from accidentally throwing a lighter in the fire—down-filled parkas are flammable!" and "holding a flashlight in your mouth for light to adjust camera settings is only a good idea if the flashlight is not metal...ouch!" Exposure is 30 seconds at ƒ/3.5 with a Canon 60D at ISO 3200.

# The Venus Aureole Effect: Minimum Aperture for Visual Detection

R.A. Rosenfeld (randall.rosenfeld@utoronto.ca)[1]
Chris Beckett (cabeckett@gmail.com)[2]
Mike O'Brien (jmobrien@accesscomm.ca)[2]
Jeff Danielson (saskdanielson@gmail.com)[2]
Rob Sheppard (grabhooks@hotmail.com)[2]
Paul Greenham (paul.greenham@mail.utoronto.ca)[3]

## Abstract

The 2012 June 5 Transit of Venus (ToV) provided a unique opportunity for scientific teams to conduct observational programs probing features of this rare Solar System event. A RASC team stationed in Regina set out to determine the minimum aperture necessary to unequivocally visually detect the aureole effect. The experiment and its results are described below. In the context of contested historical detections of the Cytherean atmosphere, this investigation used modern analogues of 18th-century equipment to aid in characterizing the potential of enlightenment optics for detecting the aureole effect. It was conducted under the auspices of the Transit of Venus Project (TVP)-Astronomers Without Borders (AWB) Experimental Archaeology program (ExARx).

## The aureole

Among the more intriguing of the phenomena observed during the ToVs of 1761, 1769, 1874, 1882, 2004, and 2012 is the Venus twilight phenomenon known as the *aureole effect*, "One of the most relevant features pertaining to ground-based studies of the Venus Atmospheric structure...observed only during transits...as a bright arc outlining—in part or entirely—the portion of Venus's disk projected outside the photosphere" (Tanga *et al.* 2012, 207). It is caused by the refraction of sunlight through Venus's outer atmosphere as seen by observers on Earth (Bergman 1761, 228; Tanga *et al.* 2012, 213-216). The aureole is by reputation a challenging and by no means presumable quarry for the visual observer, as is well attested in the early literature (Hirst 1761, 397-398; Harris 1769, 426). A reasonable question to ask in light of its observational character is: "With what minimum aperture can the aureole be positively detected?" Our ToV experiment was designed to answer that query.

## Experiment

In its essentials, the experiment consisted of observing the ToV before 1st contact, during 1st and 2nd contact, and immediately after 2nd contact for visually detectable signs of the aureole. High-quality modern small-aperture doublet refractors were placed in the hands of experienced visual observers, supplemented by observations with a Georgian-period Gregorian in the hands of an historian of science, and observations were recorded in traditional logbook media. The rationale for using modern instruments is given below.

Instrument specifications can be found in Table 1. A series of aperture stops AS1-AS7 (see Table 2, and Figure 1), ranging in diameter from 38.1 mm (1.5″) to 114.3 mm (4.5″), were placed successively in front of the object glass (O.G.) of Optical Tube Assembly 1 (OTA1) during the ToV. OTA2 was used for constant monitoring of any phenomena, with OTA3-OTA4 used more intermittently.
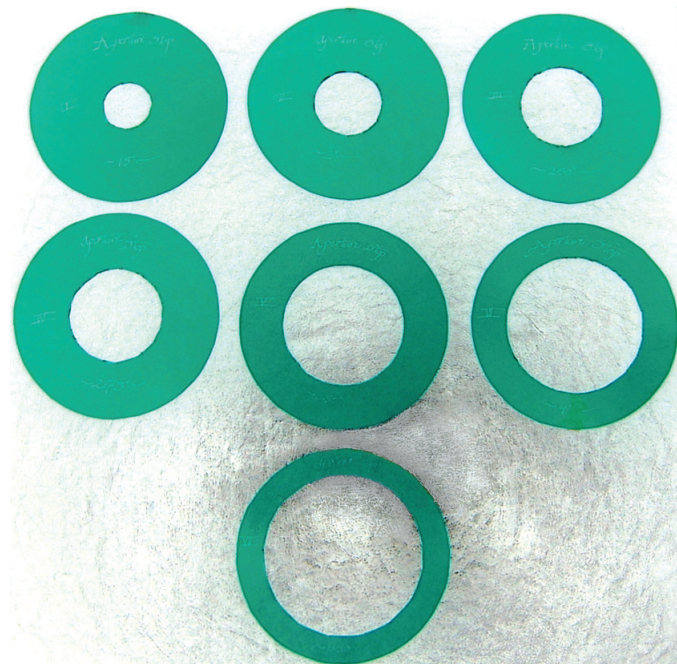


*Figure 1 — Aperture stops AS1-AS7 (38.1mm-114.3mm; 1.5″-4.5″) used on OTA1.*

The working hypothesis was that the aureole effect would not be detectable with anything less than an aperture of 101.6 mm (4″), that is, it would not be visible in OTA2 - OTA4, and only in OTA1 when fitted with AS (aperture stop) 6, AS7, or when used without an aperture stop (it was also expected to be potentially visible in OTA5). To count as a positive detection, the aureole had to be clearly visible without the use of averted vision, by more than one observer.

The primary ToV station was established on the grounds of the Saskatchewan Science Centre (longitude 104.59°W, latitude 50.43°N, elevation 577 m as), in a sheltered area with generous sightlines for viewing the ToV (Figure 2). Cloud cover was unfavourable a half hour before the ToV commenced, but cleared at approximately 20 minutes before 1st contact, and remained virtually clear until sunset. Seeing was above average at Pickering 7-7.5 (Antoniadi II), and winds were gusting moderately strong to start with but became moderate to light. The topography of the site afforded good protection from the wind.[4] For information on the second ToV station, see the final section of this paper.

*Figure 2 — Project leads evaluating the site for the primary ToV station on OTA1. Photo by Mike O'Brien.*

As the timings of the ToV phenomena were in no way crucial to the experiment, little effort was devoted to noting them in a systematic way. Chronometric data, therefore, does not figure in this report.

One member of the team (CB) originated the concept and formulated the design, another (RAR) constructed the modest experiment-specific apparatus, five (CB, RAR, MO'B, RS, PG) sourced and procured relevant commercially available equipment or original apparatus, and all (RAR, CB, MO'B, JD, RS, PG) were involved in on-site implementation.

As this experiment was conducted under the aegis of the Transit of Venus Project (TVP)-Astronomers Without Borders (AWB) Experimental Archaeology program (ExARx), its design had to fit within their parameters. The principles of best practice of experimental archaeology in astronomical application specified for the ExARx are as follows (Rosenfeld Experimental Archaeology):

- The equipment used should be that available to the original observers, or its equivalent;

- Techniques should be those of the time, place, and activity under investigation;

- Modern technicians should not be incompetent, inexperienced, or inexpert in their handling of 1 and 2 above;

- Modern technicians must be fully informed of the goals of the experiment, and be sympathetic to its aims, unless the experimental design requires them to be uninformed;

- In regard to 1 and 2 above, modern materials and technologies should play as little a role as possible in the crucial elements of the experiment. Where they are necessary, their use should be controlled, and recorded;

- Parameters, qualifications, and limits to an experiment should be clearly formulated and stated;

- Experiments in sequence should be consistent, unless the experimental design dictates otherwise;

- Experiments should be developed and run with reference to previous trials (if any);

- All possible ways that something may have been done, documented from historical sources, should be considered for investigation where practicable;

- The experiment should be reproducible if at all possible, should the opportunity for similar experiments present themselves;

- Results must be stated as accurately as possible, with all necessary qualifications, chief among which is that **a successful experiment provides only one possible way something may have been done;**

- The experiment should be scrupulously recorded, including any failures of technique, equipment, or observers, using the most appropriate modern technology;

- The experiment must be published as fully, transparently, and rigorously as possible.

The first bullet item, above, could not be fulfilled, as extant equipment (chiefly OTAs and oculars) used at 18th-century ToV stations in Canada could not be found. Some similar 18th-century apparatus was located, but its release for experimental purposes could not be obtained, with one exception (OTA5—see Table 1), hence the relevance of bullet items 5 and 6. In addition to the Georgian-period reflector, it was decided to run the experiment with modern, high-quality OTAs equipped with BK7 F2 achromatic, and ED and FL apochromatic doublet O.G.s as usable analogues to high-quality 18th-century doublet and triplet refractors. Modern theoretical analyses and historical accounts of the on-axis performance of traditional refractors show that it was in fact very good (Smith, Ceragioli, & Berry 2012, 95-119; also note their positive analysis of even earlier singlet O.G.s at 88-95, bearing out Binder's 2010 experiments; Bishop 2012, 147). This is a departure from the usual route of using poor modern instruments to replicate historical observations, a procedure for which there is little warrant (*e.g.* Jones 1991, 33, 52); such a course is rarely if ever based on long experience with actual antique instruments in original condition or accurate reproductions and familiarity with historically appropriate observational techniques. It is important to note the qualification this decision introduces into the results: **if** an 18th-century doublet or triplet O.G. could deliver on-axis performance comparable to modern achromatic or aprochromatic O.G.s for visual observation of ToV phenomena, then in a limited sense, the results of this experiment can help to characterize the performance of equipment used in 1761 and 1769. More data from critical analyses of extant 18th-century optical systems, combined with informed field use of a significant population of the surviving instruments, would aid materially in refining this approach. Preliminary results conducted by Shiltsev and colleagues lend support to the view expressed here (arXiv 1208.5286; Crease 2012). As a working principle, the use of authentic instruments or close copies should always be favoured when restaging historical

| instrument code | O.G. | F, ƒ/ | glass type, mfg | filters | eyepieces | other | observers |
|---|---|---|---|---|---|---|---|
| OTA1 | 125mm (4.92″) | 750mm, ƒ/6 | ED, Borg 125SD | Baader AstroSolar Safety Film OD=5, in a Kendrick cell | Pentax X05.1 (=147×), XW7 (=107×), XW10 (=75×) | aperture stops 38.1mm-114.3mm (RAR mfg) | CB, assisted by JD |
| OTA2 | 80mm (3.15″) | 480mm, ƒ/6 | BK7 F2, Stellarvue NHC | Lunt White Light Solar Wedge (Herschel Wedge), Baader Solar Continuum Filter (540nm) | Agena EWA 6mm (=80×), Baader Hyperion 8mm (=60×) | | RAR |
| OTA3 | 78mm (3.07″) | 630mm, ƒ/8 | Fl, Takahashi FS78 | Baader AstroSolar Safety Film OD=5, in a Kendrick cell | Televue Ethos 13mm (=48×) | | MO'B |
| OTA4 | 80mm (3.15″) | 560mm, ƒ/7 | Lunt LS80T-Hα (<0.7Å) | Etalon and blocking filter | Lunt Zoom 7.2mm-21.5mm (78×-26×) | | RS, CB |
| OTA5 | 100mm (3.94″) | ca. 1845mm ƒ/18.45 | Speculum metal, R.B. Bate, London, ca. 1830, Toronto, Department of Astronomy & Astrophysics Library, 2012.ast.5 | Baader AstroSolar Safety Film OD=5, in a Kendrick cell | Bate (Ramsden design?) 2.7mm (=228×), Bate (Ramsden design?) 10.5mm (=59×) | | PG |

*Table 1*

experiments, but when they are unavailable, running the trials with modern analogues can be a viable alternative, and it is hoped the present experiment can act as a model for such an approach.

It should also be noted that the filtering material and apparatus were modern—metallic film, and a filter admitting λ≈540 nm are without close 18th-century analogues, and the use of a Herschel Wedge belongs to the technology of the 19th century. The customary filter for ToV observations in the 18th-century was a pane of smoked glass, common window glass being recommended for the purpose (Maskelyne 1768, 7-6). By modern standards, surviving examples of common 18th-century window glass are far from homogenous, with abundant striations and bubbles. Some contemporaries, nonetheless, were impressed by their performance (Smith 1771, 24). The efficiency of filters made from that glass has yet to be thoroughly characterized, and their effect on the observation of the phenomena of the ToV has yet to be critically assessed (Koukarine *et al.* arXiv 1208.5286 appear to have used modern non-optical quality glass.). The filters used

in the present experiment—as well as the filters not used—can play no role in determining the effects of 18th-century filtering technology. This should be taken into account when evaluating the results presented here.

Bullet items 2 through 4 were broadly satisfied through basing observational techniques on published accounts of observations collected in Arlot (2004), planning sessions, and assessing the previous observational experience of the experimenters. Satisfying point 2 also met the requirements of point 8.

Due to the rarity of the event, experiments could not be "run in sequence" as specified at 7—an experiment that requires real-time observation of a ToV is practically not amenable to such procedures, and is analogous to that ultimate of non-repeatable experiments, the archaeological excavation (Barker 1982, 11-12). Nor is it repeatable diachronically as 10 demands (at least not by the same experimenters!), although it could have been repeatable synchronically. This, however, was not done systematically.

| code | diameter | ƒ/ when used with OTA1 | comments |
|---|---|---|---|
| AS1 | 38.1mm (1.5″) | ƒ/19.69 | aureole not visible |
| AS2 | 50.8mm (2″) | ƒ/14.76 | **aureole clearly visible** |
| AS3 | 63.5mm (2.5″) | ƒ/11.81 | somewhat brighter than with AS2 |
| AS4 | 69.85mm (2.75″) | ƒ/10.74 | somewhat brighter than with AS2 |
| [*3 | *76.2mm (3″)* | — | *bright image*] |
| AS5 | 88.9mm (3.5″) | ƒ/8.44 | bright image |
| AS6 | 101.6mm (4″) | ƒ/7.38 | brightest image of best definition |
| AS7 | 114.3mm (4.5″) | ƒ/6.56 | image not quite as good as with AS6 |

*Table 2 — *No AS3 was manufactured, as the requirement for this aperture class was met by the unobstructed apertures of OTA2 & OTA3 (see Table 1 for specifications)*

The requirement for point 9 was not met, because at least one major optical system (Newtonian) used to observe the 1761 & 1769 ToVs was not deployed in the trials. Points 11-13 are being met with this publication.

## Results

The results can be found in Table 2. At the primary ToV station, the aureole effect was clearly visible with an aperture of 50.8mm (2″), using AS2 on OTA1, at f/14.76. It was also visible when viewed with OTA2-OTA4, with apertures ≈80 mm (3″), at f/6-f/8 (Figure 3). Keeping the aperture constant while increasing magnification had no effect on the detection of the aureole–observing with sufficient aperture seems to have been the crucial factor (also see Shiltsev, Nesterenko, & Rosenfeld 2013). The aureole effect was not detected at the second ToV station with OTA5.
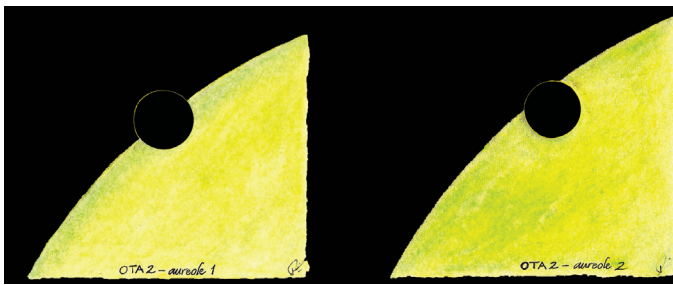


*Figure 3 — Aureole effect as viewed through OTA2 (colour is due to the Baader Solar Continuum Filter, 540nm). Drawings by R.A. Rosenfeld.*

## Discussion

Those conducting the experiment were surprised that significantly smaller apertures than expected proved effective for the positive detection of the phenomenon. Such a finding, that the minimum aperture was not the hypothesised value of 101.6mm (4″), but in practice turned out to be a surprising 50.8mm (2″)—half the predicted value—is interesting in itself. We echo Thorbern Bergman's statement of nearly two-and-a-half centuries ago: "On this occasion some phenomena were observed, which were not at all expected" (1761, 228).[5]

The results from the primary station in Regina (OTA1-4) were not matched by the results from the secondary station in Toronto (OTA5). This could be attributable to the higher elevation of the primary station (ca. 577m compared to ca.100m), and the noticeably better seeing there than at the secondary station on the day of the ToV (Pickering 7-7.5 compared to 5.5). A less significant although contributory factor may have been the more onerous education and public outreach (EPO) responsibilities on the Toronto observer manning the secondary station, diverting attention and opportunities away from detecting the aureole.

The positive results acquire an added interest when placed in the context of current work on the 18th-century reports

of observations of the aureole. A recent paper by Pasachoff & Sheehan (2012) has questioned the accuracy of all of the observations of the aureole effect during the 1761 and 1769 ToVs and in particular that of the noted Russian polymath Mikhail Vasilievich Lomonosov (1711-1765) as reported in his landmark publication on the 1761 ToV (Shiltsev arXiv 1206.3489). The presumed limitations of 18th-century equipment play a significant role in the authors' questioning of the Enlightenment detection of the Cytherean atmosphere.

Calls to re-examine the accepted narrative of the course of a scientific discovery are useful, for they can prompt both a reconsideration of how well we know what we think we know, and a review of the factual basis on which our narratives rest. Pasachoff & Sheehan's questioning of 18th-century aureole observations served as a catalyst spurring research, leading directly to the Shiltsev team's (arXiv 1208.5286) successful efforts to employ 18th-century instruments and observational techniques during the 2012 ToV. Two of their four ToV stations were successful in detecting the aureole with Georgian achromats by Dollond and West, with apertures under 76.2 mm (3″). Their findings are closely in accord with the results of the RASC Regina team's observations to determine the minimum aperture capable of revealing the aureole. It is striking that the modern instruments appeared to offer no definite advantage over the 18th-century instruments when detecting Venus's atmosphere visually. (This finding ought not to be taken to apply to the comparative observation of other types of astronomical objects with antique and modern instruments without field tests.)

Neither the Shiltsev nor the RASC results can *prove* that any particular 18th-century astronomer actually saw the aureole during the ToV. What the results *do* establish is that the atmosphere of Venus can be seen with small-aperture, high-quality refractors of either 21st- or 18th-century manufacture. Astronomers of the Enlightenment possessed in their best standard equipment the instrumental means to see the aureole. Whether any did will have to be judged through careful analysis of their observational records alone. No aureole observation can be dismissed through a sweeping dismissal of the optics of the day.[6]

## Other phenomena

The observers at the primary ToV station in Regina (using OTA1-4) independently saw an intriguing phenomenon immediately succeeding 1st contact. When enough of the planet was present on the Sun to form a discernible shape after the first "bite" into the solar disc, the planet presented the appearance of a truncated oblate spheroid (Figure 4), a phenomenon also seen by Vessey in 1874 (Russell 1892, 16-19, Pls. I, VII). This effect did not last more than a couple of minutes. One observer (CB) attributed the effect to OTA1-4 being still in the process of achieving thermal equilibrium
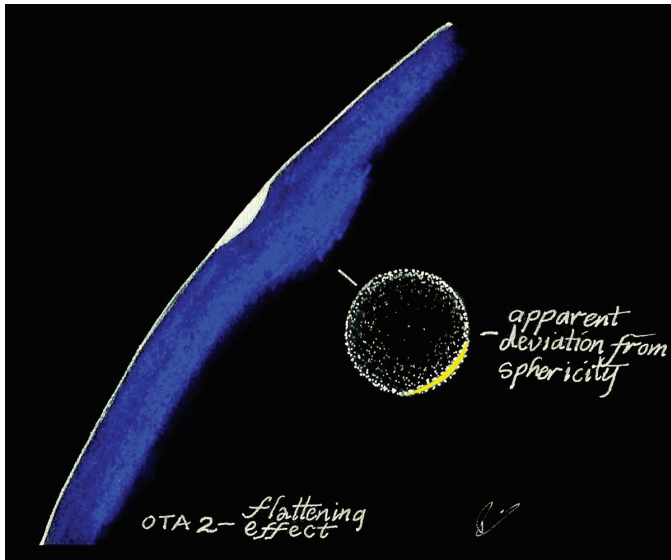
*Figure 4 — Momentary distortion of Venus's shape at beginning of the transit. Drawings by R.A. Rosenfeld.*

with the ambient air temperature, equilibrium being reached when the planet's appearance assumed the shape of a spherical cap shortly thereafter. Alternatively, he wondered whether the distortion was due to an air cell. It should be noted that none of the observers were aware of the solar disc showing similar distortion, but even if the effect were present it might have been difficult to discern in OTA1-2, as they were not used in a configuration to show more than a section of the solar disc.

One member of the team (RAR), observing with OTA2, saw the black-drop phenomenon at 2nd contact (Figure 5a). The duration of the "ligament" joining the solar limb to the trailing edge of the planet, and the latter's piriform distortion struck
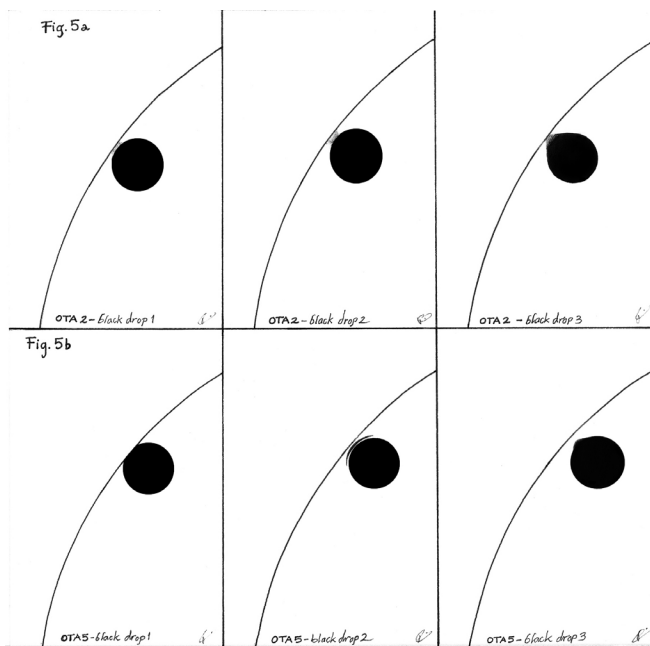


*Figure 5 — a. Stages of the black-drop phenomenon through OTA2; b. Stages of the black-drop phenomenon through OTA5 (first image shows Venus just prior to the black drop). Drawings by R.A. Rosenfeld.*

the observer as very brief, although that impression cannot be quantified, as the observer failed to time the stages of the phenomena. The ligament itself appeared as the merest hint of "smoke" never totally obscuring the Sun beneath, nor could the ligament be described as either particularly thread-like, or long.

Finally, before 2nd contact, one observer (CB) had the impression that he could just discern very faint traces of the solar atmosphere extending beyond the portion of the planet still off the solar disc through OTA1 at full aperture. To check this observation, he switched to Hα (OTA4) and saw the portion of the planet still off the solar disc framed by a small quiescent prominence. He was surprised by this, and wonders if the Hα observation really was confirmation of the white-light view at the extreme edge of visual detection, or was merely a coincidence.

We can assure readers of the integrity of the above observations, which follow Charles Messier's principle, "…but I relate only what I saw" (Messier 1769, 377).

## Observation with a Georgian Gregorian



*Figure 6 — Bate Gregorian reflector ca. 1830 (OTA5). Photo UTSIC.*

One observer (PG) stationed at Varsity Stadium, Toronto (longitude 79.40°W, latitude 43.67°N, elevation ca. 100m asl), participating in the ToV education and public outreach (EPO) event organized by the Dunlap Institute of Astronomy and Astrophysics (DI), was able to use a Georgian-period Gregorian reflector to observe the ToV (Figure 6). The Specifications of the instrument can be found in Table 1. Some haze was present, and light clouds occasionally intervened. Seeing was average at best, never exceeding Pickering 5.5 (Antoniadi III) The observer did not see the aureole during ingress, but did see the black-drop phenomenon (Figure 5b). Seeing was average at best, never exceeding Pickering 5.5 (Antoniadi III). What was particularly striking about this instrument was the very sharp quality of the images it produced, and its ability to snap into focus. The solar limb, sunspots, and the disc of Venus all had the quality of a fine copper engraving—nothing was diffuse due to the optics. Many of the public who attended the DI

event considered the view of the ToV through the Georgian telescope superior in definition to that of many of the modern instruments on site. Balancing the dual commitments to EPO and scientific observation was not always easy, as some 18th-century astronomers also remarked (Smith 1771, 24-25). ✳

## Acknowledgements

## References

### Manuscripts, Books, and Articles

Arlot, J.-E. (2004). *Les rendez vous de Vénus—Venus' rendez-vous* CD-ROM (Paris: Observatoire de Paris & IMCCE)

Barker, P. (1982). Techniques of Archaeological Excavation 2nd ed. (London: B.T. Batsford Ltd.)

Bergman, T. (1761). An Account of the Observations Made on the Same Transit at Upsal in Sweden, in *Philosophical Transactions 52*, 227-230

Binder, A. (2010). The Performance Characteristics of 17th Century Long-Focus, Non-Achromatic Refractors, in *Journal of the Antique Telescope Society 31*, 3-17

Bishop, R. (2012). Castle Frederick Observatory, in *JRASC 106, 4*, 142-149

Crease, R.P. (2012). Critical Point: Transit Watching, in *Physics World 25, 8*, 16

Harris, D. (1769). Observations of the Transit of Venus Over the Sun, Made at the Round Tower in Windsor Castle, June 3, 1769, in *Philosophical Transactions 59*, 422-431

Hirst, W. (1761). An Account of an Observation of the Transit of Venus Over the Sun, on the 6th of June 1761, at Madras, in *Philosophical Transactions 52*, 396-398

Jones, K.G. (1991). *Messier's Nebulae & Star Clusters*, Practical Astronomy Handbooks 2 (Cambridge: Cambridge University Press)

Maskelyne, N. (1768). Instructions Relative to the Observation of the Ensuing Transit of the Planet Venus over the Sun's Disk, on the 3rd of June 1769, in *The Nautical Almanac and Astronomical Ephemeris for the Year 1769* (London: Richardson & Clark), 1-47

Messier, C. (1769). Letter Addressed to Mr. Magalhaens, in *Philosophical Transactions 59*, 376-377

Pasachoff, J.M. & Sheehan, W. (2012). Lomonosov, the Discovery of Venus's Atmosphere, and Eighteenth Century Transits of Venus, in *Journal of Astronomical History and Heritage, 15, 1*, 3-14

Russell, H.C., et al. (1892). Observations of the Transit of Venus; Made at Stations in New South Wales, 9 December, 1874 (Sydney: Government of New South Wales)"

Shiltsev, V., Nesterenko, I, & Rosenfeld, R.A. (2013). Atmosphere of Venus: Replicating the 18th-Century Discovery, in Physics World

Smith, H.S., Ceragioli, R., & Berry, R. (2012). *Telescopes, Eyepieces, Astrographs: Design, Analysis and Performance of Modern Astronomical Optics* (Richmond VA, Willmann-Bell)

Smith, W. (1771). An Account of the Transit of Venus Over the Sun's Disc, in *Transactions of the American Philosophical Society 1*, 8-39

Tanga, P., *et al.* (2012). Sunlight Refraction in the Mesosphere of Venus During the Transit on June 8th, 2004, in *Icarus 218*, 207-219

Wilson, A. (1769). Observations of the Transit of Venus Over the Sun, in *Philosophical Transactions 59*, 333-338

### Web sites

arXiv, V. Shiltsev, Lomonosov's Discovery of Venus' Atmosphere in 1761

www.arXiv.org/abs/1206.3489 *(accessed 2012 September 11)*

arXiv, A. Koukarine, I. Nesterenko, Y. Petrunin, & V. Shiltsev, Experimental Reconstruction of Lomonosov's Discovery of Venus's Atmosphere with Antique Refractors During the 2012 Transit of Venus www.arxiv.org/abs/1208.5286 *(accessed 2012 September 14)*

Transit of Venus, R.A. Rosenfeld, Experimental Archaeology www.transitofvenus.nl/wp/getting-involved/experimental-archaeology/ *(accessed 2012 September 21)*

## Endnotes

1   RASC Archivist.

2   Regina Centre.

3   The Institute for the History and Philosophy of Science and Technology (IHPST) at the University of Toronto, and the University of Toronto Scientific Instruments Collection (UTSIC).

4   Reporting on the second of the 18th-century pair of ToVs, Dr. Alexander Wilson, Professor of Astronomy in the University of Glasgow, describes an almost identical experience with the clouds dissipating obligingly immediately before first contact (1769, 333-334). Unintentional humour enters his account when he states that he placed an advertisement in the local paper "...begging the inhabitants, in cases where it would not be very inconvenient, to put out their fires from three o'clock that afternoon till sun-setting." It apparently worked to ensure a smoke-free sky for the ToV: "...the politeness of the inhabitants of Glasgow, in complying with this request, was far greater than could well be expected"! Smoke from wood fires did not seem to be a problem in present-day Regina, nor in Toronto.

5   "Hac occasione phaenomena nonnulla minus expectata adparuerunt;" trs. R.A. Rosenfeld.

6   It is indeed highly likely that even a well-made single-lens O.G. of suitable focal length providing diffraction-limited on-axis performance would, in skilled hands, provide unequivocal views of the aureole; on the capabilities of these instruments see Smith, Ceragioli & Berry 2012,88-95; Binder 2010.

# Official Opening of the London Centre's Observatory

*by Rick Saunders, President, (ozzzy1@gmail.com)*
*and Peter Jedicke, Past President, London Centre*

On October 21 of last year, the London Centre officially opened the club's new observatory. A festive barbecue was held at sunset to celebrate the occasion with about 45 Centre members and guests attending. London Centre President Rick Saunders officially declared the observatory open, and National 1st Vice-President Colin Haig brought greetings on behalf of the Society. The weather was pleasant under a first-quarter Moon, and clear skies made it possible to hold the first observing session right away.

The project has a long history. Several sites were looked at over approximately 35 years with construction actually starting at one of them, only to be cut short when the land was sold. Then, in 2006, the Centre entered into negotiations with the Ontario Ministry of Natural Resources and the Elgin Stewardship Council with the aim of putting up an observatory at our dark-sky observing site at the Fingal Wildlife Management Area. Talks stretched out over many months, but finally permission to build was forthcoming. The Elgin Stewardship Council, which manages and maintains the area, were on our side and really wanted the area used by more people. The RASC promise to conduct outreach functions on the site helped them in their negotiations with the government. The stipulations set forth by the Ministry were simple: that any structures could be removed on 90 days' notice and that we have proper insurance.

The buildings all rest on an annular concrete pad that sits directly on top of an old foundation pad that we think was put in place to house fuel trucks back in World War II, when the site was an RCAF training base. The pad was strong enough to carry the weight of the structure, while allowing us to use a minimal amount of concrete in the additional construction. If we ever have to move, the buildings could be taken down, and the pads would break apart easily.

The Warm Up Room (WUR) was the first building erected, completed in 2008. It is a 2.5×4-m (~8×13 feet) building, clad in green steel. It is heated using an RV-style furnace, controlled by a thermostat and supplied from a propane tank in a concrete bunker outside the building. The inside is lit by red-lighting fixtures on a timer, so that if someone leaves the lights on, the lights will shut off automatically. There is no mains supply at the site, so we have several hundred ampere-hours of 12V battery and a large inverter to provide 120V AC mains. The batteries are automatically charged by a solar panel on the roof.



Figure 1 — Peter Jedicke, human guard dog, makes it clear who is invited and who is not. Image: Dale Armstrong.

Inside the WUR are a small shelving unit for storage and a fold-down table for people to work on. Power is supplied for computers from the inverter, and a USB connection runs from the work table to the telescope pier in Observatory One (OBS1).

The two observatory buildings—one complete, the other pending—sit on 3×3-m (10-feet square) pads with a large concrete pier base offset to the south side of each. OBS1 was designed by then-Centre President David McCarter and erected over several work parties by the membership. The structure is of 2×4 and 2×6 boards sitting on top of a deep floor plate that is bolted down to the annular pad. The roof rolls off toward the north. A full-height steel entry door is set in the north wall. OBS1 is completely clad in white steel siding.

The roof beams were laid up using 2×8s glued and screwed together. A steel U-channel is bolted to the inside of the beam and the roof's rollers run in the U-channel; 6×6 vertical posts are anchored to the existing concrete pad and hold up the far end of the beams. A "webbing" of lateral and transverse supporting 2×6s steadies the beams and verticals. Aluminum sheet is wrapped around the verticals to act as "squirrel cheaters" and we hope this will keep the red squirrels out (we had to evict a few during construction).

Inside, OBS1 is painted flat black and the floor is covered by foam panels in a checker-board black-and-white pattern. These were purchased from Lensmill Store in London and just snap together. No adhesive is used. In the northeast and northwest corners are small desks, and at the northeast corner is a 300W inverter to run a laptop and a USB connection to the telescope pier. In the south wall is a flap that can be lowered when the roof is rolled back to allow the telescope to see close to the horizon.

*Figure 2 — London members celebrate at the opening's BBQ. Image: Dale Armstrong.*

The pier in OBS1 is built from the tube and base sections of an Astro-Physics pier, bolted to a 19-mm steel plate, which is itself bolted to the concrete pier base. An Astro-Physics 1200GTO mount rides on top of the pier and has an ADM dual-dovetail saddle plate, which can accept either Vixen- or Losmandy-style dovetails. Counterweights for the mount are SkyWatcher 11-kg weights—we have four—with the hole bored out to match the AP counterweight shaft. At the moment, there is no Centre telescope on the AP1200, but Rick Saunders' Celestron 9.25″ is mounted for the time being and will remain there until London Centre obtains an optical tube.

The pier hosts a power box where 12V DC power is brought up to the mount. Inside the box are two large bus-bars of 3/8″ brass. These provide power to the various connectors and boards. The box provides four low-current power ports with RCA-type connectors, centre positive, and four high-current power ports using XLR-type connectors. The mount's power is provided by a separate XLR port. Inside the box are some DC-DC converter circuits, one of which provides 5V to a USB2.0 hub; the other provides 8V to power a DSLR camera with a suitable battery eliminator. Incoming power runs through a 250V switch and an automotive-type fuse holder, reachable without taking the cover off the box. Also in the power box is an anti-dew heat controller of Dave McCarter's design. The anti-dew controller and two power circuits are on the same circuit board, which was fabricated by Rick Saunders.

Above the power box is a circular wooden shelf with 1.25″ and 2″ holes for eyepieces. At the floor level of the pier is another circular wooden cosmetic plate that hides the hole in the floor and trims out the pier nicely. Both were fabricated by Pete Raine; they add a classy touch.

OBS2 will be a 3×3-m (10 square feet) SkyShed built to our specifications. The club members have given permission to contract with SkyShed for the provision of OBS2, and discussions with SkyShed have been finalized. This building will have a stiffer frame than the company's standard and will be
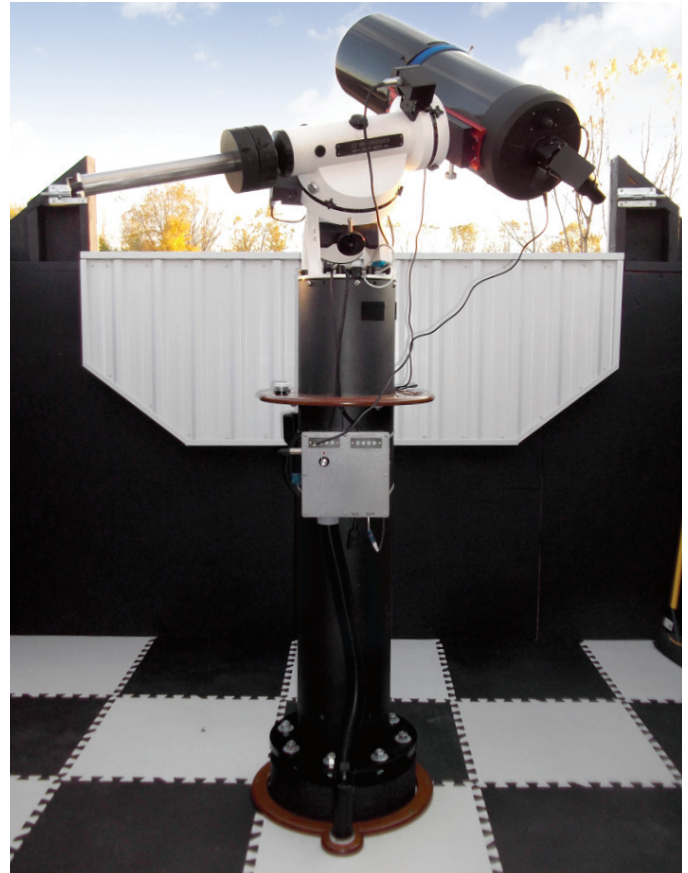


*Figure 3 — OBS1 pier and mounting. Image: Robert Duff.*

wrapped in white steel instead of pine. The standard windows and pine siding have been removed. The roof will roll off to the north, as with OBS1.

OBS2 will hold the Centre's Byers equatorial mount once a suitable pier has been fabricated. 12V will be supplied from the WUR but no USB connections, as the mount is from the pre-computer-control era and will be used for visual work. We are currently looking for a replacement optical tube, as our old 16″ Meade is in use at Western University's meteor lab.

It's been a long, LONG journey, but now London Centre finally has a facility it can be proud of and that will become the centrepiece of many of the Centre's functions. To all of those who assisted in construction and to those who provided moral support and advice, London Centre offers heartfelt thanks. Future generations of amateur astronomers owe you a debt of gratitude. ✷

*Rick Saunders became interested in astronomy after his father brought home a 50-mm refractor and showed him Saturn's rings. Previously a member of both Toronto and Edmonton Centres, he now belongs to the London Centre and is mostly interested in DSLR astrophotography.*

*Note added in proof: The OBS2 building was installed by SkyShed in November and is awaiting the coming of spring before its interior can be finished and the mount installed.*

# My Fast-Light Mirror

*By Roman Unyk, Edmonton Centre*
*(UnykFamily@shaw.ca)*

Wouldn't a 406-mm (16-inch) mirror weighing about 6 kg (13 lbs) be great? What if it also had a short focal length and was relatively easy to figure! The design I will present evolved over some time, but it wasn't till 2005 that I started using *PLOP* (*PL*ate *OP*timizer finite-element analysis) to quantify my guesses.

Before going further, I would first like to add a few words about what amount of deformation is acceptable. An optical system is considered capable of diffraction-limited performance when the final wavefront error produces a Strehl ratio greater than 0.80. This is the Raleigh criterion. A perfect optic has a Strehl ratio of 1.0. The word "final" is bolded for a reason. In order for a telescope to actually operate at this level, every optical component must be fashioned to a higher level AND the mounting of these components must not significantly detract from their performance.

So what can we get away with? Opinions vary, but it seems to me that a mirror cell that doesn't decrease a mirror's Strehl by more than 0.05 would be acceptable. Since nothing works perfectly, let's use a Strehl decrease of 0.03 as our guide. In other words, a perfect mirror would be decreased to a Strehl of 0.97, still excellent. Using the equations at the end of this article, this limit is equivalent to a $7.0 \times 10^{-6}$ mm RMS surface-error contribution from the cell, or 1/36 wavefront error. More stringent tolerances would be in order for speciality telescopes and vice versa.

Very thin mirrors require intricate cells, and edge support is problematic. Conical mirrors don't need edge support but are not really light. High-tech cellular designs can be very light but are also very expensive. My compromise mirror cross section is a cost-effective monolithic solution that is significantly lighter than a conical blank. It has a very thin edge with a significantly convex back and is supported at its centre of gravity in a simple 6-point, 3-bar cell. Unfortunately, *PLOP* only works with concave or convex mirrors that have a flat back. However, there is a way, with a little bit of hand waving, to fool *PLOP* into evaluating mirrors with curved rear surfaces.

First hand waving argument:

If we look at a mirror created by slumping a blank such that the front and rear surfaces have the same radii of curvature, it is equally thick all over but slightly saucer shaped. Even at f/3, the amount of sag is only about 2 percent of the mirror's diameter. For all intents and purposes, this is small, and the disk will behave like a simple flat plate. It can be modelled in *PLOP* as a flat mirror (infinite focal length or sagitta of zero). *PLOP* shows that, pound for pound, a slumped-blank design is stiffer than the standard flat-back design.
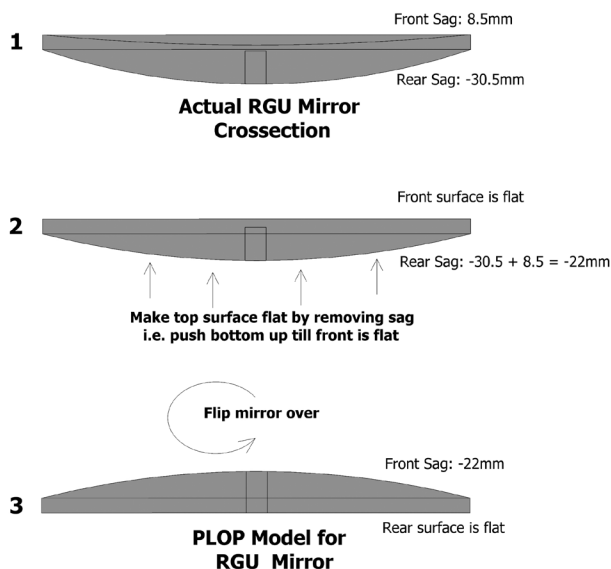
Second hand-waving argument:

For relatively thin mirrors, a point pushing up on the back surface would cause this surface to bend upward, deforming the front surface outward by a similar amount. This would generally be true even if the front and rear surfaces had different radii of curvature. In other words, the basic shape and magnitude of the distortions calculated by *PLOP* for the top surface of the mirror would, in essence, be the same on the rear surface.

If we put both the hand-waving arguments together, we can, with reasonable certainty, model the proposed mirror profile using *PLOP* (see Table 1). Figure 1 shows how this is done.

Enough of theory and design, it was time for the rubber to meet the road. But how "fast" to go? Tele Vue Naglers are guaranteed to work well down to f/4 and the original Paracorr was workable at f/3.5. In 2006, I settled for f/3.3. The prototype mirror then was also a little larger, 419 mm (16.5″), and weighed 7.1 kg (15.7 lbs).

| *PLOP* Model: | |
|---|---|
| Mirror Diameter: | 406 mm (16 inch) |
| Thickness: | 10 mm |
| Sagitta: | -22 mm (front sag minus rear sag) |
| Diagonal size: | 100 mm |

| *PLOP* Results: | | | | |
|---|---|---|---|---|
| Cell Type | Surface      RMS | Wavefront Error | Strehl | Cell r/R |
| 6pt-3bar | 3.2e-6mm | 1/78 | 0.994 | 0.484 |
| Siliconed ring | 2.5e-6mm | 1/100 | 0.996 | 0.500 |

*Table 1 — PLOP model and results for 6.1-kg f/3 mirror. These are phenomenal numbers for a very light mirror in such a simple cell. The second entry shows what is possible if one could evenly distribute the load around a circle. It was these results that started me thinking about supporting the mirror resiliently on a metal ring.*

**1** Actual RGU Mirror Crossection

Front Sag: 8.5mm
Rear Sag: -30.5mm

**2**

Front surface is flat
Rear Sag: -30.5 + 8.5 = -22mm

Make top surface flat by removing sag
i.e. push bottom up till front is flat

Flip mirror over

**3** PLOP Model for RGU Mirror

Front Sag: -22mm
Rear surface is flat

NOTE: Vertical height exaggerated by a factor of 2 for clarity

*Figure 1 — The three steps needed to allow modelling of curved-back mirrors with* PLOP.

I am fortunate in knowing Barry Arnold, an excellent optician. Barry likes to work thin mirrors on a cell to ensure they are evenly supported. This is where I ran into my first snag. The mirror was so light that it tipped easily when a weighted tool was placed near the edge. The solution was to hold the blank in place by resiliently mounting it to a steel ring using a 10-mm-thick by 10-mm-wide bead of silicone and then bolting the ring to the turntable. As an extra precaution, a ring of plywood was built up close to the blank's edge. Electrical tape was then lightly applied to seal the gap.

The following are Barry's comments:

1. The most difficult portion of working the blank was generating the rear surface. Next time I'd have the glass supplier provide a fully generated blank.
2. Siliconing the blank onto a steel ring worked very well. The blank stayed put even when polishing with a weighted tool right at the edge.
3. I expected there to be issues working a mirror with such a thin edge, but figuring was unremarkable. It went very smoothly and parabolizing at f3.3 was less difficult than expected. Perhaps the shape had something to do with how well it went.
4. The final figure is very smooth. I wouldn't hesitate making another such mirror, even a larger faster one.

The mirror was finally done, and I was desperate to get outside and try it out. So I just re-siliconed the mirror back onto the steel ring and put it into a hastily made tube assembly. Within a month of a very successful first light, I had the tube mounted
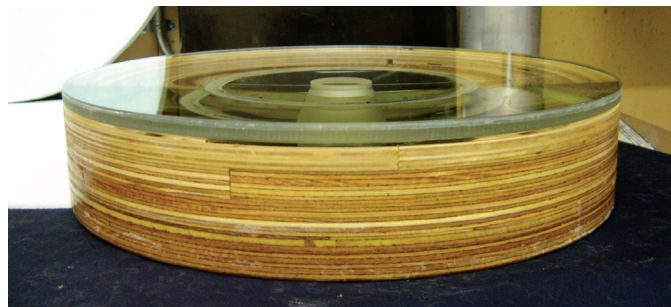


*Figure 2 — Mirror on turntable.*

on an Alt/Az mount with Dob-style altitude disks. I have used the telescope many times, and performance is basically very good even when the telescope is significantly tilted. Since the mirror was only mounted on a silicone ring, not a proper cell as originally planned, this was not expected.

Not too long after the telescope was completed, *PLOP* version 3 with Z88 analysis was made available. Although it still didn't handle mirrors with curved backs, it did allow me to roughly examine performance when tilted. The reason I can only say "roughly" is that the previous hand-waving arguments don't hold up well when the mirror is tilted. Hanging the mirror from a silicone ring attached to the rear is considerably different than attaching the ring to the front. The centre of gravity is much closer to the front, so the resulting bending moment is proportionally less. Even so, trying a variety of designs attempting to mimic a silicone ring support, seems to indicate that it might allow near-diffraction-limited performance even at significant tilts. Likely not great performance, but certainly not terrible. The difference should still be able to be seen.
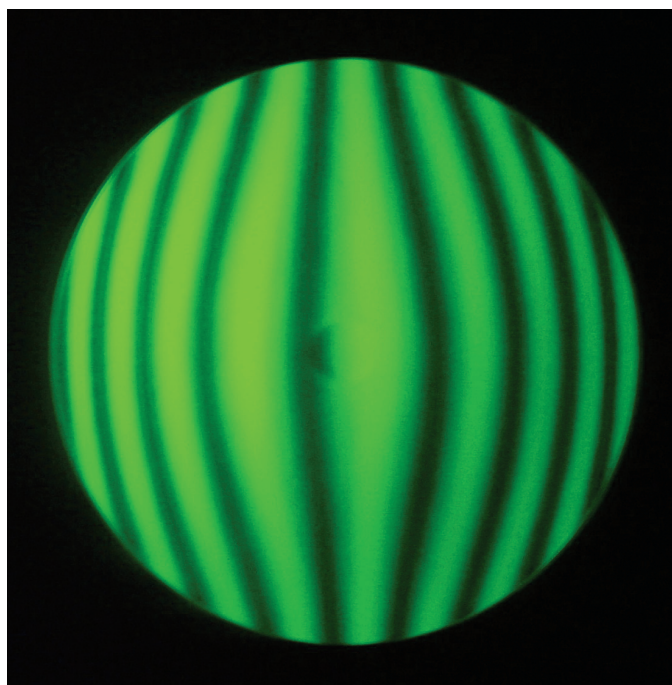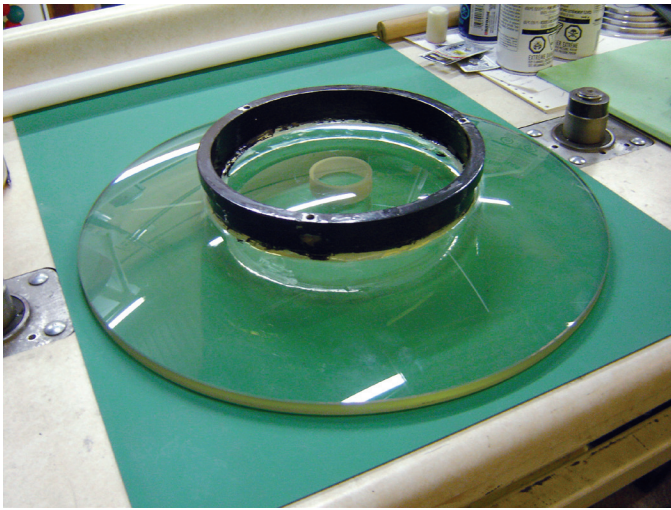


*Figure 3 — Mirror under test.*

*Figure 4 — Mirror face-down showing ring.*



*Figure 5 — Prototype scope at the 2008 SSSP.*

There are many real-world factors that combine to hide imperfect optics—poor seeing, a changing figure during cool-down, tube currents, collimation issues, and eyepiece limitations are just a few.

Poor seeing and tube currents are easily identified. With the addition of a fan and some time, there will eventually be a night where these are not the limiting factors. The low-weight mirror cools quickly. The fan concentrates flow over the rear centre because the thin edge requires no extra assistance.

I thought proper collimation would be more difficult to attain and maintain than it has turned out to be. A solid tube, stiff secondary holder design, and a primary mirror cell with no play does the job. It seems I only need to touch up the collimation after I have taken something apart. Normal transportation doesn't seem to be a problem. My latest modification has been to split the tube in half and motorize two of the mirror's collimation bolts. I assumed I would need to touch up the collimation every time I put the two halves together, but this doesn't appear to be necessary. However, I'm sure that a larger and faster telescope with a truss tube would be a different

proposition. Remote collimation adjustment would likely be much appreciated.

In my opinion, the major factor limiting excellent performance is that few eyepieces can handle fast optics well. The Airy disk for a fast mirror is smaller (3.8 microns for an f/3 compared to 6.3 at f/5 or 12.7 at f/10), so eyepieces simply have to be better to get at the available detail. The steeper light cone is very troublesome. To my knowledge, there is no eyepiece made that can provide diffraction-limited performance over a substantial field at f/3. It is for these reasons that, in 2006, I settled for an f/3.3 prototype. At the time, even this choice was pushing the envelope. It was slightly beyond what the original Paracorr was designed to handle and the combination at f/3.8 was near the limit of many Naglers. My mirror was very good, but the other optics made for a combination that is not truly diffraction limited. It may be that the crude silicone ring support allows the mirror's figure to change when the telescope is significantly tilted, but the change is not so great as to make itself noticeable above the other aberrations.

*Figure 6 — Latest reincarnation with my T-bar EQ table, collimation drives, and ArgoNavis controller.*

The existing telescope works very well as is. Since I mostly use low powers, the Airy disk is too small to see. More important are basic seeing conditions, transparency, and cleanliness of the optics. Nevertheless, I have had recent occasion to observe Jupiter under excellent seeing conditions. At 330×, detail was astounding and the Galilean moons clearly showed disks of different sizes. Not bad for an f/3.3 scope!

I must also add that the scope is a joy to use. Even after I added my modified equatorial platform, I have no need of a step stool and I'm just 5′ 7″ tall. The field of view with my older 16-mm Nagler is very nice, but a 21-mm Ethos would be staggering. Imagine a 1.3-degree field at 76× and with a 5.5-mm exit pupil—perfect for my aging eyes.

The saga doesn't end here. I have just taken delivery of a Supremax 33″ blank already generated for my next project, a 559-mm (22″) f/2.9 mirror weighing 13 kg (28.5 lb). Barry Arnold feels confident the mirror will turn out well. A 15-point cell should work nicely, but I will again see if I can get away with a siliconed ring. This time I'll need to include centre-of-gravity support to eliminate the bending moments that would be imposed if the mirror were to simply hang from the rear ring. Nothing like pushing limits even further!

To finish-off, I provided Table 2 with data for f/3 mirrors of various diameters, all mounted on a 6-pt, 3-bar cell with support at the 50-percent zone, all with 10-mm edge thickness and 25-percent central obstruction. Surface deformations by *PLOP* with Z88. Best results will be obtained by supporting the mirror at its centre of gravity. ✴

## Notes:

1   *PLOP* is available at www.davidlewistoronto.com/PLOP

2   Wavefront error calculations assume a wavelength of 500 nm ($5\times10^{-4}$ mm)

3   Simplified Strehl calculation is based upon the formula: Approximate Strehl = $1/\exp_e[(4\pi\,RMS_{surface}/\lambda)^2]$ where "$\exp_e$" is the exponent to base "e" and RMS surface error and wavelength $\lambda$ are in the same units (mm for *PLOP*). The above is derived from equation 4.8 taken from Jim Burrows' Web page: http://home.earthlink.net/~burrjaw/atm/atm_math.lwp/atm_math.htm, which in turn references H.R. Suiter, Star Testing Astronomical Telescopes, (Willmann-Bell, Richmond, 1994, ISBN 943396-44-1)

4   $RMS_{total} = SQRT\,(RMS_1^2 + RMS_2^2 + RMS_3^2 + \cdots + RMS_n^2)$

*Roman Unyk has been a member of the RASC since 1969 and is a professional mechanical engineer who's been making telescopes since grade school. He also believes that there are few things more satisfying than observing the heavens with a telescope fashioned by one's own hands.*

| Mirror Diameter mm (inch) | Edge Thick mm | Front RofC mm (inch) | Rear RofC mm (inch) | Finished Weight kg (lb) | Surface RMS (Z88) mm | Wavefront Error @500nm | Strehl Ratio |
|---|---|---|---|---|---|---|---|
| 317 (12.5) | 10 | 1900 (75.0) | -737 (-29.0) | 2.7 (6.0) | $2.6\times10^{-6}$ | 1/96 | 0.996 |
| 362 (14.25) | 10 | 2170 (85.5) | -737 (-29.0) | 4.0 (8.8) | $2.8\times10^{-6}$ | 1/90 | 0.995 |
| 406 (16) | 10 | 2440 (96.0) | -737 (-29.0) | 5.8 (12.8) | $3.1\times10^{-6}$ | 1/81 | 0.994 |
| 457 (18) | 10 | 2740 (108) | -737 (-29.0) | 8.6 (18.9) | $3.5\times10^{-6}$ | 1/71 | 0.992 |
| 508 (20) | 10 | 3050 (120) | -737 (-29.0) | 12.4 (27.4) | $4.0\times10^{-6}$ | 1/63 | 0.990 |
| 559 (22) | 10 | 3350 (132) | -737 (-29.0) | 17.5 (38.6) | $4.5\times10^{-6}$ | 1/56 | 0.987 |
| *508 (20) | 11 | 3050 (120) | -1050 (-41.3) | 9.7 (21.3) | $2.2\times10^{-6}$ | 1/114 | 0.997 |
| *559 (22) | 12 | 3350 (132) | -1100 (-43.3) | 13.3 (29.3) | $2.2\times10^{-6}$ | 1/112 | 0.997 |
| *610 (24) | 13 | 3660 (144) | -1150 (-45.3) | 17.8 (39.2) | $2.4\times10^{-6}$ | 1/104 | 0.996 |

*Table 2 — * Indicates values for a 15pt, 6-bar, 3-triangle cell, with 12 points (on 6-bars) on the 63% zone and 3 points on the 10% zone at the tips of 3 triangles. The triangles are supported so the three points have a relative force of 1.6′ that of the outer points. These designs would be worth exploring with a finite-element analysis program capable of properly modelling the actual mirror while tilted, including CofG support.*

# Through My Eyepiece

## What's Up!

*by Geoff Gaherty, Toronto Centre*
*(geoff@foxmead.ca)*

As I write this, it's early December, and I've just received my annual pre-Christmas treat: the new edition of the *Observer's Handbook.*

Nearly every year, I spend a few hours with my new Handbook, seeing what the astronomical future has in store for me. Looking back at past editions on my bookshelf, all the way back to 1957, I see that most copies are well worn from much use. In truth, the Handbook is probably the most-used book in my library. It's become a lot thicker and more colourful over the years, but the layout and content remain much the same.

The first thing I do is to check the opening pages, where the editor alerts me to changes and important events. This year there is an interesting article by Jay Pasachoff that actually refers to a 2012 event, which hasn't happened yet as I write this: a planetary conjunction on 2012 December 21. This *isn't* the grouping that has preoccupied so many Internet sites, the supposed alignment of the Sun, Earth, and centre of the galaxy, which is of no significance. It also isn't the impossibly rare alignment of all the planets, all eight of them in a straight line, something that not only isn't going to happen in 2012, but has never happened in the entire history of the Solar System.

Instead, Jay is writing about a much more interesting event: a transit of Venus visible not from Earth, but rather from the planet Saturn. In 1957, the year of my first Handbook, this would have been an a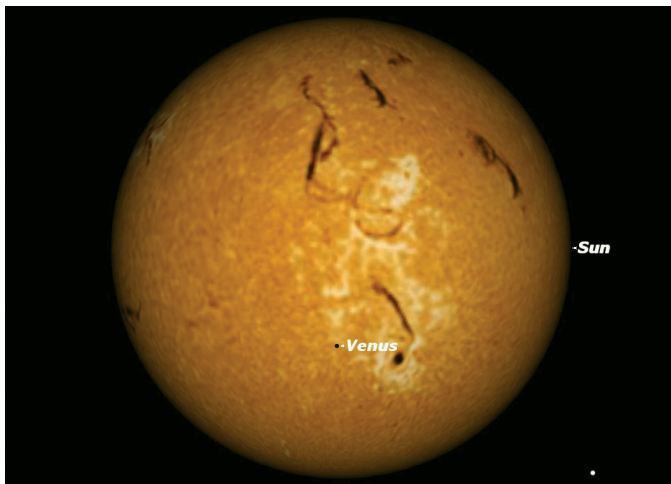bsurdly irrelevant piece of trivia. In 2013, Jay calmly tells us that he is actually going to observe this transit *from* Saturn, with the help of the *Cassini* probe currently in orbit there. Such a possibility existed only in my wildest dreams in 1957, as would be the idea that I would be able to sit down at my personal computer and watch the event myself through *Starry Night.*

After last year's transit of Venus and annular and total solar eclipses, this year is a bit of a disappointment, in fact nothing much visible from Canada. Oh well, 2017 is only four years away...

The periodic-comets page doesn't include two one-time visitors that *may* prove spectacular. No one wants to jinx us by promising great comets in advance, but keep an eye out for Pan-STARRS (C/2011 L4) in March and ISON (C/2012 S1) in November. If these are even half as nice as *Starry Night* predicts, we should be in for a very special treat.



*Figure 2 —* Starry Night *views of Comet Pan-STARRS (left) and Comet ISON (right) at their closest approach to the Sun.*

Figure 2 above shows what Pan-STARRS is supposed to look like as seen from the University of Toronto Campus on March 12 according to *Starry Night.* The right-hand depiction shows Comet ISON on November 29; note the spectacular length of the tail.

Lunar occultations, when the Moon passes in front of a star, are quite common, but always a treat to see. Occultations of stars by planets are much rarer, but the Handbook promises three this year, two of them visible from Canada. Mars will occult a 7th-magnitude star on August 18, visible from western Canada, and Venus will occult a 7th-magnitude star on November 21, visible from southeastern Ontario.

All in all, 2013 is shaping up to be an interesting year. ✷

*Geoff Gaherty received the Toronto Centre's Ostrander–Ramsay Award for excellence in writing, specifically for his JRASC column, Through My Eyepiece. Despite cold in the winter and mosquitoes in the summer, he still manages to pursue a variety of observations. He recently co-authored with Pedro Braganca his first iBook:* 2012 Venus Transit.



*Figure 1 —* Starry Night *view of the transit of Venus from Saturn.*

# A DIY Anti-dew Heat Controller

*by Rick Saunders, London Centre*
*(ozzzy@bell.net)*

Lately, at every monthly meeting in London, I've run a segment that I call "Cheap stuff from China" that highlights inexpensive electronics or other bits and pieces available on eBay that can be used by amateur astronomers to add to their bag of tricks. One of the items that I showed our members was a variable-speed motor controller that can handle ten amperes of current and does a great job of controlling an anti-dew heat strip such as those sold by Kendrick Astro Instruments.



*Figure 1 — The PWM motor controller.*

DC motor speed is controlled in the same fashion that anti-dew strips are, by turning the current on and off rapidly and varying the "duty cycle"—the ratio of the time the current is on to that when the current is off. This is known as Pulse Width Modulation or PWM. A quick search on eBay using the term "pwm motor controller" brought up a list of many parts. I whittled it down to those that had a "Buy Now" value along with "Free Shipping" and came up with the item shown in Figure 1. This part cost me about $8. I couldn't buy the parts to build it for that little, much less the time involved in construction.

Once the part arrived on this side of the ocean, I drove to the local electronic parts store and bought a Hammond case, a handful of RCA connectors (female), and two banana-plug connectors (again female). With these in hand, I had everything I would need to build the anti-dew controller.

The first step was to drill holes to mount the board. Notice that it comes from the factory with brass standoffs (Figure 1). I hunted through my collection of old computer screws and found four that would fit. Then I removed the standoffs and placed the board on the bottom of the plastic case to locate the holes, which were then drilled with a Dremel tool and 1/8″ drill bit. I mounted the board in the top of the box and configured the bottom as a lid (Figure 2). This makes things simpler.

With the board mounted in the box, the next task was to position the two banana plugs that I would use to bring power into the device. I like these, as they carry a lot of current and are colour coded. Following convention, I used the red one
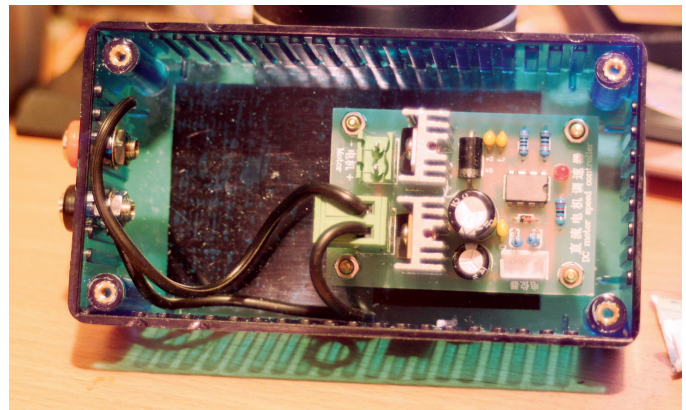


*Figure 2 — Top view of the controller*

for positive and the black one for ground (negative battery terminal). These were run to the connector on the board labelled "power." The board designers were nice enough to include detachable screw terminals for both power and motor... er... heater connections. The board is labelled + and – (Figure 2); don't mix them up. With the connectors in place, the body of the unit is finished.

Next, I had to locate where the potentiometer would sit on the lid. I found the centre using my calipers like a set of compasses and scratched a cross where the pot would sit. I then drilled/ Dremeled a suitable hole. The pot has two "ears" that are



*Figure 3 — Bottom view of the controller*

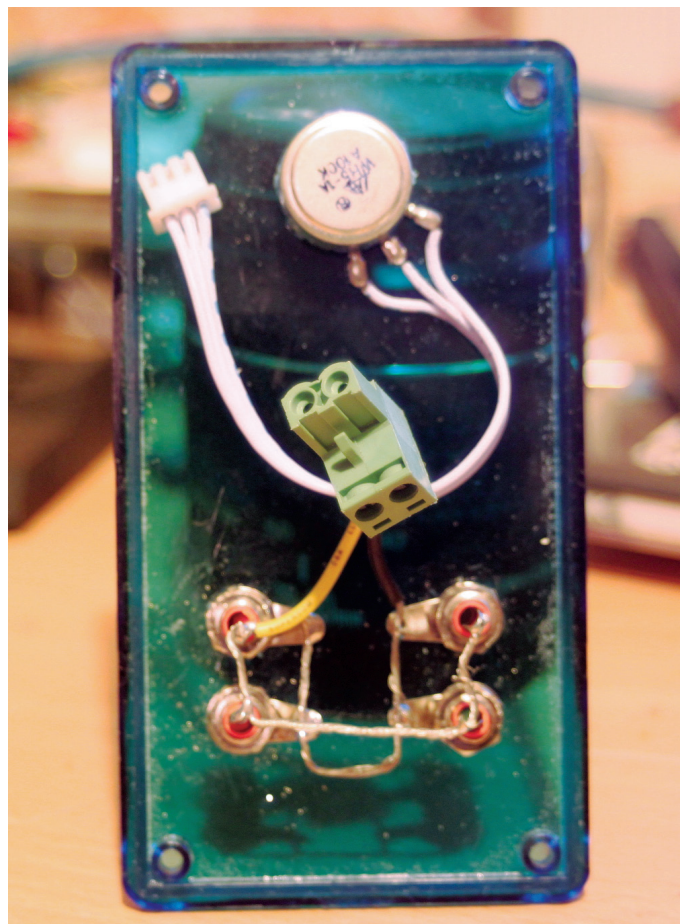supposed to fit into holes in the panel on which it is mounted to keep it from rotating. I positioned the pot and, using a small drill in the Dremel, located where these holes should be, then drilled them out. As you can see in Figure 3, the pot has a very long lead going to the board. This can be coiled up or, as I have done, cut shorter and re-soldered to the pot.

The last thing to do is to mount some connectors to the lid that will allow our heat strips to be plugged in. I chose to put four on, and again used my calipers as a compass to mark where I would drill holes. These were then carefully drilled with a 1/8″ bit, opened up with a conical grinder (you can use a 1/4″ drill bit), and then cleaned of the melted plastic.
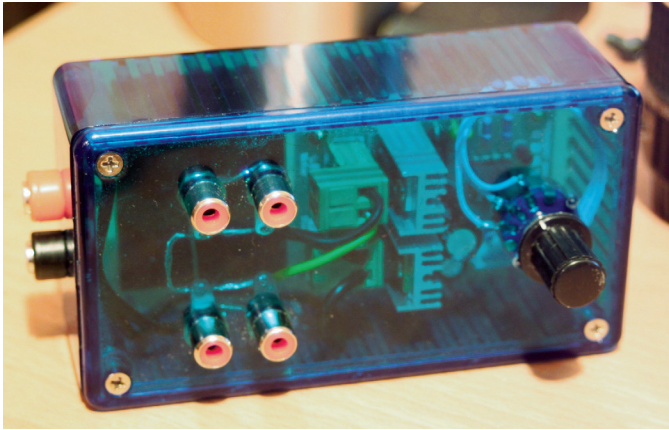


Figure 4 — The completed antidew controller.

To wire the connectors, I stripped all but 5 cm of insulation from a 150-cm 20-ga wire. I ran the wire from one RCA plug centre lead to the other until I had all four connected, then repeated the task with another 150 cm of wire to connect all four outer leads together. When I finished, I trimmed the two wires, stripped off about 3 mm of insulation, and tinned (coated with solder) the two wire ends. These were placed into the terminal labelled "motor." With anti-dew strips, polarity isn't an issue.

With all the drilling and wiring done, the only thing left was to put some Velcro on the bottom to allow it to "ride" my mount, and to screw the lid into place. This anti-dew heat controller cost less than $20, took about an hour to build, and works just fine. I didn't mount an LED on the outside of the case, as there is one on the board and the case is transparent (Figure 4). Should you like an opaque case, you can just desolder the LED and solder in a lead to go to an LED on the outside of the box.

The next project is a triple-voltage supply box, using cheap stuff from China. ✳

*Rick Saunders became interested in astronomy after his father brought home a 50-mm refractor and showed him Saturn's rings. Previously a member of both Toronto and Edmonton Centres, he now belongs to the London Centre and is mostly interested in DSLR astrophotography.*

# Imager's Corner

## *Images Plus*

*by Blair MacDonald, Halifax Centre*
*(b.macdonald@ns.sympatico.ca)*

When I retired my old CCD camera and first started using a DSLR for my imaging, I went looking for a decent program for stacking and calibrating images. I came across *Deep Sky Stacker* and was very pleased with the results in the early going. Eventually I started to run into some stacking issues, and having to take darks each time I went imaging was becoming a pain, not to mention a great waste of imaging time. Several fellow DSLR imagers told me about *Images Plus* so I decided to give it a try.

My first impression after using the software was that its author did an excellent job on the image processing, but had a rather quirky interface that didn't necessarily follow the usual *Windows* standard, as it had some very strange menu conventions. Since my day job involves electrical engineering (yes, I'm a geek) with a large amount of digital-signal processing, I could see the strange logic in the menu names, and I was very impressed with the calibration and stacking capabilities of the software. I decided to fork over some hard-earned dollars and buy a copy of the program. Since that day, *Images Plus* has gone through several iterations and has grown into an excellent processing package that makes most tasks easy and intuitive.

Let's start with the calibration capabilities—after all, this was one of the main reasons I purchased the program in the first place. Like a lot of software out there, *Images Plus* completely automates image calibration and stacking. You simply tell it what light, dark, and other calibration frames to use and it
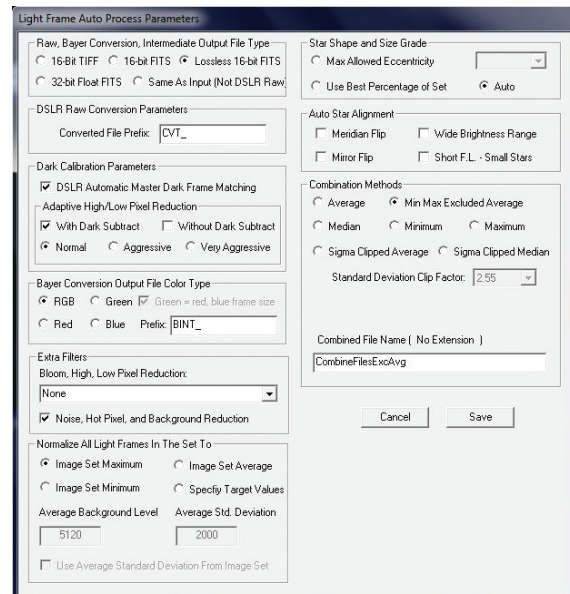


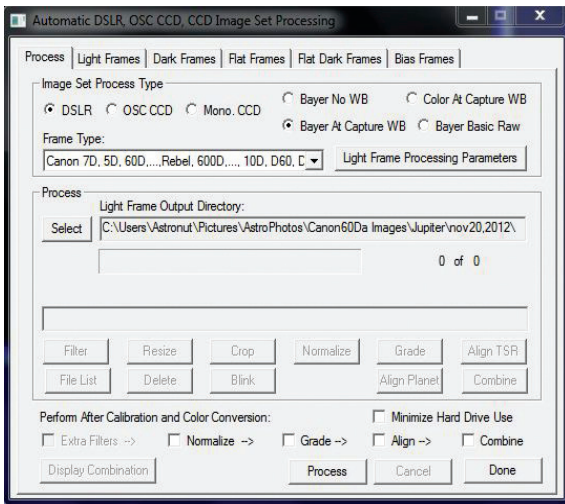Figure 1 — Light-frame processing parameters dialogue

Figure 2 — Automatic image-set processing dialogue

pretty much takes it from there. One thing that stands out is the ability to auto-scale darks to minimize the noise in the final calibrated image. This allows me to create a dark library, even though the DSLR I use has no temperature regulation. The software permits me to create a master-dark library and reuse darks over about a five- to ten-degree temperature range, so it is ideal for DSLR image calibration. The light-frame processing parameters dialogue is shown in figure 1.

This dialogue gives the user control of the stacking parameters as well, and it offers the usual bevy of options, from stacking modes to meridian-flip modes. The rest of the process is pretty much fully automated, with one more dialogue to select camera type and how you want to handle colour data.

Once you click the process button, the software automatically calibrates each image, identifies stars in the image, aligns the images by colour channel, and produces the final output. All processing is done in 32-bit floating-point, so scaling is rarely an issue. In addition to the fully automatic modes, there are several manual modes where the user selects up to three stars for use in alignment.

A welcome addition for planetary imagers is that *Images Plus* also automates aligning and stacking data from video files, and the camera-control system allows remote control of your camera for both still and video capture over a USB or other connection.

There is a whole host of processing features, from true HDR capability, various contrast-stretch methods, smoothing and sharpening functions, as well as various colour-balancing and saturation-control capabilities.

Sharpening capabilities run the gamut from kernel filters, wavelet based multi-resolution smoothing and sharpening, a variety of deconvolution routines, including an adaptive Richardson-Lucy algorithm, and several contrast-based sharpening algorithms that are particularly useful for lunar
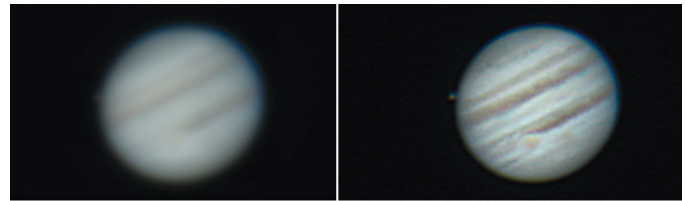


Figure 3 — Left: unprocessed image; right: image processed with statistical-difference sharpening

and planetary images. Figure 3 demonstrates the effectiveness of the statistical difference contrast-based sharpening for planetary imaging.

With the advent of version 5, *Images Plus* now has the ability to combine images with various combine modes and masks, duplicating the functionality of layers and masks in more general image processors. There are some well-thought-out mask-generation tools that allow masks based on luminance, colour, saturation, edge and area detection, and high-pass filtering.

As I've mentioned before, all processing is carried out in 32-bit floating-point resolution, so saturation due to stretching is pretty much a thing of the past, at least up until you set the black-and-white point for display. The software is also multi-threaded and can use multiple cores to speed processing. You can even process multiple images through iterative functions, such as deconvolution, at the same time. There is an unlimited undo feature, as each processing step produces temporary files that are deleted automatically when you finish with an image. The entire processing history can be displayed and even copied and applied to another image.

There are some areas that could use some improvement: the paint function only contains a square brush of limited size; painting on masks does not show the result in real time (you have to click on the apply button); and there is no transparent view of the mask so you can see what you are painting. In addition, there are still some quirks in the interface that are not the normal *Windows* standard, but the processing capability of the package more than makes up for an ever-decreasing list of quirks. Each new version of *Images Plus* adds well-thought-out refinements, and with the latest version, it has taken a big leap into high-end image processing.

Remember, this column will be based on your questions, so keep them coming. You can send them to the list at hfxrasc@lists.rasc.ca or you can send them directly to me at b.macdonald@ns.sympatico.ca. Please put "IC" as the first two letters in the topic so my email filters will sort the questions. ✶

*Blair MacDonald is an electrical technologist running a research group at an Atlantic Canadian company specializing in digital signal processing and electrical design. He's been a RASC member for 20 years, and has been interested in astrophotography and image processing for about 15 years.*

# Second Light

## M31 Surprise

*by Leslie J. Sage*
*(l.sage@us.nature.com)*

The Andromeda galaxy—M31—and some of its companions are well known to amateur (and professional) astronomers. Dwarf companion galaxies are generally believed to be leftovers from the time of galaxy formation, as giant galaxies grew by accreting smaller ones. This is the picture that has arisen from simulations of the growth of structure in the early Universe and has been very successful in explaining why clusters of galaxies lie in filaments and sheets. Rodrigo Ibata of the University of Strasbourg and his colleagues have now discovered that about half of the dwarf companions of M31 lie in a planar sheet with a radius of ~400 kpc, but a thickness of just 14 kpc (see the 2013 January 3 issue of *Nature*).

Dwarf galaxies were a bit of a problem for the standard cosmology for a while. The simulations that are so good at predicting large-scale structure also predict far more dwarfs than we see around the Milky Way and M31. It has recently become clear, though, that the answer to that problem lies in what happens with normal matter—the simulations only track the dark matter, because that dominates the normal matter by a factor of about 5. The normal matter, though, forms clouds of gas, then stars, and subsequently supernovae, and the energy from stellar winds and supernovae is sufficient to make many dwarfs very dark in the present era.

There have been suggestions that some of the Milky Way's dwarf galaxies form a co-planar group, possibly associated with streams of atomic hydrogen gas, and it was shown just this year that a subset of globular clusters—the so-called "young halo clusters"—orbit in the same plane. One way to form such a plane/disk of galaxies is if the Milky Way and another large galaxy passed near each other in the early Universe, ripping a stream of gas out of the Milky Way. This stream then formed the dwarf galaxies and globular clusters.

M31 has a huge angular extent on the sky—about 4 degrees, or 8 times that of the full Moon. This makes mapping it and its surrounding area very challenging, requiring many pointings with a telescope. The pan-Andromeda archeological survey by the Canada-France-Hawaii Telescope imaged about 400 square degrees of the halo around the galaxy, finding many new dwarfs. Ibata and his colleagues then determined distances to and velocities of these dwarfs, to plot their true positions and motions relative to M31 (see Figure 1.)

To their surprise, it turns out that about half of the dwarf galaxies lie in a plane that is very close to the line between M31 and the Milky Way. They then looked at the velocities of the galaxies in that plane, and found that almost all of the dwarfs show common orbital motion, with the southern galaxies approaching us (relative to M31) and the northern ones going away. The chance of this being random is vanishingly small.

The distribution of dwarfs in this plane is rather lopsided, with most of the galaxies between M31 and the Milky Way. Ibata is confident that this lopsidedness is real, and not an artifact of an incomplete survey. With the plane pointing at the Milky Way, the case for tidal dwarfs (as proposed for the plane of dwarfs around the Milky Way) seems to me to be the most
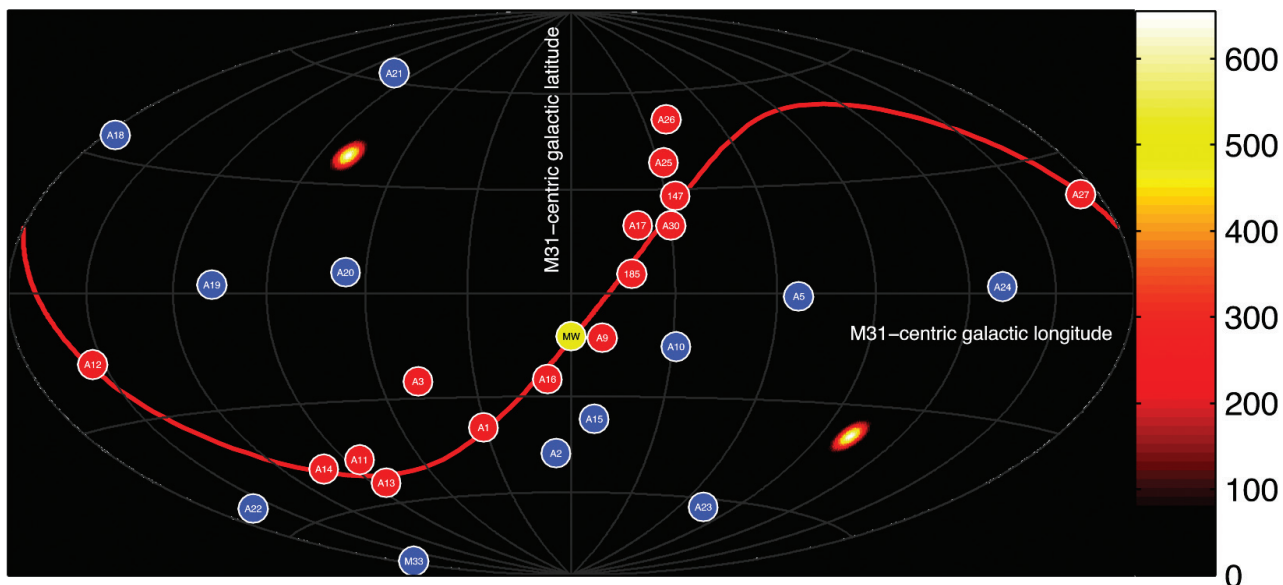


*Figure 1 — Dwarf galaxies' positions as they would be seen from the centre of M31. The plane of M31's disk lies along the equator of this projection. The red symbols show the co-planar galaxies, while the blue ones are dwarfs not associated with the plane. The direction to the Milky Way is shown in yellow.*

Figure 2 — This is an interactive 3-dimensional PDF (for the on-line PDF Journal). The red symbols are again the co-planar galaxies, and the blue ones the "normal" ones. The z direction is parallel to the line between M31 and the Milky Way. The thinness of the plane is most easily seen looking down the z axis. (Give it time to load—it takes over a minute on some computers. You need to view it using Adobe Reader or Adobe Acrobat; Preview on an Apple computer will not work.)

likely explanation. The problem with that, however, is that there is evidence for dark matter associated with at least some of the galaxies, while the argument goes that galaxies formed from tidal processes should not have dark matter associated with them.

However they formed, they are now an observational fact that models of the early Universe will have to explain eventually. Next time you turn your binoculars towards M31, give a thought to the disk of galaxies spinning along that plane. ✳

*Leslie J. Sage is Senior Editor, Physical Sciences, for* Nature Magazine *and a Research Associate in the Astronomy Department at the University of Maryland. He grew up in Burlington, Ontario, where even the bright lights of Toronto did not dim his enthusiasm for astronomy. Currently he studies molecular gas and star formation in galaxies, particularly interacting ones, but is not above looking at a humble planetary object.*

# On Another Wavelength

## Observations in Taurus

*by David Garner, Kitchener-Waterloo Centre*
*(jusloe1@wightman.ca)*

Taurus is often overshadowed by its neighbour Orion, but there are several very interesting features in Taurus that are certainly worth getting out your telescope for. Taurus has two very well-known clusters and what became the first object in Messier's catalogue, M1.

The brightest star in the constellation is Aldebaran ($\alpha$ Tauri). To find it, just follow the three belt stars of Orion off to the right. With an apparent magnitude that varies between 0.75 and 0.95, it is not only the brightest star in the constellation but also one of the brightest stars in the night sky. Compared to our Sun, a G2 V-type star, Aldebaran is a K5 III star in the red giant stage of its evolution. Its mass is only 1.7 times that of our Sun but it has swollen up to 40 times larger. At its current state, its core is still fusing hydrogen and is not yet hot enough to begin fusing helium.

Taurus, as part of the zodiac, is intersected by the ecliptic (dark solid line in Figure 1), such that the Moon and the planets can often be found in the constellation Taurus during some part of each year. Aldebaran, at a declination of +16° 30′, is close enough to the ecliptic to be occulted by the Moon. The next event in Canada will occur on the morning of 2015 March 25.

Aldebaran appears to be a member of the nearby Hyades open cluster, but the distance between them indicates it is not. The star is only 65 light-years away, whereas the Hyades are about 150 light-years distant. The Hyades span about 5° of the sky and can be viewed in their entirety with binoculars. The four brightest stars of the Hyades are all red giants that have now evolved off the main sequence. The cluster consists of a roughly spherical group of hundreds of stars of approximately the same age (625 million years) and mostly within 18 light-years of each other.
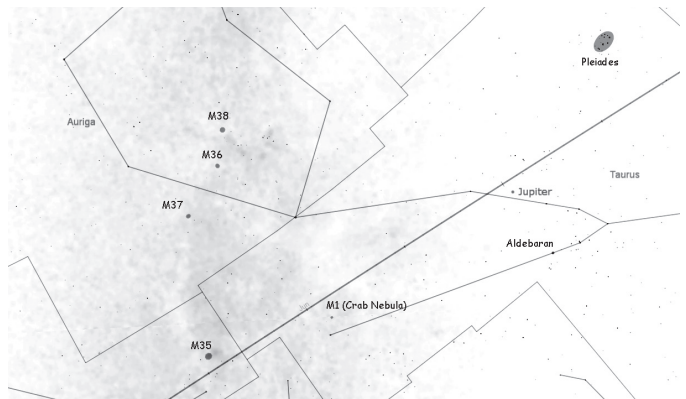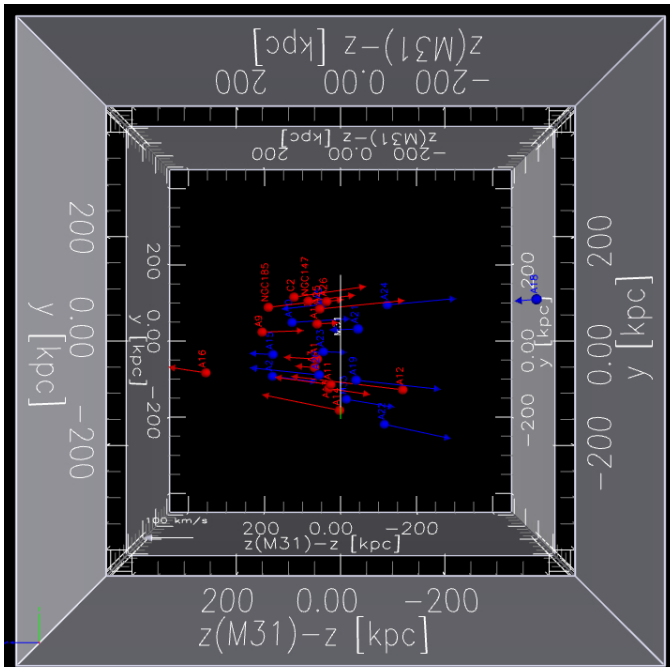


Figure 1 — A map of the constellation Taurus.

*Figure 2 — The Crab Nebula, courtesy of Brian McGaffney, Kingston Centre, and Peterborough Astronomy Association. The image was taken here at the Nutwood Observatory. The telescope is a carbon-fibre Ceravolo 300-mm astrograph, with an Apogee U16m CCD camera and 50-mm Astrodon filters. Acquisition was achieved by guided data using a WO 110 for approximately 8 hrs. This image is an (Hα+L) (R+Hα) G B stack.*

The Pleiades cluster, also called the Seven Sisters or M45, is the most obvious cluster to the naked eye in the night sky. At approximately 400 light-years distant and with a core radius of only 8 light-years, the cluster consists of many hot, blue stars that make a beautiful image for amateur astrophotographers. Many astrophotos of the Pleiades have shown nebulosity around the cluster. This nebulosity is a result of the cluster passing through a particularly dusty region of the interstellar medium and is caused by that dust reflecting the blue light of the hot, young stars.

In 1771, Charles Messier observed the position of the cluster and included it as number 45 in his famous list of comet-like objects. Including the Pleiades seems curious since most objects in his catalogue were much fainter and easily confused with comets. The Pleiades has easily discernible stars and bears no resemblance to a comet.

The Crab Nebula (M1, SN 1054) is a supernova remnant, first observed by John Bevis in 1731. His observation corresponds to earlier naked-eye records written by Indian, Arab, and Chinese astronomers in 1054. The Crab Nebula thus became the first object identified with a historical supernova explosion. Its strange name, the "Crab Nebula," was based on a crab-like drawing made by Lord Rosse around 1844.

The Crab Nebula (Figure 2) is the remnant of a Type II supernova. The nebula has a diameter of 11 light-years and lies at a distance of 6500 light-years; spectroscopic measurements show that it is expanding at 1500 kilometres per second. The progenitor star is a massive star that ran out of fuel to power its fusion reactions and collapsed in on itself, resulting in a massive rebound explosion. This progenitor, called the Crab

Pulsar, is a spinning neutron star approximately 30 km in diameter that emits pulses of radiation about 30 times per second. In X-ray and gamma-ray observations, the Crab is the strongest source in the sky. M1 appears as a blue oval-shaped central region
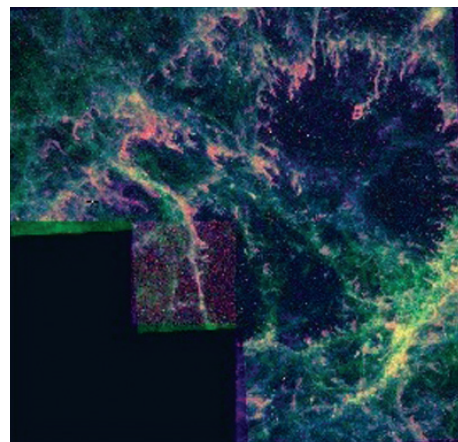


*Figure 3 — Crab Nebula Filaments. Image credit: HST WFPC-2*

surrounded by a mass of filaments (Figure 3) that are the remnants of the progenitor star's atmosphere, consisting mostly of helium, oxygen, and sulphur gas.

Similarly to Aldebaran, the Crab Nebula lies approximately 1½° from the ecliptic and can therefore be occulted by the Moon and planets. The nebula can be found easily, about 1 degree north and 1 degree west of Zeta Tauri, a 3rd-magnitude star close to Aldebaran. The Crab Nebula can be seen under clear dark skies, and with a 4-inch telescope, appears as a nebulous oval patch. ✶

*Dave Garner teaches astronomy at Conestoga College in Kitchener, Ontario, and is a Past President of the K–W Centre of the RASC. He enjoys observing both deep-sky and Solar System objects and especially trying to understand their inner workings.*

# 2012 RASC National Awards—Highlights of Award Citations

*Mary Lou Whitehorne*
*Past President*
*Chair, Awards Committee*

## Qilak Award for Astronomy Outreach and Communication

### Colleen O'Hare, Okanagan Centre

*The Beyond IYA collaboration of RASC/CASCA/FAAQ jointly developed the Qilak Award in 2010 and it was granted for the first time in 2012. Each year, three Qilak Awards will be given, one by each of the sponsoring organizations.*

*Qilak is the Inuit word that means the entire sky: the celestial sphere and all that it contains: the Sun, the Moon, and the stars.*

*The Qilak Award/Prix Qilak is intended to recognize individual Canadian residents or teams of residents who have made an outstanding contribution, during a particular time period, either to the public understanding and appreciation of astronomy in Canada, or to informal astronomy education in Canada, and to promote such activities among the members of the sponsoring organizations.*

*The awards are not designed to recognize achievement in formal astronomy education or achievement by a person or team of persons in the performance of their regular duties in their job or profession.*

Colleen O'Hare joined the Okanagan Centre in December of 2004. One year later, she was the "Member of the Year" for her exceptional motivation and energy in support of Centre EPO.

- As Outreach Director, Colleen began to organize membership and outreach programs.

- Actively sought out and developed new avenues to promote astronomical EPO.

- Energetic communicator, encouraging participation and involvement by all.

- Kept careful, complete records of all outreach activities—valuable in advancing our observatory project.

- Now in its third season, the facility offers a free public night every Friday.

- Colleen's outreach records were the key in identifying funding sources necessary to this public outreach initiative.

- Colleen gives presentations from the "Sky Theatre" amphitheatre to guests of the observatory.

- Colleen started, and for several years ran, the Centre's NOVA and NOVA Junior Programs, nurturing and promoting educational development.

- For many years Colleen has participated in, and led astronomy classes with the Society for Learning in Retirement.

- In a 10-month period in 2011, Colleen led the Okanagan Centre membership in nearly 100 outreach events, reaching over 6000 members of our community.

This pace of over 100 events a year, with thousands of people, has been the norm since Colleen engaged her outreach program of excellence, changing the face of astronomy in the Okanagan.

## Simon Newcomb Award

### Randall Rosenfeld, Unattached Member

*The Simon Newcomb Award is intended to encourage members of the Society to write and publish astronomy-related articles of general interest to our membership and beyond, and to recognize the best of these contributions through an annual award. The Simon Newcomb Award looks for originality, literary merit, scientific accuracy, and educational value in the work of candidates for this award.*

Here are the highlights of Randall's nomination for this award:

Randall Rosenfeld arrived on the RASC scene like a bright nova in 2008. Unlike any other nova, he continues to show amazing staying power, contributing to nearly every issue of the *Journal*—21 articles totalling some 98 pages in barely three years. His "Astronomical Art and Artifact" columns often highlight neglected aspects of RASC history and usually feature some aspect of his eclectic interests, such as his outstanding talent for drawing. He is also carrying out a valuable service by writing obituaries of the Society's

distinguished late Honorary Members. His articles are invariably well written, and well researched. Randall's literary ability was recognized by a prize in the Boeing-Griffith Observatory Science Writing Contest in 2008 for his essay "From Uraniborg to Yerkes; A Fragile Monumentality." In 2009, he received the Ostrander-Ramsay Award of the RASC Toronto Centre for excellence in astronomical writing. The members of the History Committee are proud to nominate our Chairman, Randall Rosenfeld for the 2012 Simon Newcomb Award.

## Chilton Prize
### Holly Ayles, New Brunswick Centre

*The Chilton Prize is awarded to an amateur astronomer, resident in Canada, in recognition of a significant piece of astronomical work carried out or published during the year.*

- Holly is 14 years old and a member of NB Centre's Education Committee.

- In 2011, she began a project, *Does Light Pollution Exist in the Village of New Maryland?* Using the RASC's Sky Quality Meter, she measured and mapped sky quality and light pollution in and around her hometown.

- Holly presented her project at the Bliss Carmen Middle School Science Fair, winning first place.

- She again won first place at the District Science Fair.

- Holly then won a Bronze medal at the River Valley Science Fair.

- She and a friend transformed the presentation into a poster project, La Pollution Lumineuse (Light Pollution), for a Statistics Canada contest, winning first place in provincial and national competitions.

- Her poster went to the International Statistical Literacy Project–Poster Competition 2010-2011 in Dublin, Ireland, where it again won first place.

- Holly Ayles is a bright young student of which the New Brunswick Centre is very proud.

- She has shown how much can be accomplished by our youth.

## Service Award: Three Awards in 2012
### James Edgar, Fred Smith, and Roland Dechesne

*The Service Award recognizes the contributions of members who, at either the National or Centre levels, have made a significant contribution to the life and vitality of the Society. It is given in recognition of outstanding service, rendered over an extended period of time, where such service has had a major impact on the work of the Society and/or of a Centre of the Society.*

These are some highlights of the Service Award citations for these three deserving candidates:

## James Edgar, Regina Centre

- Joined RASC in 2000 and has not looked back for even a moment.

- Since 2001, served as pre-production proof-reader for the *Journal* and the Handbook.

- Proof-reader for the *Observer's Calendar* and the *Bulletin*.

- Since 2006, competently filled the crucial role of *Journal* production manager and advertising coordinator.

- For many years has coordinated and overseen production and printing of the *Annual Report*.

- For several years, he has actively participated on the Awards, Constitution, Finance, Publications, Board Pilot, and Executive committees.

- For several years, he has moderated and coordinated the RASC's various email distribution lists and worked to maintain and update the Society Web site.

- From 2004 to 2007, he was National Recorder. From 2007 to present, he is the National Secretary (which now includes the Recorder duties).

- In this role, he has completed extensive updates and revisions to the RASC *Manual* and many other Society documents and files.

- Through James's work, the RASC has a newly invigorated Public Speaker Program, which James promotes and administers successfully.

- At the local level, he writes a regular astronomy column for Saskatchewan newspapers and conducts extensive school and community astronomy outreach programming.

James has been a stalwart of our National Committee structure, keeping committees working cooperatively and progressively toward the goals and objectives of the Society. He does it all with patience, grace, warmth, and humour.

James Edgar has participated actively in all aspects of national RASC business, working long and enthusiastically to promote the RASC, to encourage participation in Society activities, in sharing knowledge with others, and in the public awareness of science in general and astronomy in particular.

## Fred Smith, St. John's Centre

Long-time member of the St. John's Centre

- Executive Committee member for more than 15 years, including several years as President.

- Attendance record at public and executive meetings of more than 97%.

- Always been the liaison between the St. John's Centre and Memorial University—meeting space, parking, equipment storage space, and speakers.

- Frequent speaker, media contact, and liaison with other groups.

- Key player in obtaining funds and proposal for the "Universe Centre," a provincial observatory/planetarium/ meeting centre.

- Co-Chair for the 1994 GA and member of the organizing committee for the 2004 GA.

- Heavily involved with the Canada-Wide Science Fair, serving on the organizing committee and judging for RASC awards at regional and Canada-wide fair.

- Valued and frequently called-upon member of the St. John's Centre.

- Fred has given much of himself for the advancement of astronomy at the local and provincial level and is a deserving candidate for the Service Award.

## Roland Dechesne, Calgary Centre

- For his outstanding contributions to the Calgary Centre of the RASC over many years.

- Member of the RASC since 1977.

- Twice served as president of the Calgary Centre.

- Currently Past President and Chair of the Membership & Promotion Committee.

- Roland's efforts and commitment to the Society have been numerous, consistent, of high quality, and with excellent follow-through.

- Initiated, developed, and maintains the Calgary Centre's presence on social media including Facebook, Twitter, and the Calgary Meetup Group.

- Regular public speaker at RASC and University of Calgary-sponsored public events as well as many non-RASC events.

- Active and involved member of Council for many years.

- Key person in helping to create public star nights in the community of Vulcan, Alberta.

- Leadership role in research and education on Light Pollution Abatement.

- Researching roadway lighting laws in Canada and in the US.

- Taken the lead in helping to develop responsible lighting policies and in communicating light-pollution issues with individuals, communities, and local and regional governments.

- Provided assistance to the Lethbridge Astronomical Society and Waterton Lakes National Park to develop responsible-lighting protocols.

- Roland's multi-level and long-term engagement with astronomy has had a significant positive impact on the RASC as a whole.

- He continues to show passion and excellence in all that he undertakes.

## President's Award
## Randall Rosenfeld, Unattached Member

*Established in 2008, this award is to be given at the President's discretion, usually once a year, to a member who has made an important contribution to the Society. The intent of this award is to recognize a significant contribution that might not fall under the criteria for any of the RASC's other national awards.*

Randall Rosenfeld appeared on the RASC national scene in 2008, when he accepted the role of Archivist for the Society. Randall possesses remarkable talent, energy, and knowledge of astronomical history. He has been active on three committees: as past-chair of the Membership and Promotion Committee, and as current chair of both the Green-Laser Pointer Committee and the History Committee.

As Archivist, he oversaw the reorganization of the Society's library, the preservation of its most valuable holdings, the digitization of several significant holdings, and the placing of these on the Society's Web site. Randall has taken an active interest in the astronomical artifacts that the Society has accumulated over the years, researching them and seeing that they are appreciated and preserved. As an artist familiar with techniques from past centuries, Randall has made our members more aware of our pre-CCD, pre-photographic recording heritage and has encouraged other members to contribute to the Society.

His contributions have been many in recent years, and not all of them are described here. This award particularly acknowledges his outstanding work in preserving the RASC's material history: our library, our artifacts of value and historical significance, and our scientific heritage. It is individuals who make things happen. The RASC is fortunate to have Randall Rosenfeld in its ranks.

The full citations for all of the 2012 national Award winners can be found on the Society Web site: www.rasc.ca/awards

# Rendezvous with the Stars!

## 54th General Assembly of the Royal Astronomical Society of Canada
### June 27 - July 1, 2013

Come explore Thunder Bay, Canada's gateway to the west while attending the 54th General Assembly of the RASC. With features like the Sleeping Giant, Kakabeka Falls, Old Fort William (with the brand new David Thompson Observatory), and situated on the largest inland lake in the world, there is lots to see and do.

The GA is taking place on the beautiful campus of Lakehead University, located in the heart of Thunder Bay and on the banks of the McIntyre River. Most activities will be in the Advanced Technology & Academic Centre (ATAC) building. While you are there, don't forget to visit Mars! The Lakehead University Virtual Reality Environment (LUVRE) recreates stereoscopic 3D environments – as if you were really there.
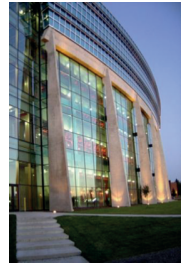
## Accommodations

Lakehead University will play host to us for the weekend. Guests can choose from a shared apartment-style room or a traditional dorm style accommodation.

## Night Sky Photo Workshop

We will be hosting a three part night sky photography workshop, that will be instructed by Dennis Mammana. His photos capture the heavens in ways rarely seen, and incorporate the celestial with the terrestrial to provide a unique perspective for the viewer.

## Tours

There are four tours to select from.

**Tour #1** – Friday June 28 – Fort William Historical Park with the David Thomson Observatory. From the fur trade to 21st century tech in one day!

**Tour #2** – Monday July 1 All Day – Slate Islands – featuring shatter cones from meteor impacts (limited availability and weather permitting). Requires travel by boat.

**Tour #3** – Monday July 1 AM – Ouimet Canyon, Eagle Canyon, Amethyst Mines, Terry Fox Monument. After viewing spectacular scenery, visit the spot where Canadian hero Terry Fox ended his run.

**Tour #4** – Monday July 1 PM – Kakabeka Falls and Founders Museum.

## Speakers

**Dr. Sara Seager** from MIT will be our first keynote speaker after the Wine and Cheese. She will deliver a talk entitled – *Exoplanets and the Search for Habitable Worlds.*

The Ruth Northcott Memorial Lecturer will be **Dr. Raymond Carlburg**. He is the Canadian lead on the Thirty Meter Telescope from University of Toronto, and will be delivering a talk about the background of the project, why Canada is involved and it's current state of development.

Our banquet speaker will be **Dennis Mammana**. Dennis was an invited photographer with the IYA The World at Night (TWAN) project, and his talk will be entitled – *One People, One Sky.*

**More information at www.rasc.ca/events**

# Astrocryptic

*by Curt Nason*

## ACROSS

1. One beast starts another in the sky (5)
4. Gases up around the Mobil sign (7)
8. He was a lion of our society; an all nighter, perhaps (7)
9. A very large one in New Mexico or across Barrayar (5)
10. Satellite in song let arts evolve with science (7)
11. His theory of cosmology was not in the cards, according to him (5)
12. Her deep-sky selections have drawback in strange oiled uses (6,7)
15. Rocket arrives from alternative Beta Centauri (5)
17. A movie aid and his father in a crater by Tempel's wall (7)
20. Asteroid turns hydroxide into potato state (5)
21. Soy components grown around Mount Kobau (7)
22. Orion's lead follows the French in test of Saturn's satellite (7)
23. TNO discovered with retrograde motion in clandestine operation (5)

## DOWN

1. Dishonest person steals the head of Beta Pegasi (5)
2. Aries backed you around London's first Past President (4,3)
3. Ironically, it heavily forms the basis of observational astronomy (5)
4. The most rascally optician can somehow tree a cop lover (5,8)
5. Nobelist in electroweak interactions detected aura around volcanic residue (7)
6. He studies impact craters or maybe an explosive prominence (5)
7. Membership benefit obtained in risky new subscription (3,4)
12. She rewrote vital ET information into her work on Cepheids (7)
13. Closely follows eclipse makers (7)
14. Agent unloaded real estate in a rilled crater (7)
16. I am back in the Spanish method of reporting comet discoveries (5)
18. Porros alternatives have much overhead (5)
19. Volcano on Mars or right in Asia (5)
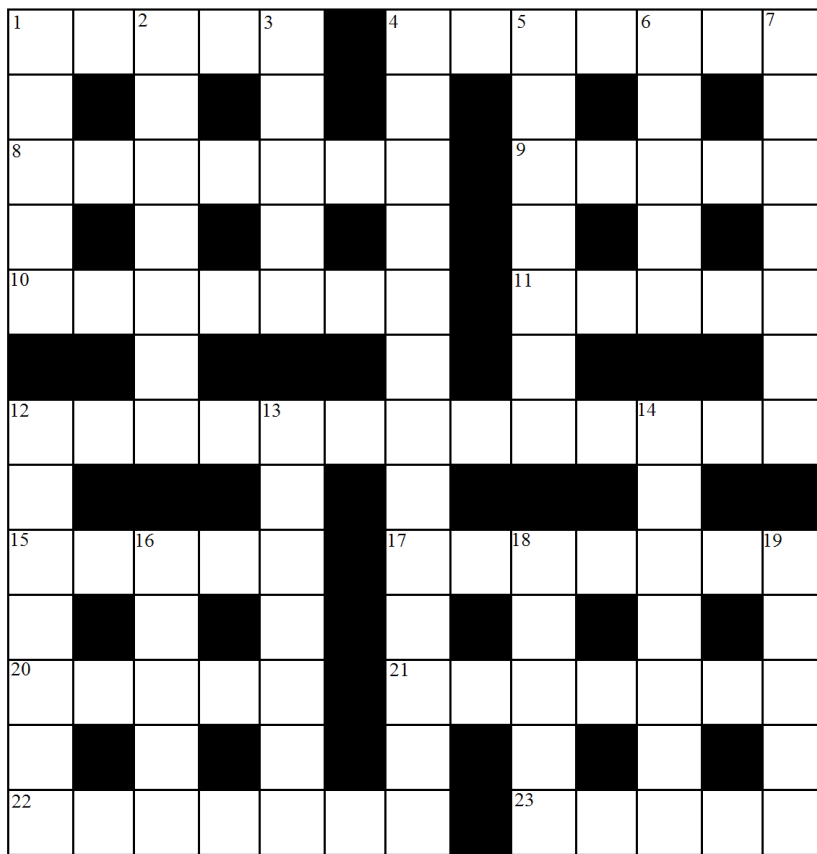
# It's Not All Sirius—Cartoon

*by Ted Dunphy and Kurt Nason*



Felix picked the wrong day to go to Gale Crater!

Ted Dunphy/Curt Nason
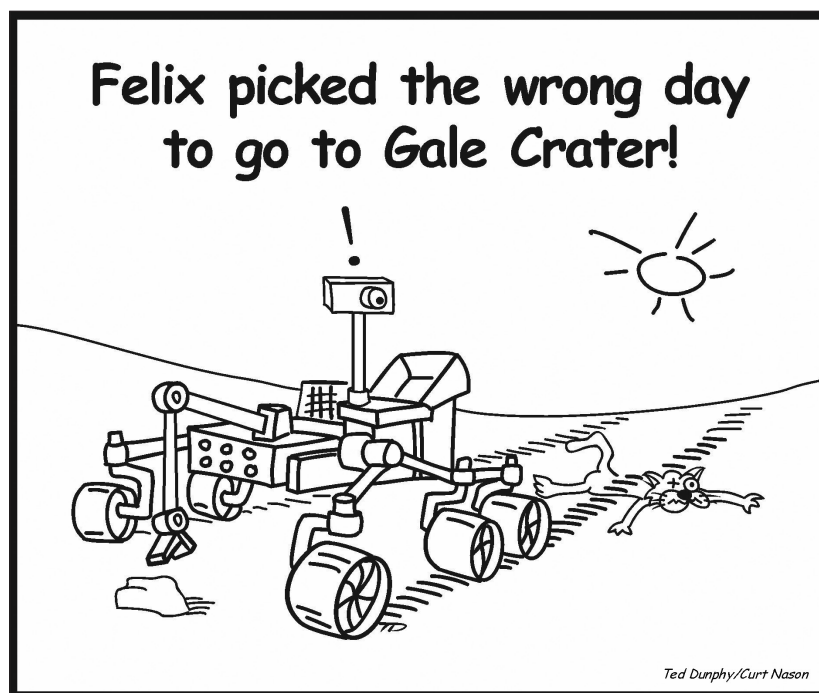
# THE ROYAL ASTRONOMICAL SOCIETY OF CANADA

## Executive committee and appointed officers for 2013 | Comité exécutif et membres attitrés pour 2013

| | |
|---|---|
| **Honorary President** | Jim Hesser, Ph.D., Victoria |
| **President** | Glenn Hawley, B.Sc., B.Ed., Calgary |
| **1st Vice-President** | Colin Haig, B.Sc., M.Sc., Hamilton |
| **2nd Vice-President** | Chris Gainor, B.A., M.Sc., Ph.D., Victoria |
| **Secretary/Recorder** | James Edgar, Regina |
| **Treasurer** | Denis Grey, B. Math., M.B.A., Toronto |
| **Past President** | Mary Lou Whitehorne, Halifax |
| **Editor of Journal** | Jay Anderson, B.Sc., MNRM, Winnipeg |
| **Editor of Observer's Handbook** | David M.F. Chapman, M.Sc., Halifax |
| **Editor of The Beginner's Observing Guide** | Brenda Shaw, Toronto |
| **Editor of Observer's Calendar** | Paul Gray, Halifax |
| **Executive Director** | Deborah Thompson, CAE, Toronto |

## Centre addresses/Adresses des centres

The most current contact information and Web site addresses for all Centres are available at the Society's Web site: www.rasc.ca

**Belleville Centre**
C/o Greg Lisk, 11 Robert Dr
Trenton ON  K8V 6P2

**Calgary Centre**
250, 300 5th Ave SW
PO Box 20282
Calgary AB  T2P 4J3

**Charlottetown Centre**
C/o Brian Gorveatt,
316 N Queen Elizabeth Dr
Charlottetown PE  C1A 3B5

**Edmonton Centre**
C/o Telus World of Science
11211 142 St
Edmonton AB  T5M 4A1

**Halifax Centre**
PO Box 31011, Halifax NS  B3K 5T9

**Hamilton Centre**
C/o Mr. A. Blanchard, 2266 Lakeshore Rd W
Oakville ON  L6L 1G8

**Kingston Centre**
PO Box 1793, Kingston ON  K7L 5J6

**Kitchener-Waterloo Centre**
305 – 20 St George St, Kitchener ON  N2G 2S7

**London Centre**
C/o Peter Jedicke, 82 Barrydale Cres
London ON  N6G 2X4

**Mississauga Centre**
PO Box 98011, 2126 Burnhamthorpe Rd W
Mississauga ON  L5L 5V4

**Centre francophone de Montréal**
C P 206, Station St-Michel
Montréal QC  H2A 3L9

**Montréal Centre**
17 Kirkland Blvd, Unit 121
Kirkland QC  H9J 1N2

**New Brunswick Centre**
C/o Emma MacPhee
26 Wilson Rd, Riverview NB  E1B 2V8

**Niagara Centre**
C/o Dr. Brian Pihack
4245 Portage Rd
Niagara Falls ON  L2E 6A2

**Okanagan Centre**
PO Box 20119 TCM
Kelowna BC  V1Y 9H2

**Ottawa Centre**
1363 Woodroffe Ave, PO Box 33012
Ottawa ON  K2C 3Y9

**Prince George Centre**
7365 Tedford Rd
Prince George BC  V2N 6S2

**Québec Centre**
2000 Boul Montmorency
Québec QC  G1J 5E7

**Regina Centre**
PO Box 20014
Regina SK  S4P 4J7

**St. John's Centre**
C/o Randy Dodge, 206 Frecker Dr
St. John's NL  A1E 5H9

**Sarnia Centre**
C/o Marty Cogswell, 6723 Pheasant Ln
Camlachie ON  N0N 1E0

**Saskatoon Centre**
PO Box 317 RPO University
Saskatoon SK  S7N 4J8

**Sunshine Coast Centre**
5711 Nickerson Rd
Sechelt BC  V0N3A7

**Thunder Bay Centre**
286 Trinity Cres
Thunder Bay ON  P7C 5V6

**Toronto Centre**
C/o Ontario Science Centre
770 Don Mills Rd
Toronto ON  M3C 1T3

**Vancouver Centre**
1100 Chestnut St
Vancouver BC  V6J 3J9

**Victoria Centre**
3836 Pitcombe Pl
Victoria BC  V8N 4B9

**Windsor Centre**
C/o Greg Mockler
1508 Greenwood Rd
Kingsville ON  N9V 2V7

**Winnipeg Centre**
PO Box 2694
Winnipeg MB  R3C 4B3

# Journal

## Great Images

*Stef Cancelli and Kerry-Ann Lecky-Hepburn describe this image of M106 and NGC 4248 as "a golden horseshoe collaboration" and a "Franken-Galaxy" because of the varied optical systems at different focal lengths that were used from two different locations. In total, there are 19 hours and 40 minutes of data collected. Kerry-Ann used a C6 at f/10 with a QHY-8 camera while Stefano employed a Vixen VC200L at f/9 with a ST10XME camera. In their words, "having that much data really helps overcome our less-than-ideal shooting locations and mediochre seeing."*